APTAMER FUNCTIONALIZED NOBLE METAL PARTICLES FOR BIOANALYTICAL AND BIOMEDICAL APPLICATIONS

By

EMIR YASUN

A DISSERTATION PRESENTED TO THE GRADUATE SCHOOL
OF THE UNIVERSITY OF FLORIDA IN PARTIAL FULFILLMENT
OF THE REQUIREMENTS FOR THE DEGREE OF
DOCTOR OF PHILOSOPHY

UNIVERSITY OF FLORIDA

2013

To my beloved family

ACKNOWLEDGMENTS

First of all, I would like to thank Allah for giving me the strength and dedication to come to the point where I am right now. Alhamdulillah! Praise be to Allah, who had guided me to this felicity, never could I have found guidance, had it not been for the guidance of Allah.

Then I would like to give special thanks to my patient and encouraging research advisor, Dr. Weihong Tan. He was truly supportive and always there for me when I need him. He was the one, who showed me the path going to success with his wisdom and huge experience in both academic and daily life. I would like to thank him for accepting me in his group and for the opportunities he offered.

Also I would like to thank my committee members; Dr. W. David Wei, Dr. Rebecca A. Butcher, Dr. Ben Smith, Dr. Valentin Craciun and Dr. Gregory Schultz for their precious inputs that ease the progress of my research.

I don’t know how I can show my gratitude to the ones, who brought me to this earth; I always felt their prayers from overseas, my beloved family. I hope you will be proud of me and I know this is nothing compared to the things you offered to me until this age, but please take this accomplishment as a fruit of the tree you have been taking care of for all these years.

I would like to thank the warm family of Tan Group Members as well. I would like to especially thank Dr. Kwame Sefah, Dr. Basri Gulbakan, Dr. Mohammed Ibrahim Shukoor, Dr. Elizabeth Jimenez, Dr. Suwussa Bamrungsap for their trainings and unconditional helps during my research. I also would like to thank Ismail Ocsoy, Huseyin Erdal, Sena Cansiz, Tao Chen, Da Han, Chunmei Li (a visiting scholar), Inci

Barut (a visiting scholar), Liping Qiu, Diane Turek, Cheng Cui, Denisse Janvier (My K12 student), Cuichen Sam Wu for their sincere friendship and support.

I also would like to thank to my former and current roommates; Berik Uzakbaiuly, Serdar Yedier, Ismail Hakki Sahin since they make the life more joyful all these years in Gainesville.

TABLE OF CONTENTS

page

LIST OF FIGURES

LIST OF ABBREVIATIONS

AMA	Ammonium hydroxide methylamine
AuNC	Gold nanocage
AuNP	Gold nanoparticle
AuNR	Gold nanorod
AuNS	Gold nanoshell
BSA	Bovine Serum Albumin
CELL-SELEX	Cell-Systematic Evolution of Ligands by EXponential enrichment
CTAB	Cetyltrimethylammonium bromide
DDA	Discrete Dipole Approximation
EGF	Epidermal growth factor
FBS	Fetal bovine serum
FITC	Fluorescein isothiocyanate
Hb	Hemoglobin
HPLC	High pressure liquid chromatography
LDI	Laser desorption ionization
MS	Mass spectrometry
NIR	Near-infrared
PAI	Photoacoustic imaging
PBS	Phosphate buffered saline
PCR	Polymerase chain reaction
PDGF	Platelet-derived growth factor
PEG	Polyethylene glycol
PI	Propidium iodide
PSS	Polystyrene sulfonate

PTK7	Protein tyrosine kinase-7
SDS-PAGE	Sodium dodecyl sulfate polyacrylamide gel electrophoresis
SMS	Silver microsphere
SPR	Surface plasmon resonance
TEM	Transmission electron microscopy

Abstract of Dissertation Presented to the Graduate School
of the University of Florida in Partial Fulfillment of the
Requirements for the Degree of Doctor of Philosophy

APTAMER FUNCTIONALIZED NOBLE METAL PARTICLES FOR BIOANALYTICAL AND BIOMEDICAL APPLICATIONS

By

Emir Yasun

December 2013

Chair: Weihong Tan
Major: Chemistry

Noble metal particles, especially gold (Au) and silver (Ag) have been exploited in a broad range of biological applications due to their unique intrinsic features that depend on their physical appearance or optoelectronic properties, which can be tuned with the change in the size or shape of those particles. Thus, this tunability enables gold nanoparticles (AuNPs) to be used in biomedical diagnostic and therapeutical applications.

In photothermal therapy applications, nanomaterials, which can absorb efficiently in NIR region, are utilized since the healthy tissue or cells can't absorb at this spectral region. Among AuNPs, gold nanorods (AuNRs) are one of the best candidates for hyperthermia therapy of cancer cells with their high absorption cross-sections and tunable absorption maxima in NIR region. When this unique optical property is combined with the specificity against cancer cells utilized by aptamer conjugations, AuNRs become to be one of the most important nanoparticles employed in both cancer cell sensing and therapy. However, one drawback of AuNRs is having the surfactant CTAB on their surface, which can cause nonspecificity and cytotoxicity. In this research,

the side effects of CTAB are passivated by BSA modification, where the nonspecificity and cytotoxicity are dramatically decreased prior to the NIR treatment.

Recognition of changes in the rare cancer protein abundances can lead the early diagnosis of cancer, so capturing these low abundance proteins has a great significance. In this research, firstly, aptamer conjugated AuNRs were used to capture 1ng of α-thrombin effectively from plasma samples as model system. Then both aptamer conjugated AuNRs and silver microspheres (SMSs) are used to capture the biomarker proteins of a colon cancer cell line, DLD-1. Gold and silver surfaces can easily be modified through thiolate chemistry, compared to the tedious modification steps for the magnetic particles, so more aptamer immobilization can be achieved for AuNRs and SMSs, which can increase the possibility of binding to the target protein. Furthermore, SMSs offer a novel separation method, gravitational separation owing to their heavy nature. In this way, there is no need for an external stimuli to separate the captured proteins and protein isolation can take only seconds.

CHAPTER 1
BACKGROUND

Cancer Biomarkers

Cancer is a general name for a group of diseases in which abnormal cells grow out of control and spread. This abnormal cell proliferation can be induced by the alteration of certain proteins or, in other words, biomarkers, where the alteration can occur with the changes in expression levels, posttranslational modifications or with the genetic mutations.[1-5] Recognition of these changes can facilitate the early diagnosis, predicting the progression of cancer and lead to the targeted therapy strategies.

Most of the cancer-related proteins found are membrane associated proteins, since they can easily be accessible. For instance, vascular endothelial growth factor (VEGF), epidermal growth factor (EGF) and platelet-derived growth factor (PDGF) are commonly known membrane associated proteins and their abnormal activity can trigger cancer initiation and progression.[6-8]

In the recent studies, even though it is estimated that the membrane proteins constitute the 30% of the overall cell proteins, only less than 5% of this total is recognized by 2D-Gel electrophoresis and MS techniques.[9] There are various reasons for this limited success. The limitation is generally due to the lack of robust, sensitive and specific capturing probes.[2] Being robust basically refers to the stability of the probe and its binding efficiency to the target protein. Sensitivity refers to the capability of the enrichment of these proteins present in attomole or zeptomole amounts in biological fluids.[3] Early studies showed that these amounts can be in the concentration range of 1-10 ng/mL in plasma.[10,11] Specificity is another necessity, since these low abundance proteins should be specifically captured among plasma proteins vary over at least 12

orders magnitude.[1,10] Therefore, it is still a challenge to identify specific protein markers associated with the corresponding cancer type. In order to target the specific protein, antibody conjugated magnetic beads have been used to isolate membrane proteins using whole cellular lysates, but the major problem with antibodies is the difficulty in generating cell specific antibodies.[12,13] Thus, cell-Systematic Evolution of Ligands by EXponential enrichment (cell-SELEX) method provides an opportunity to generate probes that are called as aptamers to bind to their target cancer cells with high specificities and affinities.[14,15] Generation of aptamers for various cancer types will definitely ease and diversify the diagnostic, therapeutic applications as well as the cancer biomarker discovery studies.

Aptamers

Aptamers are single-stranded oligonucleotides (DNA or RNA) that bind to their specific target molecules, such as small bio-molecules and proteins, with affinities equal to those of antibodies. They are generally shorter than 100 bases. They have certain tertiary structures, which allow them to bind to their target molecules specifically through Van der Waals, hydrogen bonding or electrostatic interactions.[16,17] Aptamers have been generated by repeated rounds of in vitro selection with the method called Systematic Evolution of Ligands by EXponential enrichment (SELEX). Also this method is further applied for cells to find cell specific aptamers, so the new method is called as cell-SELEX. The aptamers generated with cell-SELEX can specifically bind to the biomarkers expressed by targeted tumor cells.

Characteristics of Aptamers

Compared to other affinity tags, aptamers have many advantages, including small size, nontoxicity, relatively easy preparation and functionalization with no batch-to-batch

variations and easy surface immobilization via their functional groups.[15,18-21] Thus, they can be easily functionalized simultaneously with attaching groups and fluorescent dyes (fluorophores) to be tethered on the surface of a scaffold nanoparticle for both targeting and imaging purposes.

Cell-SELEX

In the selection process, target cells are incubated with a random unselected library of DNA with 10^{15} distinct sequences. Then the unbound sequences are washed off and bound sequences are eluted by heating the cells at 95°C. The collected sequences are then incubated with the control cell lines to remove the sequences that bind to the common biomarkers on the cell membrane. After gathering the pool of sequences that only bind to the target cell line, they are amplified with PCR and used for subsequent rounds of selection. This round is iterated until the pool is fully enriched for the target. Finally, the enriched pool is sequenced and the sequences of the possible aptamers are identified by looking at resembling sequences.

Applications of Gold Nanorods in Cancer Cell Sensing and Therapy

Through the developments in controlling the shape of gold nanoparticles (AuNPs), synthesis of gold nanorods (AuNRs) can be considered as a milestone discovery in the area of nanomaterial based cancer treatments. Besides having tunable absorption maxima at near infrared (NIR) range, AuNRs have superior absorption cross section at NIR frequencies compared to other gold nanoparticles. When this unique optical property is combined with the specificity against cancer cells utilized by affinity tag conjugations, AuNRs become to be one of the most important nanoparticles employed in both cancer cell sensing and therapy. In this section, the impact of the size and shape

control of the AuNPs, especially AuNRs, on cancer cell treatments and a range of aptamer conjugated AuNR applications are discussed.

The Importance of Size and Shape Control of Gold Nanoparticles

Gold nanoparticles (AuNPs) have been extensively used in biomedical applications due to their biocompatibility, facile synthesis, easy surface functionalization and tunable physical properties.[22-24] Their sizes and shapes can be varied for a particular biological application such as labeling, delivering, heating and sensing.[23,25] Sizes of AuNPs depend on the nature of the reducing agent that reduces the gold precursor and the molar ratio of the reducing agent or stabilizer to gold precursor used in the synthesis route.[26,27] Different shapes of AuNPs can generally be synthesized either by using rigid templates such as porous alumina, polycarbonate membranes and carbon nanotubes or surfactants as soft templates.[27-34] Surfactants, which are also known as capping agents interact with different growing faces of the nanoparticles to confine their shape, whereas rigid templates act as a mold to constrain the area of the metal precursor reduction.[35] For the shape control of nanoparticles, using surfactants eliminates the tedious steps of rigid template preparation and dissolving the rigid template contents to release the prepared nanoparticles at the very end. The change in the size and shape of AuNPs affects their absorption maxima that can vary in vis-NIR range. Color of the nanoparticles also changes depending on the absorption maxima variations. This tunability of the optical absorption facilitates various biomedical applications including, but not limited to, colorimetric detection assays for proteins[36-39], DNAs[39-42] and cancer cells[43] that operate in vis range; photothermal therapy[44-49], photoacoustic imaging[50-55] and heat-induced drug delivery[56] that operate in NIR range.

Tuning the SPR band of plasmonic nanoparticles to NIR range

Nanoparticles that have significant absorption in the tissue optical window (600-1300 nm), which is also known as NIR, are promising sensing and therapeutical agents for cancer cell treatments, since healthy tissue doesn't absorb at this spectral region.[57] Moreover, in longer wavelengths the scattering of the light is minimized. Thus, the combination of the minimal scattering and NIR absorption allow deep tissue penetration.[25,58,59] This penetration depth can be 1-10 cm depending on the tissue types.[59,60]

When AuNPs absorb light, the oscillating electromagnetic field of the light triggers the polarization of the conduction band electrons on the surface of the nanoparticles and the polarized electrons go through collective coherent oscillations with respect to the positive ions in the metallic lattice, these oscillations are called as surface plasmon oscillations (Figure 1-1). Since surface plasmon oscillation has the same frequency with the incident light, it is also known as surface plasmon resonance (SPR).[59]

SPR frequency highly depends on the size and shape of the nanoparticles as it was indicated before for the absorption maxima. For spherical AuNPs, there is only one SPR frequency, around 520 nm in the visible region, which is responsible for the intense red color of the spherical AuNPs. For the AuNRs, there are two SPR frequencies as known as longitudinal and transverse bands (Figure 1-1). Transverse band is for the electron oscillations that take place along the transverse direction (Figure 1-1) and it is a weak absorption band in the visible region similar to the SPR frequency of the spherical AuNPs. Longitudinal band is related to the electron oscillations along the longitudinal direction (Figure 1-1) and it is a strong absorption band in the vis-NIR region.[59,61]

The excited surface plasmon electrons relax in two different ways: they can either emit the light that has the same energy as the incident light, known as SPR scattering, or they can transfer the absorbed energy to the metallic lattice in the form of thermal energy. Subsequently, hot lattice cools down by phonon-phonon interactions and the heat is transferred to the surrounding medium.[25,59,61] This forms the basis of all plasmonic nanoparticle based photothermal therapy applications. Since the SPR band of nanoparticles contains both the scattering and absorption components, tuning the shapes and sizes of the nanoparticles can change their scattering and absorption properties dramatically.[62] For example, when the aspect ratio of the AuNRs increases, longitudinal band undergoes a red shift and while the scattering component increases, the absorption component of the longitudinal band decreases.[63] Therefore, for NIR imaging applications, larger AuNRs that have high scattering efficiency and for photothermal applications, smaller AuNRs that have high absorption efficiency can be preferred.

Comparison of the NIR-absorbing gold nanoparticles

The most commonly used NIR-absorbing AuNPs for cancer cell sensing and therapies are gold nanoshells (AuNSs), gold nanorods (AuNRs) and gold nanocages (AuNCs). Since scattering and absorption properties of those AuNPs determine their efficiency in cancer cell treatments, these properties were compared by Discrete Dipole Approximation (DDA) method after adjusting their structures to tune their SPR bands to 800 nm. In order to have the SPR band at 800 nm, AuNRs should have an aspect ratio of 3.6 with the width length of 20 nm, AuNSs should have a gold shell thickness of 3.2 nm with a silica core diameter of 50 nm and AuNCs should have an inner edge length of 50 nm with a wall thickness of 6 nm. According to the DDA results, the absorption and

scattering cross-sections for AuNRs and AuNCs are comparable to each other and they are much larger than those for the AuNSs.[58,62] The extinction cross-section coefficients of the AuNRs and AuNCs are more than 2 times larger than that of AuNSs. This huge absorption cross-section makes AuNRs and AuNCs good candidates as photothermal therapy agents.[62] For example, heating per gram of gold for AuNRs is at least six times faster than that for AuNSs.[64]

Besides their easily tunable structures for a particular cancer cell treatment, AuNRs should be further modified with affinity tags such as antibodies or aptamers to achieve specificity against cancer cells, while avoiding the interference with healthy cells.

Synthesis, Growth Mechanism and Surface Modification of Gold Nanorods

Besides the rigid template methods, AuNRs have been synthesized by many different surfactant based methods such as photochemical[65], electrochemical[66] reduction methods and seed-mediated[27,32-34,59] method. So far, seed-mediated method is the most efficient method to synthesize AuNRs. In this method, there are two steps: first step is the synthesis of the seed AuNPs and second step is the growth of these seeds into nanorods. Firstly, single crystalline, seed AuNPs in the sizes of less than 4 nm are prepared by the reduction of $HAuCl_4$ (auric acid) with ice cold $NaBH_4$ (sodium borohydride) in an aqueous CTAB (cetyl trimethylammonium bromide) solution. Secondly, the growth solution is prepared by introducing ascorbic acid, as a mild reducing agent, into an aqueous CTAB solution of $HAuCl_4$ and $AgNO_3$ (silver nitrate) to reduce Au^{3+} to Au^{1+}. When the seed solution is added to the growth solution, seed AuNPs can catalyze the reduction of the Au^{1+} to Au^0 on their surface by the present ascorbic acid. This leads the gold atoms to be added on the surface of the seed

nanoparticles, resulting in the growth of the nanorods. The role of the CTAB is to be the shape templating surfactant. There are numerous hypotheses about the templating mechanism of CTAB in the rod formation. In one of them, it is believed that CTAB is preferentially bound onto (110) or (100) faces of gold and it leaves the (111) face for the gold atom addition that results in the nanorod growth along the (100).[67] In the other mechanism, after the ascorbic acid reduction of auric acid in the growth solution, $AuCl_2$ binds to CTAB to form the $AuCl_2$-CTAB complex. This complex binds to the tip of the seed AuNPs in a faster rate than to side faces, so that it leads to nanorod growth.[68] The addition of silver nitrate to the CTAB solution results in the immediate formation of AgBr. It has been claimed that Ag^+ ions adsorb onto the surfaces of AuNPs in the form of AgBr and Ag^+ is reduced to Ag atoms on the side (110) face of the nanorods in a faster rate than on the (111) end face. This avoids the gold addition to the side faces and thus results in nanorod growth. The aspect ratio of the AuNRs can easily be tuned by either varying the amount of seed solution or the amount of silver nitrate that are added to the growth solution.

Besides their unique optical properties, in order for AuNRs to show their efficacy in cancer cell treatments, their surfaces should be modified to further stabilize them in biological fluids and to allow targeted cancer treatments.

CTAB coating on the surface of AuNRs provides the stability in their aqueous solutions, but it was proven that in biological fluids such as serum, CTAB capped AuNRs can easily be precipitated. In order to avoid the precipitation and increase the circulation times of AuNRs in vivo, their surfaces are modified with polyethylene glycol (PEG).[64] After the PEG modification, AuNRs exhibited a circulation time of 17 hours and

they maintained their longitudinal SPR band during this circulation time.[64] PEG protection can also decrease the nonspecific binding to the surfaces of AuNRs.[5,69,70] In order to PEGylate the surface of AuNRs, thiol [48] modified PEGs are used to form covalent bonds between the sulfhydryl groups of PEG and the gold surface, which are also known as thiolate bonds.

Specificity against the cancer cells can be achieved by tethering the affinity tags such as antibodies or aptamers on the AuNR surface for sensing and therapy applications. Antibodies can be adsorbed onto AuNR surface by the hydrophobic interactions with the polymer, polystyrene sulfonate (PSS) that is previously adsorbed on the AuNR surfaces through electrostatic interactions.[45] Surface of the CTAB-capped AuNRs are positively charged, so the negatively charged PSS polymer can easily be adsorbed on the surface of AuNR via electrostatic interactions, followed by the adsorption of antibodies through the hydrophobic interactions with the PSS polymer.

As another affinity tag, aptamers are single-stranded oligonucleotides that bind to their specific target molecules, such as small bio-molecules and proteins, with affinities equal to those of antibodies. As it was discussed before, aptamers can easily be modified with attaching groups in the synthesis process, such as sulfhydryl [48] and amine ($-NH_2$) groups. So sulfhydryl [48] modified aptamers can be tethered to the surface of AuNRs through thiolate bonds. On the other hand, aptamers can be functionalized with attaching and signaling groups (fluorescence, electrochemical and etc.) simultaneously, so they can be used for both targeting and sensing purposes.

Cancer Cell Sensing with Affinity Tag-Conjugated Gold Nanorods

Affinity tag conjugated AuNRs make use of fluorescence, light scattering and photoacoustic imaging techniques in order to sense the cancer cells. AuNRs are

particularly preferred in these methods for follow up in hyperthermia therapy of cancer cells. Fluorescence is provided by the fluorophore modified affinity tags that are attached to the AuNR surface. Light scattering and photoacoustic imaging are due to the intrinsic properties of gold nanorods.

Fluorescence imaging of cancer cells

Molecular recognition on specific cell surfaces plays a key role for diagnosis and therapy of cancer cells. The affinity tags responsible for molecular recognition in cancer cells, such as aptamers and antibodies can sometimes have weak binding strengths towards their molecular target, which is also known as biomarker, on cancer cells. This can diminish the signaling and binding affinity towards those targets. Therefore, instead of using single aptamers for molecular recognition, multiple aptamers can be conjugated on a scaffold nanoparticle to generate a multivalent binding platform, which can enhance the signaling and increase the possibility of binding. AuNRs are good scaffold candidates for the multiple aptamers to conjugate, since they can be used as photothermal therapeutic agents following the detection of cancer cells. Yu Fen *et al.* showed that by using the fluorescein (FITC)-labeled multiple aptamers conjugated to AuNRs, the fluorescence intensity coming from the cell surface is enhanced more than 300 folds compared with those obtained from individual aptamers according to the flow cytometric measurements.[70] In this fluorescence signal amplification experiment, the KK1HO8 aptamer that has a weak binding affinity (K_d ~296 ± 41 nM) towards K-562 cancer cells was chosen (Figure 1-2). Thus, multiple aptamer conjugated AuNRs can be a remedy for the cases of cancer cells having low expression levels of biomarkers on the cell membrane as binding sites or having aptamers with weak binding affinities toward their binding sites on the cell membrane.

Light scattering imaging of cancer cells

As it was discussed before, AuNRs can also be used as scattering contrast agents in dark field imaging. Xiaohua Huang et al. used anti-epidermal growth factor receptor (anti-EGFR) monoclonal antibodies conjugated AuNRs to target two malignant oral epithelial cell lines (HSC and HOC) and a nonmalignant epithelial cell line (HaCat) is chosen as a control.[45] Since EGFR is over-expressed on the cytoplasmic membrane of the malignant cells, the antibody conjugated AuNRs can bind to the malignant cell lines in a higher affinity compared to the nonmalignant cell line. After the incubation with each cell line for 30 min at room temperature, the excess AuNRs are washed off. AuNRs that bound to the malignant cell lines strongly scatter orange to red light detected by dark-field microcsopy due to their strong longitudinal surface plasmon oscillation in NIR region (Figure 1-3). This type of strong scattering can easily be distinguishable compared to those from the nonmalignant cell line. Since nonmalignant cell line also shows scattering as a background, in order to quantify the bound AuNRs on each cell type, absorption spectra of the cell samples incubated with antibody-conjugated AuNRs are taken and the longitudinal band intensities of AuNRs are compared. The absorption intensities for the malignant cell line samples are two times higher than that for the nonmalignant cell line. However, this is not a fair comparison of the EGFR expression levels for the malignant and nonmalignant cell lines, since some of the AuNRs bind to nonmalignant cell lines via nonspecific interactions, possibly caused by the hydrophobic interactions between the PSS on the AuNRs surface and cell membrane. In spite of this nonspecific binding, the cancer cell lines can still easily be distinguished from the noncancerous cells by the highly efficient scattering properties of AuNRs in NIR region.

Photoacoustic imaging of cancer cells

The basic principle of the photoacoustic imaging [52] is the detection of the sonic waves generated by the thermo-elastic expansion of the heated tissue by a laser treatment (Figure 1-4).[71] The sonic waves are detected by the ultrasonic transducers and converted to electrical signals, followed by processing those electrical signals to form an image.

PAI makes use of the high optical contrast of the biological tissues. For example, because of the high optical absorption of hemoglobin (Hb), PAI can image blood vessels successfully.[58] Some in vivo studies showed that the ratio between the optical absorption contrasts of normal and tumor tissues in the breast can be as high as 1:3 in NIR region due to the extremely increased vascularity in the tumors.[72-74] Therefore, in contrary to the light scattering imaging, PAI requires the contrast agents to have high optical absorption. Owing to their large absorption cross-sections in NIR region, AuNRs are good contrast agent candidates for PAI. The principal of the PAI is very similar to the one for photothermal therapy, since heating of the target is involved in both, so it is highly possible to combine these two modalities.[58]

Since nanoparticle based, targeted PAI of cancer is still rather a new technique, there are not so many examples to represent its potentials, especially for the ones, where aptamers are used as affinity tags. The in vivo PAI of human prostate cancer is achieved by antibody conjugated AuNRs.[53] In this study, antibody conjugated AuNRs are designed to have an absorption band in the range of 700-840 nm to be optimal in vivo applications and a single layer of cells is monitored by PAI. In another in vivo study, AuNRs in different aspect ratios are conjugated to antibodies to specifically target human epidermal growth factor receptor 2 (HER2) and EGFR, which are over-

expressed in OECMI and Cal 27 oral cancer cell lines, respectively. The aspect ratios of the AuNRs that are conjugated to HER2 or EGFR antibodies are tuned to have SPR bands of 785 nm and 1000 nm, respectively. These two probes are used to target HER2 or EGFR on both oral cancer cell lines, in vivo and in vitro, while switching the irradiation wavelength to either 800 nm or 1064nm for PAI. By matching the irradiation wavelength with the SPR bands of the probes, the corresponding molecular targets for the oral cancer cell lines are successfully monitored by PAI. Even though both probes were not used in the same mice to detect the molecular signatures for the two different cells, by only switching the irradiation wavelength, this work can open new avenues for multiple biomarker detection on cancer cells or for determining heterogeneous population of cancer cells in a lesion.[75]

Cancer Cell Therapy with Aptamer-Conjugated Gold Nanorods

There are mainly two methods of administering cancer cell therapy via plasmonic nanoparticles. The first one being photothermal therapy via the heat generation induced by the relaxation of the excited surface plasmon electrons, and the second one being the heat-induced drug delivery to cancer cells.

Photothermal therapy of cancer cells

Cells are highly sensitive to temperature variations, and temperatures above 42°C can result in cell death. Hyperthermia is an anti-cancer therapy that aims to increase the temperature of the cancer cells above normal levels to cause cell death. Excessive heating can induce the denaturation of proteins or the disruption of organized biomolecular assemblies in the nucleus and cytoskeleton of the cells.

In photothermal therapy, NIR lasers are involved for deep tissue penetration and thermal treatment of tumors. This type of therapy requires specificity against cancer

cells, in order not to be destructive for the healthy cells and it also requires sufficient heat generation to kill the targeted cancer cell. Aptamer conjugated AuNRs can satisfy both of these requirements with the specificity provided by the aptamers and efficient heat generation provided by the AuNRs.

Yu Fen et al. from Tan lab used aptamer-conjugated AuNRs for selective photothermal therapy in a suspension cell mixture[47] (Figure 1-5). In this study, two cancer cell lines are chosen for the cell mixture, CCRF-CEM cell line is chosen as a target and NB-4 cell line is used as a control cell line. The chosen sgc8c aptamer can bind to the membrane protein of CCRF-CEM cell line, but it can't bind to any molecular signature on NB-4 cell line. Also random DNA library is chosen to serve as a control indicating the specificity against CCRF-CEM is only because of the sgc8c aptamer. After the sgc8c aptamer and random DNA library are immobilized on the surface of AuNRs, the two cell lines are incubated with the AuNR conjugates separately. Followed by washing off the unbound AuNR conjugates from the cell solutions, the samples are exposed to a laser light of 808 nm at 600 mW for 5 minutes. Cell death is determined by PI dye staining and monitored by flow cytometry. While CEM cells that labeled with sgc8c aptamer conjugated AuNRs show a cell death percentage of 93 (±11), the percentage of dead cells before and after the laser irradiation remains the same for NB-4 cell line (Figure 1-6). Also the percentage of dead cells before and after illumination for the CEM cells incubated with random DNA library conjugated AuNRs remains almost the same (2% change) as well. These show the high selectivity of aptamer conjugated AuNRs against their target cells. Eventually, aptamer conjugated AuNRs are incubated with a suspension cell mixture of NB-4 and CCRF-CEM cell lines. After the

NIR laser irradiation, 50 (±1)% of target (CEM) cells are damaged, while 87 (±1)% of control (NB-4) cells remain intact. These are promising results for the future in vivo photothermal therapeutic applications, since it is demonstrated that aptamer-conjugated AuNRs are highly selective against the targeted cancer cells and are able to efficiently destroy the targeted cancer cells with minimal damage to the surrounding cells.

Heat induced drug delivery to cancer cells

Even though AuNPs can be efficient photothermal agents by tuning their sizes and shapes, their nonporous nanostructures exhibit low loading capacities for an effective drug or gene delivery to cancer cells. In order to solve this, Kang et al. engineered a drug delivery platform based on AuNRs coated with DNA cross-linked polymeric shells[56] (Figure 1-7). In this design, acrydite modified DNA (strand 1) is polymerized on AuNR surface through copolymerization reactions. Also another acrydite modified DNA (strand 2) is polymerized together with acrydite modified sgc8c aptamer separately. These two polymerized structures are then linked to each other by a linker DNA that is partially complimentary to each strand 1 and strand 2 to form a polymeric shell on AuNR. During this AuNR based nanogel formation, an anti-cancer drug, Dox is introduced to be encapsulated in the gel. The basic principle of the drug release in this system is the gel-to-sol transition of the gel layer on the AuNR surface caused by the elevated temperatures upon the NIR irradiation, in which the encapsulated Dox can be released. This transition depends on the melting temperatures of the linker DNA and the two complementary DNA segments (strand 1 and strand 2). In this case the melting temperature is in the range of 35-41°C, but it can be easily tuned by changing the number of hybridized base pairs in the linkage. According to the flow cytometry tests,

even though acrydite modified sgc8c aptamers undergo a polymerization reaction, they can still specifically bind to their target cells (CCRF-CEM).

Finally, the drug release of this system is tested by incubation of the target (CCRF-CEM) and control (RAMOS) cells with the Dox loaded AuNR based nanogels-sgc8c, followed by exposure to the laser (808 nm at 600 mW). Increasing the irradiation time up to 10 min results in the cell death percentage of 67(±5%) for CEM cells, while the percentage of dead cells remained almost the same (less than 10% change) for RAMOS cells. Also the same experiment is done with the AuNR based nanogels-sgc8c without any Dox loading, but the cell death percentage remains almost the same (less than 8% change) for CEM cells. This can indicate that there is minimal contribution from photothermal effect of AuNRs, but the cell damage is mainly due to the drug delivery. This study can be inspiring for in vivo applications, where the targeted and controlled drug delivery is a big challenge due to the side effects of the drugs. This system shows that combining the unique features of aptamers and nanoparticles can be a solution for the challenges encountered in real biological applications.

Overall Look At the Cancer Treatments of Gold Nanorods

Simple changes to the size and shape of AuNPs can give rise to a variety of biomedical applications, since those changes also affect their optical/electronic properties. As it was discussed in this chapter, by tuning the aspect ratio of AuNRs, their optoelectronic properties can be changed to apply for the desired cancer treatment. However, intrinsic properties of AuNPs are not sufficient to solve the challenges encountered in cancer cell treatments, since without targeting the specific cancer cells, these unique properties can be only left to bench tops. Thus, aptamers as targeting tags have an important role in cancer treatments. Currently, not all of the

cancer types have their own aptamers, but by time more aptamers will definitely be selected, which can increase the diversity of the cancer treatments.

Moreover, despite the superior properties of AuNRs, there is also a drawback due to the presence of CTAB on their surface, which is a highly cytotoxic polymer in their higher concentrations. Since the CTAB content on the surface of AuNRs can vary from batch to batch variations and high concentrations of AuNRs can be required according to the treatment (especially in vivo), the side effects of CTAB should be minimized for optimal results.

Silver Microsphere as a Novel Separation Platform

In contrary to other particles that can be isolated by centrifugation or application of a magnetic field, silver microspheres offer a novel separation method, gravitational separation.[76-78] They can easily go down by the gravity in their solutions due to their heavy nature. Thus, there is no need for an external stimulus. Also the synthesis route is fairly easy as well. Silver nitrate is used as the silver precursor and hydroxylamine is used as a reducing agent to reduce silver cations. The formation of the particles takes a few minutes. Also surfactants as templating agents are not used in the synthesis of silver microshperes. So the surface of the silver microsphere is very clean without surfactants and it can accommodate more functional groups on its surface. The surface modification can easily be achieved through thiolate chemistry. Recently, they have been used in DNA separations.[76-78] The target DNA is hybridized with the complementary DNAs on the surface of the silver microspheres and they can be separated easily by earth gravity. As a result, silver microspheres offer a rapid, low cost, high yield synthesis route with a novel separation method.

Overview of the Dissertation

In this dissertation, the intrinsic properties of gold nanorods and silver microshperes as noble metal particles are combined with the specificity provided by the aptamer conjugations to be utilized in cancer therapy and biomarker discoveries. However, the combination of these two is not always enough to achieve the desired goal, so also the surface of those particles are further modified to obtain improved results.

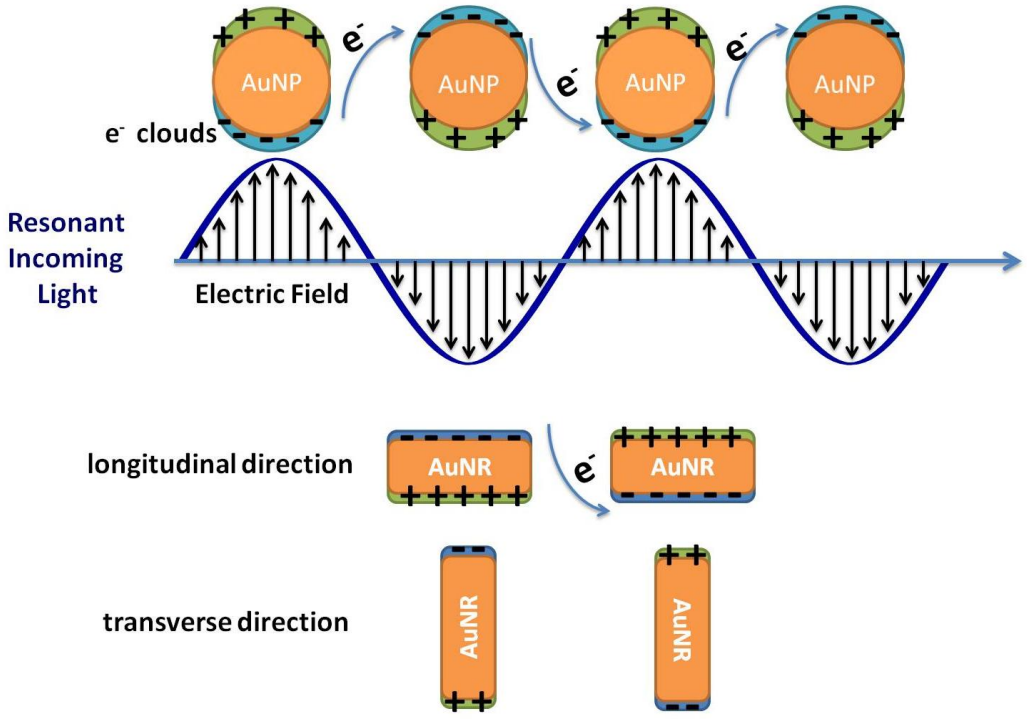

Figure 1-1. Surface Plasmon oscillations in spherical gold nanoparticles (AuNPs) and gold nanorods (AuNRs).

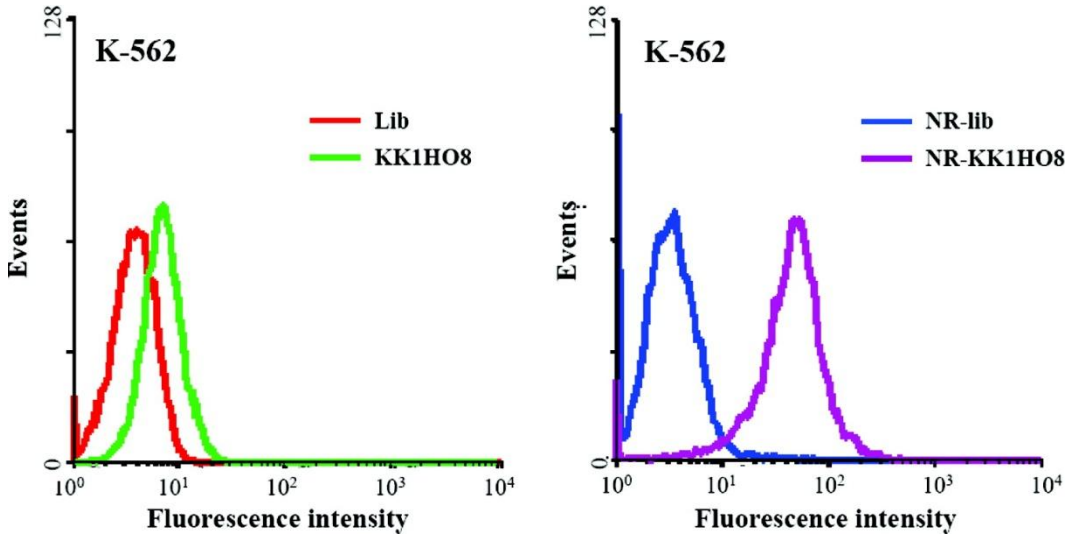

Figure 1-2. Binding assay of KK1HO8 (50 nM) and NR-KK1HO8 conjugates (1.88 nM) toward K-562 cells. The red and blue curves in the flow cytometric assay represent the background binding of unselected DNA library (lib) and NR-conjugated library (NR-lib), respectively. There was an increase in binding capacity of the NR-KK1HO8 conjugates (purple curve), whereas there was only a slight change for free KK1HO8 (green curve) with K-562 cells. Adapted with permission from Ref (70). Copyright © 2008 American Chemical Society

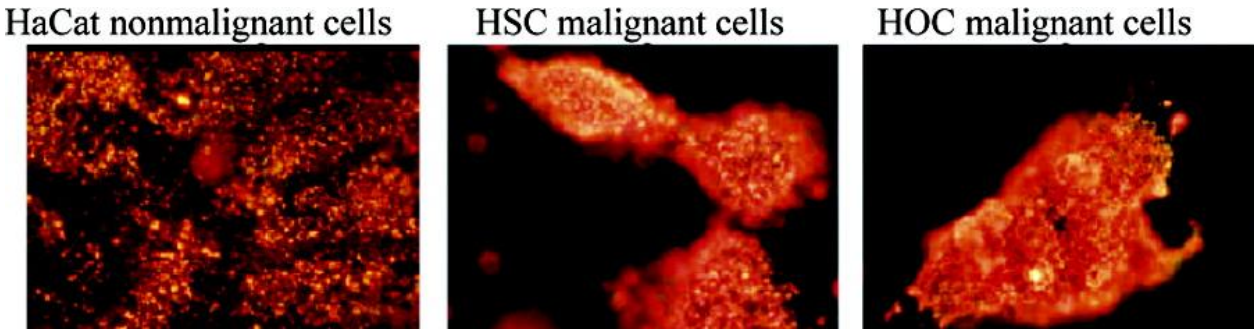

Figure 1-3. Light scattering images of anti-EGFR/Au nanorods after incubation with cells for 30 min at room temperature. Reproduced with permission from Ref (45). Copyright © 2006 American Chemical Society

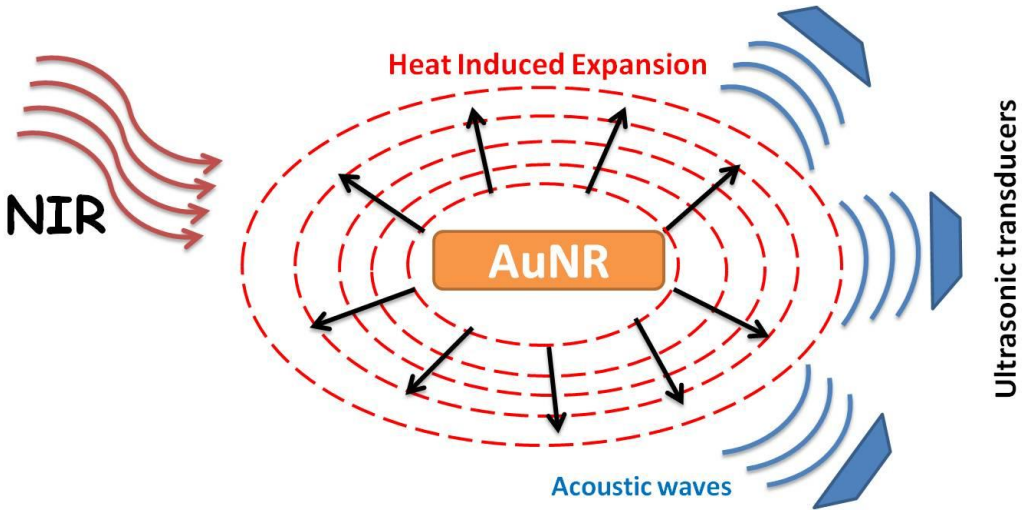

Figure 1-4. Photoacoustic imaging mechanism

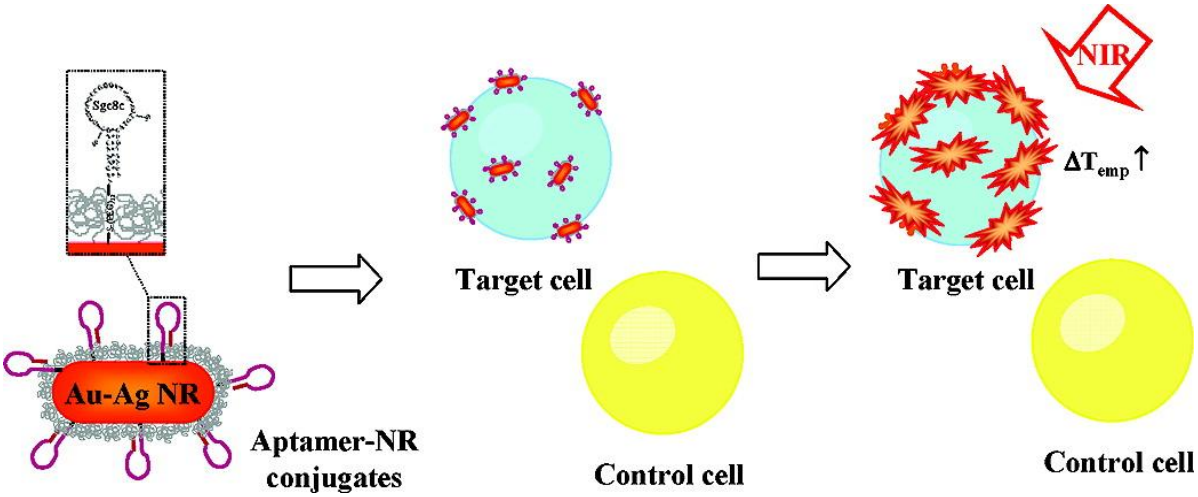

Figure 1-5. Selective Photothermal Therapy of Cancer Cells by Aptamer-conjugated AuNRs. Adapted with permission from Ref (47). Copyright © 2008 American Chemical Society

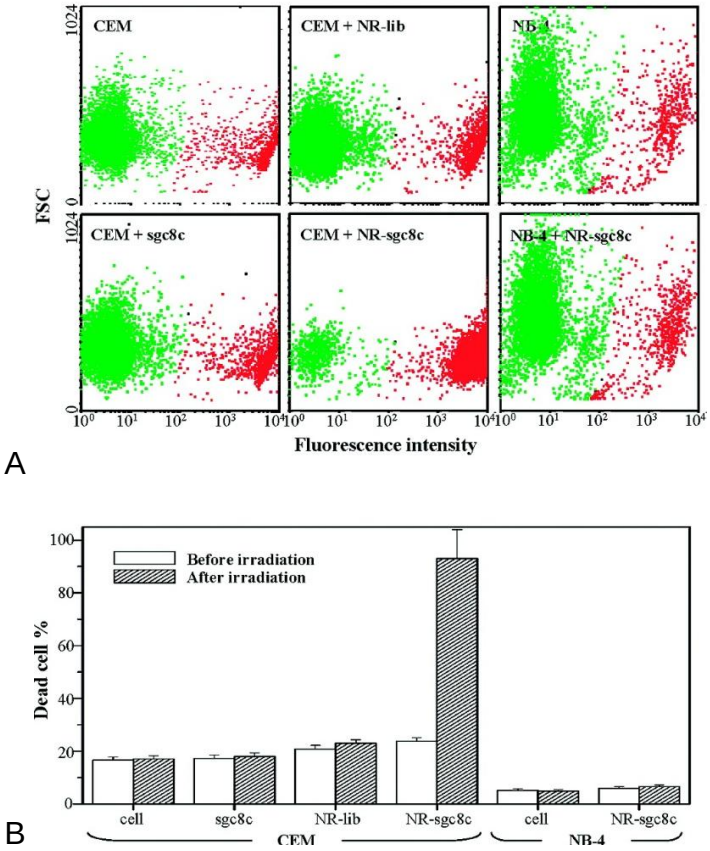

Figure 1-6. Live and dead cells analysis of with or without NR-aptamer treated cells. A) Flow cytometric comparison between live and dead cell populations of CCRF-CEM cells (target cells) and NB-4 cells (control cells) without NRs and those labeled with sgc8c (50 nM), NR-lib (0.25 nM), and NR-sgc8c (0.25 nM). A total of 10 μL of the cell suspensions is irradiated with NIR light (808 nm) at 600 mW for 5 min. Dead cells are then stained with PI dye, diluted in buffer, and determined by flow cytometry. B) Bar chart demonstrating the dead cell percentages of CCRF-CEM cells (target cells) and NB-4 cells (control cells) in all experimental conditions before and after NIR irradiation. Reproduced with permission from Ref (47). Copyright © 2008 American Chemical Society

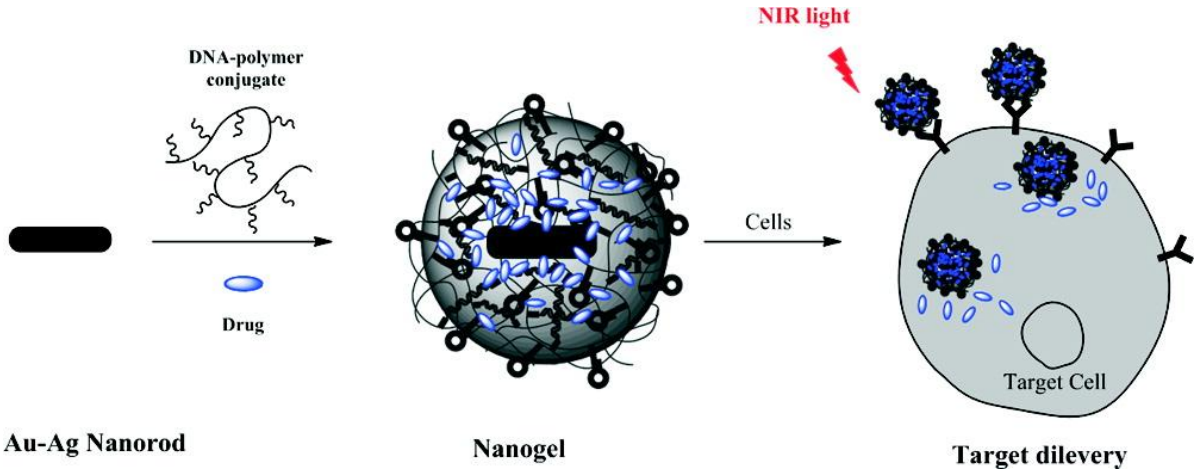

Figure 1-7. NIR responsive drug delivery platform based on AuNRs coated with DNA cross-linked polymeric shells. Adapted with permission from Ref (56). Copyright © 2011 American Chemical Society

CHAPTER 2
APTAMER CONJUGATED BSA MODIFIED GOLD NANORODS AS HIGHLY SELECTIVE PHOTOTHERMAL THERAPY AGENTS WITH NEGLIGIBLE CYTOTOXICITY

Introduction

The emergence of gold nanorods (AuNRs) has attracted lots of attention with their high absorption cross-sections and tunable absorption maxima in NIR region.[79] For instance, the extinction cross-section coefficients of the AuNRs are more than 2 times larger than those of gold nanoshells (AuNSs)[62], which are the first examples of AuNPs that can absorb in NIR region. The large absorption cross-sections in NIR region facilitate the efficient energy absorption in NIR and so the efficient conversion of this absorbed energy to thermal energy. Heating per gram of gold for AuNRs is at least six times faster than that for AuNSs.[64] Therefore, AuNRs are indeed good candidates as photothermal therapy agents. Gold nanorods own these exclusive properties to their unique shape, which is confined by the surfactant, cetyltrimethylammonium bromide (CTAB) that is present as a double layer on the surface of AuNRs.[67,68,80] Besides confining the shape, cationic CTAB can also stabilize AuNRs in their colloidal dispersions.[81] Despite these beneficial roles, CTAB can also cause some side effects when its concentration is increased in cell experiments. It has been demonstrated that, CTAB can be toxic to many types of cells.[82-86] It is also reported that both the released monomers and the double layer structure of CTAB can cause cytotoxic effects on the treated cells.[82,83,85,87] Moreover, since CTAB is positively charged, it can cause some nonspecific binding as well through the electrostatic interactions with the negatively charged cell surface.[81]

There are various reported strategies to reduce the cytotoxic effects of CTAB. One of the strategies is to coat the CTAB bilayer with polyelectrolytes such as polystyrene sulfonate (PSS) through electrostatic interactions.[82,85] In this way, the bilayer structure of CTAB is encapsulated and can't interact with the cell membrane. Another strategy is to avoid the release of CTAB monomers by fixing them via polymerization.[88] Also thiol terminated ligands can replace the CTAB from the surface of the gold nanorods and reduce cytotoxicity.[86]

In this work, CTAB on the surface of gold nanorods was passivated by the BSA (Bovine Serum Albumin) protein coating of the gold nanorod surface where the interactions between the cell surface and CTAB were blocked. It was reported that serum proteins can interact with CTAB through electrostatic interactions.[82] So positively charged CTAB can easily interact with the negatively charged BSA. This allows BSA to form a layer on CTAB. Albumin is the most abundant protein in human plasma. Therefore, it is better to use a natural molecule without any immunogenicity to encapsulate CTAB instead of using polyelectrolytes.

Materials and Methods

Cell Culturing

CCRF-CEM (CCL-119 T-cell, human acute lymphoblastic leukemia) as target cells and Ramos (CRL-1596, B-cell line, human Burkitt's lymphoma) as control cells were cultured at 37 °C under a 5% CO_2 atmosphere. The cell culture medium consists of RPMI 1640 medium (American Type Culture Collection), 10% heat inactivated fetal bovine serum (FBS, Invitrogen, Carlsbad, USA) and penicillin-streptomycin (100 IU/mL, GIBCO).

Preparation of AuNR Seed Solution

Five mL 0.2 M CTAB solution and 5 mL 0.5 mM $NaAuCl_4$ solution were mixed in a 50 mL plastic tube, and then 0.6 mL 0.01 M freshly prepared $NaBH_4$ was added. Following sonication for 3 min, the mixture turned brownish-yellow. This reaction mixture was protected from the light with aluminum foil and placed in a water bath at 25˚C for 1 h.

Preparation of AuNR Growth Solution

Fifty mL 0.2 M CTAB solution and 50 mL 1 mM $NaAuCl_4$ solution were mixed in a 100 mL glass bottle. Then 3.00 mL or 2.50 mL 0.004 M $AgNO_3$ (60 or 50 µM Ag^+ as the total concentration) was added to this mixture, followed by 0.7 mL 0.0788 M ascorbic acid. After addition of ascorbic acid, the color of the solution changed from dark yellow to colorless. Then 0.12 mL of the seed solution was added, and the overall mixture was protected from the light with aluminum foil. Finally, the reaction mixture was placed in a water bath at 25˚C for 1 h. The solution changed to dark pink within 30 min.

Synthesis of AuNRs

Forty mL 0.5 M Glycine (adjusted pH 8.0) was prepared in a 200 mL glass bottle, and 60 mL DI water was added, followed by 100 mL of the growth solution. The reaction mixture was protected from light with aluminum foil and was placed in a water bath at 25˚C for 12 h.

Removing Excess CTAB from AuNRs

Aliquots (25 mL) of nanorod solution were added to centrifuge tubes and were centrifuged at 14000 rpm for 8 min. For each fraction, 22.5 mL of the supernatant was removed and replaced with 22.5 mL DI water. The solutions were again centrifuged at 14000 rpm at 25°C for 5 min. Then 22.5 mL of the supernatant was removed from each

fraction and replaced with 22.5 mL 0.5 mM CTAB solution. The centrifugation step was repeated with the CTAB solution twice at the same speed and temperature for each fraction, and, finally, 2.5 mL of the solution was collected from each fraction.

Characterization of AuNRs

After removing excess CTAB, all fractions were combined to have approximately 10 times concentrated gold nanorod solution. Then this nanorod solution was diluted 1:20, and the UV/Vis spectrum was taken using a Cary Bio-300 (Varian, Walnut Creek, CA) to find its concentration. Two characteristic absorbance peaks were obtained as transverse band and longitudinal band. TEM images of gold nanorods were obtained with a JEOL TEM 2010F transmission electron microscope on a copper grid. The sizes of gold nanorods prepared with 50 µM of silver cation were calculated as 52 ± 4 nm and 14 ± 1 nm in length and width, respectively. The sizes of the ones prepared with 60 µM of silver cation were calculated as 70 ± 9 nm and 14 ± 1 nm in length and width, respectively. The sizes were calculated with FemtoScan software.

Synthesis of Aptamer: sgc8c

The aptamer that was selected to target the CCRF-CEM cell line: sgc8c, 5`-ATC TAA CTG CTG CGC CGC CGG GAA AAT ACT GTA CGG TTA GA-3`. The selected aptamer was coupled with 5′-thiol modifier for conjugation to the gold nanorod surface and were labeled with fluorescein (FITC, FAM) at the 3′-end using 3′-(6-fluorescein) CPG to detect and quantify the aptamer modification on the gold nanorod surface. Also, two hexaethyloxy-glycol units (EG_6) were added between the thiol and sgc8c sequence as a spacer. The aptamer was synthesized by solid-state phosphoramidite chemistry at a 1-µmol scale using an ABI3400 DNA/RNA synthesizer (Applied Biosystems, Foster City, CA). The completed sequence was then deprotected in AMA (ammonium

hydroxide/40% aqueous methylamine 1:1) at 65 °C for 20 min and further purified using a ProStar HPLC (Varian, Walnut Creek, CA) with a C18 column (Econosil, 5 µm, 250×4.6 mm) from Alltech (Deerfield, IL). A Cary Bio-300 UV spectrometer (Varian, Walnut Creek, CA) was used to measure the absorbance to quantify the concentration of the product sequence.

Aptamer Immobilization to the Surface of AuNRs

Before aptamer immobilization, 0.1 mM 5` S-S tagged sgc8c was incubated with 5 mM TCEP in 50 mM Tris/HCl (pH=7.5) buffer for 1 hour at room temperature to reduce S-S to SH groups. Then a 100 µL sample of 1 nM gold nanorod solution was centrifuged at 14000 rpm at 25°C for 3 min. The supernatant was removed, and the precipitate was resuspended in 100 µL 2 mM CTAB. Then 0.1 nM gold nanorod was incubated with 0.1 mM thiol-PEG (MW 5000) and 20 nM of the TCEPylated sgc8c in DNA grade water for 12 hours at room temperature. Then the reaction solution was centrifuged at 14000 rpm at 25°C for 5 minutes to remove the unbound aptamers, SH-PEG as a supernatant and concentrate the gold nanorod solution. The precipitate was resuspended in DI or DNA grade water and briefly sonicated. The concentration of the aptamer conjugated gold nanorods is evaluated by measuring the absorbance of the final solution via a Cary Bio-300 UV spectrometer (Varian, Walnut Creek, CA).

Cell Incubation and Flow Cytometry Analysis

The binding affinities of sgc8c conjugated AuNRs with or without BSA were determined by incubating CCRF-CEM or Ramos cells (1×10^6 cells/mL) with AuNRs-sgc8c in a 200 µL binding buffer [Dulbecco's PBS with calcium chloride and magnesium chloride (Sigma), containing glucose (4.5 g/L), $MgCl_2$ (5 mM), yeast tRNA (Sigma, 0.1 mg/mL) and BSA (Fisher Scientific, 1.0 mg/mL)] at 4°C for 30 min or at 37°C for 2h. In

the presence of BSA, the concentration of BSA was varied as 1, 5 and 20 mg/mL. Then cells were washed twice with 0.5 mL washing buffer [Dulbecco's PBS with calcium chloride and magnesium chloride (Sigma), containing glucose (4.5 g/L) and $MgCl_2$ (5 mM)]. Finally, the cells were suspended in 200 µL binding buffer and subjected to flow cytometry analysis by counting 10,000 events on a FACScan cytometer (Becton Dickinson Immunocytometry Systems, CA, USA) while using channel 1.

Cytotoxicity Assay

The cytotoxicity of AuNRs-sgc8c to CCRF-CEM and Ramos cells was evaluted by incubating 1×10^6 cells/mL of CCRF-CEM or Ramos cells with AuNRs-sgc8c in 200 µL binding buffer in the presence or absence of BSA at 37 °C for 2 h under 5% CO_2 atmosphere. Cells were then washed twice with washing buffer, and then incubated at 37 °C for another 48 h under 5% CO2 atmosphere. Followed by washing twice, cells were suspended in binding buffer and propidium iodide (PI; Invitrogen, Carlsbad, CA, USA) at room temperature for 15 min to test cell viability. Dead cells can accumulate the dye and show red fluorescence, which was analyzed by flow cytometry while using the channel 3.

Results and Discussion

Tuning the Size of AuNRs

Gold nanorods were prepared by seed mediated method.[33,89-91] Their sizes were tuned by changing the concentration of the silver nitrate in the growth solution. Since low concentrations of silver cation allow less growth[33,68], the sizes of the gold nanorods prepared with the growth solution containing lower concentration of silver cation were smaller in terms of length. Previous reports showed that the optimum size for efficient cellular uptake for gold nanoparticles is around 50 nm.[92] Therefore, in this study, it is

preferred to use the gold nanorods with the dimensions 52 ± 4 nm and 14 ± 1 nm in length and width, respectively (Figure 2-1 A).

Quantification of Aptamers Immobilized on AuNR Surface

The average number of aptamers immobilized on the surface per gold nanorod was found by dividing the concentration of aptamers immobilized on the surface by the concentration of the gold nanorods used in conjugation.[47,70] In order to find the concentration of the bound aptamers, the concentration of the unbound aptamers was subtracted from the overall aptamer concentration that was used in the modification. The concentrations of the aptamers were evaluated using a fluorescence standard calibration curve for standard solutions of the sgc8c aptamer modified with FITC dye (Figure 2-2 A). According to these calculations, approximately 160 sgc8c aptamers were immobilized on each gold nanorod surface. Also the aptamer immobilization can be monitored by the zeta potential change of AuNRs before and after the aptamer immobilization. Since CTAB is a highly cationic surfactant, before the aptamer immobilization, the surface of the AuNRs is highly positively charged (Figure 2-2 B). After the aptamer conjugation, the surface of the AuNRs became negatively charged due to the negative charges on the aptamers (Figure 2-2 B).

Specificity Test of sgc8c and sgc8c Conjugated AuNRs

Sgc8c aptamer can specifically bind to the CEM cancer cell line, but due to the lack of its biomarker protein on the Ramos cancer cell line, it can’t bind to Ramos cells. Different concentrations of the FITC modified sgc8c aptamer were incubated with both cancer cell lines at 4°C and they didn’t show any nonspecific binding to the Ramos cells (Figure 2-3 A). However, when the concentration of the AuNRs conjugated with sgc8c aptamer was increased, a huge nonspecific binding to Ramos cells was observed

(Figure 2-3 B). Since this nonspecific binding didn't occur with similar concentrations of only sgc8c aptamers incubated with Ramos cells, this nonspecific binding was caused by the increased concentrations of AuNRs. When the concentration of the AuNRs is increased, the positively charged CTAB content will be increased as well. This can increase the possibility of electrostatic interactions between the positively charged CTAB and negatively charged cell membrane, even though the overall surface charge of the AuNRs is negative after the aptamer immobilization.

The same trend of nonspecific binding also occurred when the AuNR-sgc8c conjugate was incubated with Ramos cells (control cells) at 37°C for 2 h. The nonspecific binding was evident when the Ramos cells were incubated with 0.3 nM AuNR-sgc8c and it was increased with the increase in the concentration of AuNRs (Figure 2-5 A).

Cytotoxicity of AuNRs

When the concentration of AuNRs increases, the CTAB content also increases and so its cytotoxic effects both on the target and the control cells. In Figure 2-4, when the incubation concentration of AuNR-sgc8c was increased beyond 0.3 nM, the cytotoxic effects could be seen from the decreased value of events in the flow cytometry measurements. The decrease in the events indicates the low count of the cells, or, in other words cell death. Same cytotoxic effects could be seen when AuNR-sgc8c was incubated with Ramos cells (control cells) at 37°C for 2 h (Figure 2-5) due to the nonspecific binding of AuNRs. In this incubation, even PI staining results showed that when the concentration of AuNRs was 0.3 nM and higher, the percentage of Ramos cell viability decreased to around 60% (Figure 2-5 B).

BSA Modification of AuNRs to Avoid Cytotoxicity and Nonspecificity

In order to decrease its cytotoxic effects, the nonspecific binding of the CTAB to the cells should be prevented. Nonspecific binding of the CTAB is mostly due to the interactions between the positively charged CTAB and negatively charged cell surface (due to the proteins and phospholipids).[81] Thus, cytotoxic effects of CTAB can be minimized, if the interaction between the cell surface and CTAB can be blocked. In this study, BSA (bovine serum albumin) protein was used to coat the CTAB bilayer on the surface of the AuNRs. BSA can coat the surface of the AuNRs through electrostatic interactions (Figure 2-6), since BSA (pI = 4.7) is negatively charged and CTAB is positively charged at pH 7.4 (binding buffer).[82,93]

In order to optimize the BSA concentration that is required for coating the AuNR surface to minimize the interactions between the CTAB and the cell surface, CEM cells were incubated with AuNRs (0.47 nM) that were treated with different concentrations of BSA at 37°C for 2 h. After the incubation, according to the PI staining results, AuNRs treated with 5 and 20 mg/mL BSA showed much lower toxicity compared to the untreated AuNRs and AuNRs treated with 1 mg/mL BSA (Figure 2-7). However, the cell viabilities were similar for the cells that were incubated with the AuNRs treated with 5 or 20 mg/mL BSA. Thus, 5 mg/mL was chosen to be the optimal concentration of BSA to coat the AuNR surface. As it can be seen in Figure 2-7, the toxicity decreased when the percentage of the bound AuNRs decreased as well. This can indicate that the interactions between the CTAB and cell surface are the main cause of the toxicity.

Since 0.3 nM and higher concentrations of AuNRs showed an evident cytotoxicity against the cells they bound to after incubation at 37°C for 2 h (Figures 2-4, 2-5 and 2-7), the concentrations of the AuNRs that would be treated with BSA were chosen to be

0.3 and 0.47 nM. When CEM cells (target cells) were incubated with AuNR-sgc8c (0.47 nM) that were treated with 1, 5, 20 mg/mL BSA, again 5 and 20 mg/mL BSA treatment decreased the toxicity dramatically and similarly (Figure 2-8 A, C). These results correlate with the ones obtained for the AuNRs without aptamer modification (Figure 2-7). The cell viabilities of both CEM and Ramos cells decreased dramatically after the incubation with untreated AuNR-sgc8c (0.47 nM) (Figure 2-8). However, the cell viabilities of both the CEM and Ramos cells were recovered almost completely, if they were incubated with 5mg/mL BSA treated AuNR-sgc8c (0.47 nM) (Figure 2-8 C). The same trend occurred when CEM and Ramos cells were incubated with 5mg/mL BSA treated AuNR-sgc8c (0.3 nM) at 37°C for 2 h (Figure 2-9). Since the concentration of the AuNRs is lower this time, its toxic effects were not as severe as before (Figure 2-9 C). The toxicity decreases with the decrease in the concentration of AuNRs because CTAB concentration also decreases.

As it was seen in Figure 2-7, AuNRs that were not modified with aptamers could bind to CEM cells due to the electrostatic interactions between the CTAB and cell surface. This nonspecific binding was also observed in the confocal images of the Ramos cells (control cells) that were incubated with AuNR-sgc8c (0.5 nM) at 37°C for 2 h (Figure 2-11 A). The green signal is due to the emission of the FITC dye on the sgc8c aptamers. The signal is weak, since confocal microscope only collects the emission from a certain area, but flow cytometer integrates the emission signal generated by each cell until the arranged cell number is reached. On the other hand, when Ramos cells were incubated with BSA treated AuNR-sgc8c (0.5 nM) at 37°C for 2 h, no signal was observed as an indication of lack of nonspecific binding (Figure 2-11 B).

BSA modification of the AuNRs can be monitored by SDS-PAGE technique (Figure 2-10). After incubating the AuNRs (0.1, 0.3 and 0.5 nM) with 100 µg of BSA for 2 h, the excess BSA was washed off and the captured BSA on these AuNRs and a standard BSA (10 µg) sample were loaded in a 4-12% Bis-Tris SDS-polyacrylamide gel for electrophoresis. Since AuNRs can't run into the gel (Figure 2-10 A, lane 9), the captured BSA was eluted by heating the AuNR-BSA at 95°C for 5 minutes before loading into the gel. The band intensities of the captured BSA increased with the increase in the concentration of the AuNRs that were used in the incubation as expected (Figure 2-10 A lanes 3, 5 and 7).

In the light of these results, it can be concluded that BSA modification of AuNRs minimized the interactions between the CTAB and the cell surfaces. This avoids CTAB to show its toxic effects on the cells even if high concentrations of AuNRs are employed. This can really ease the progress of the biological applications, especially in vivo applications, where high concentrations of AuNRs are needed.

Conclusion

This study emphasizes the vital role of the surface modification of the gold nanorods in their biomedical applications. Despite the high specificity of aptamers and high NIR absorptivity of gold nanorods, the conjugation of these two is not enough to get efficient results in targeted photothermal therapy of cancer cells due to the presence of cytotoxic CTAB on the surface of gold nanorods. These toxic effects of high concentrations of gold nanorods should be taken under control before the laser treatment. In this study, BSA encapsulation of CTAB on the surface of AuNRs minimized the interactions between the CTAB and the cell surface. In other words, nonspecific binding to the cells was dramatically decreased by BSA coating. In this way,

CTAB couldn’t show its toxic effects both on the target and control cells before the laser treatment. Thus, aptamer conjugated BSA modified gold nanorods are efficient and highly selective photothermal therapy agents with negligible cytotoxicity.

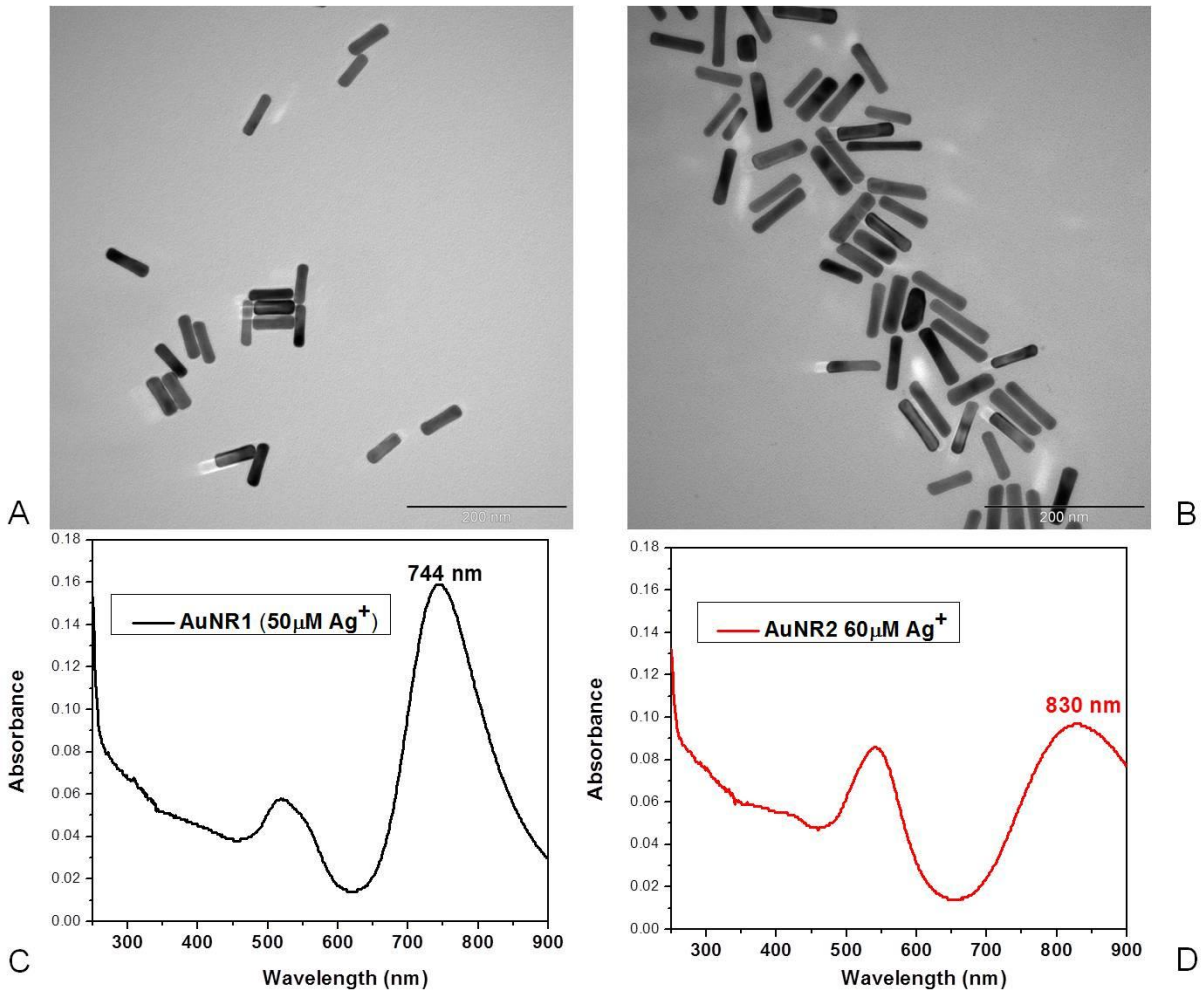

Figure 2-1. Characterization of AuNRs. TEM images of the gold nanorods prepared with A) 50 μM of Ag^+, B) 60 μM of Ag^+ with the dimensions 52 ± 4 nm, 14 ± 1 nm and 70 ± 9 nm, 14 ± 1 nm in length and width, respectively. Absorption spectra of gold nanorods prepared with C) 50 μM of Ag^+, D) 60 μM of Ag^+ with longitudinal bands at 744 nm and 830 nm, respectively.

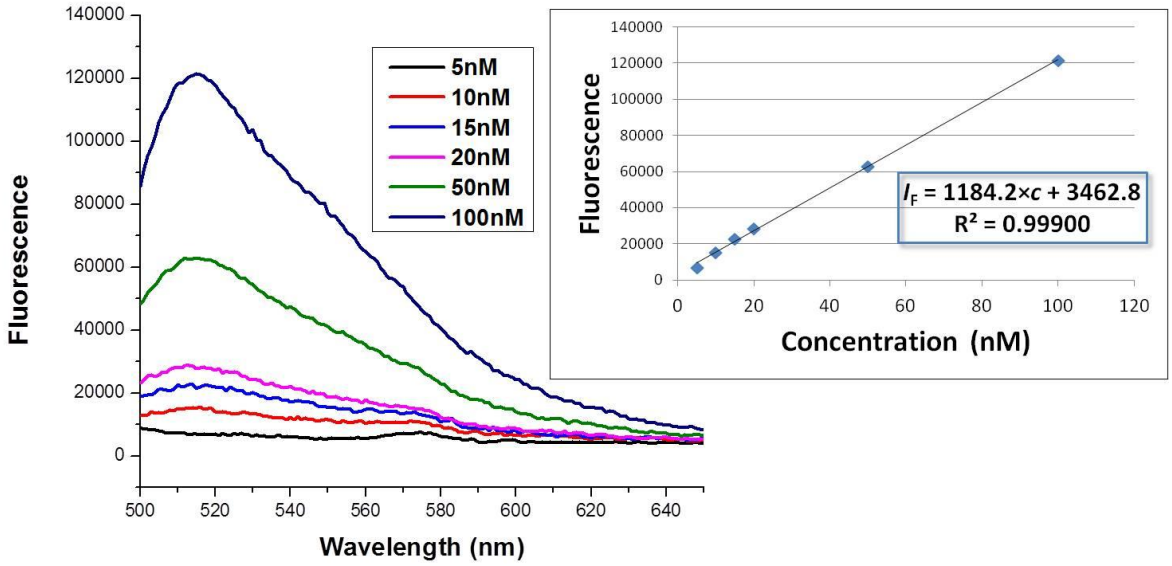

A

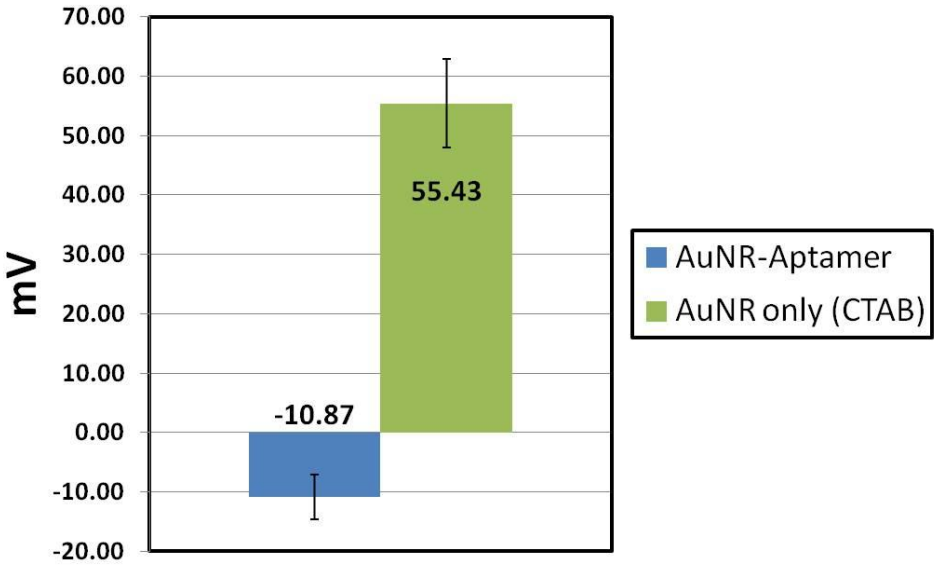

B

Figure 2-2. Detection of aptamer immobilization on the gold nanorod surface. A) Fluorescence standard calibration curve for the sgc8c aptamer modified with FITC dye. B) Zeta potential of gold nanorods before and after aptamer immobilization.

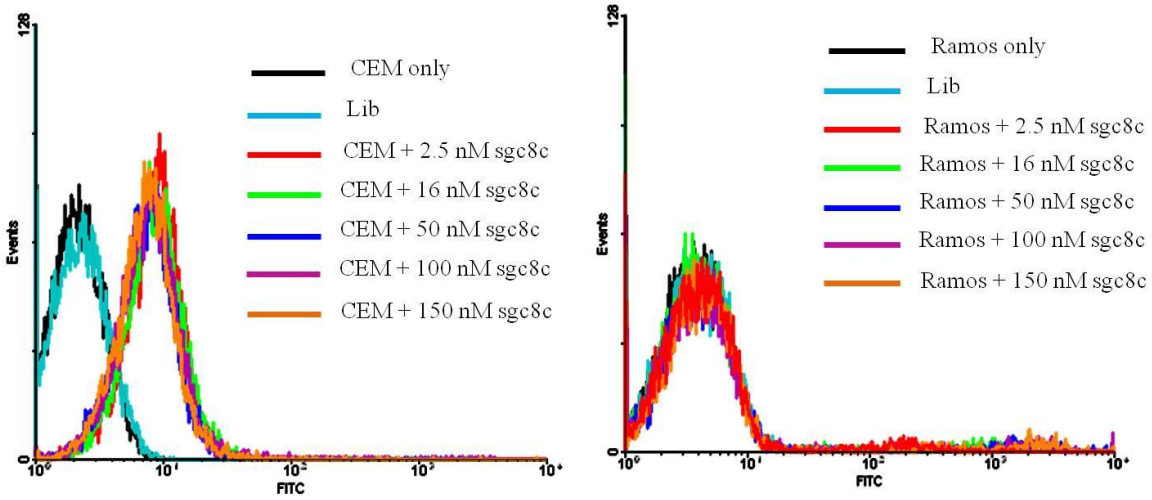

A

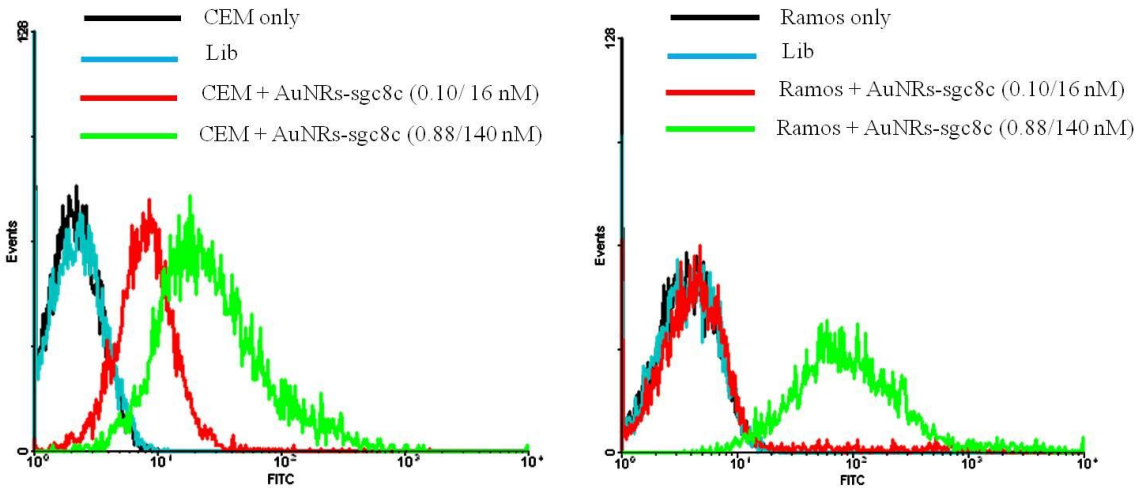

B

Figure 2-3. Specificity test of A) only sgc8c aptamer, B) sgc8c conjugated AuNRs under different concentrations. The first concentration is for the AuNRs and the second concentration is for the aptamers.

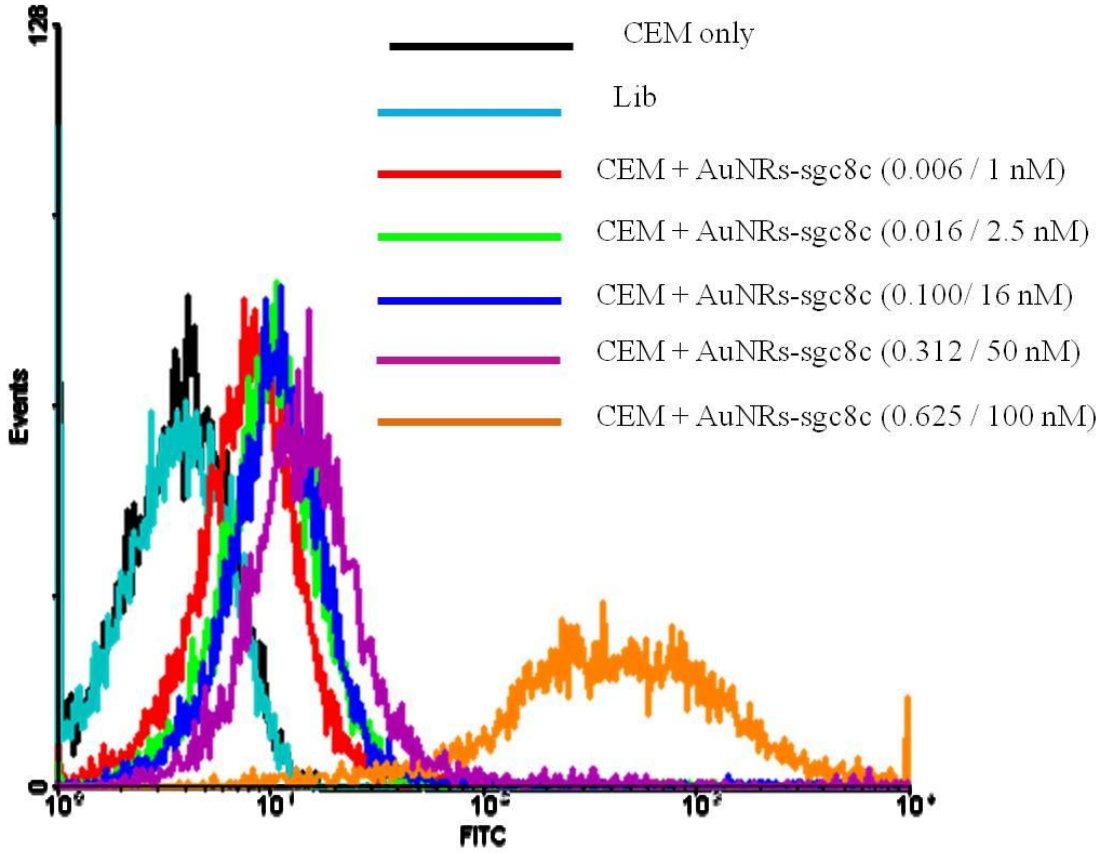

Figure 2-4. Flow cytometric assay to monitor the binding of AuNR-sgc8c with CEM cells (target cells) under different concentrations. Cells were incubated with AuNR-sgc8c at 37°C for 2 h. The first concentration is for the AuNRs and the second concentration is for the aptamers.

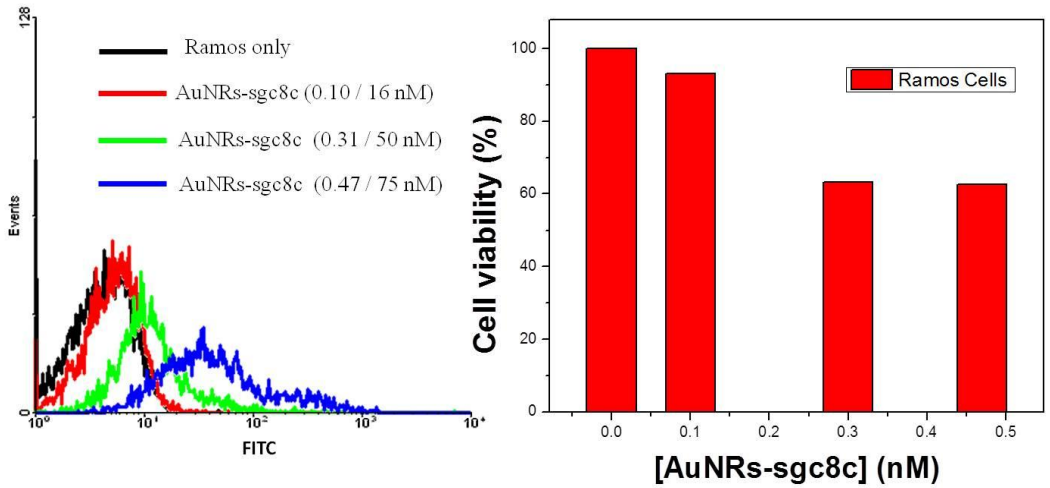

A B

Figure 2-5. Cytotoxicity and nonspecificity test of AuNR-sgc8c to the Ramos cells. A) Flow cytometric assay to monitor the binding of AuNR-sgc8c with Ramos cells (control cells) under different concentrations. B) Cell viability of Ramos Cells after the incubation with AuNR-sgc8c at 37°C for 2 h. The first concentration is for the AuNRs and the second concentration is for the aptamers.

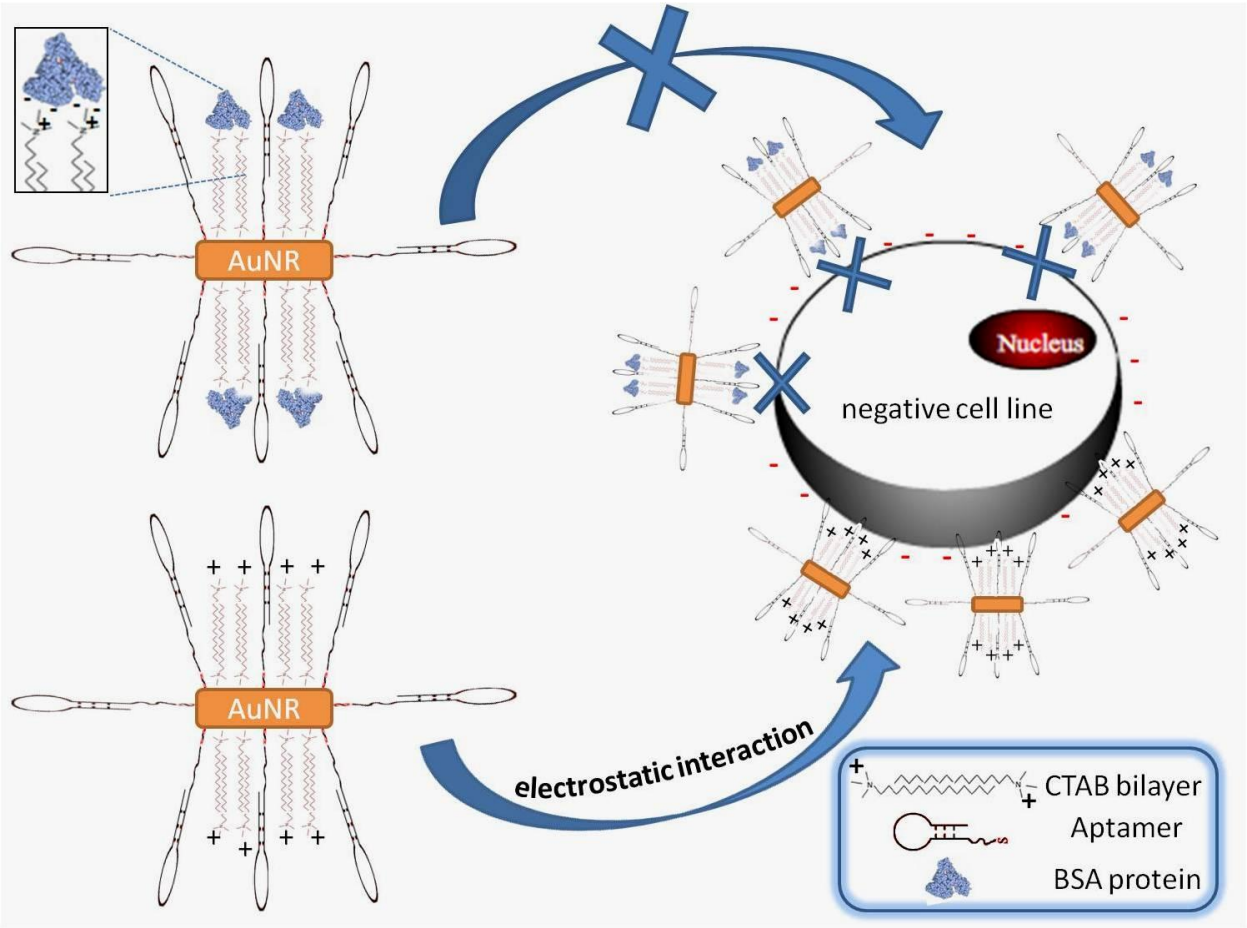

Figure 2-6. The scheme of avoiding the nonspecific binding to control cell lines with BSA modification of AuNR-sgc8c.

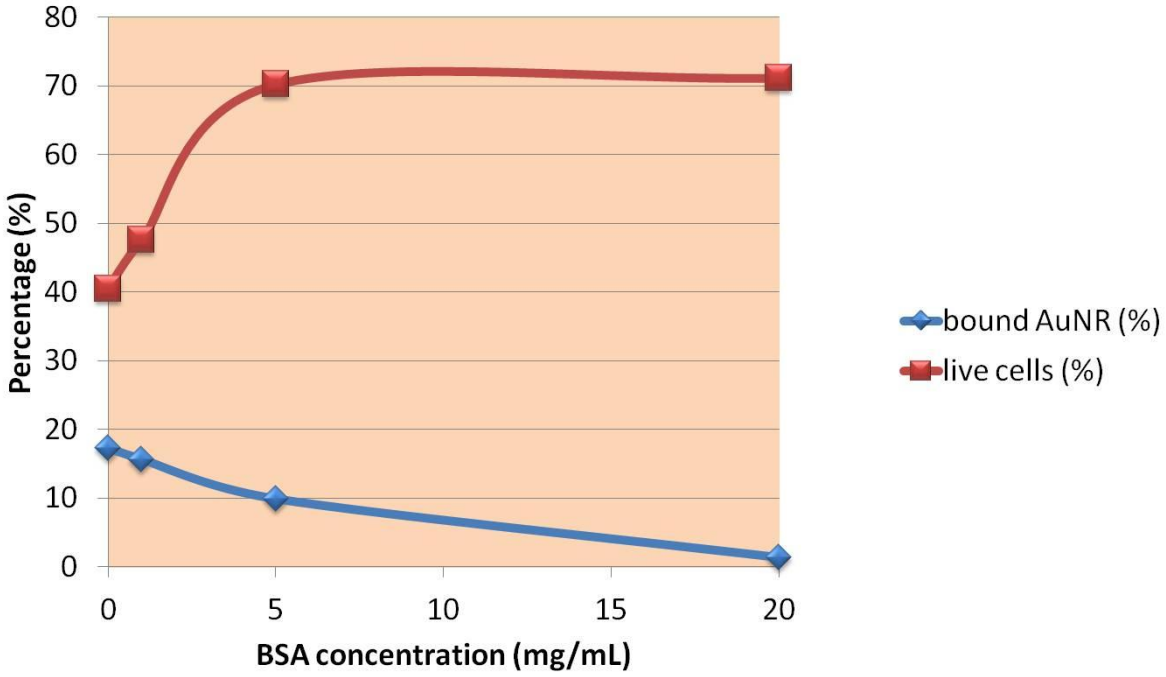

Figure 2-7. Cell viability of CEM cells incubated with AuNRs only (0.47 nM) at 37°C for 2 h under different concentrations of BSA (1, 5 and 20 mg/mL). Cell viability was analyzed by PI staining. Bound AuNRs were analyzed with absorption measurements.

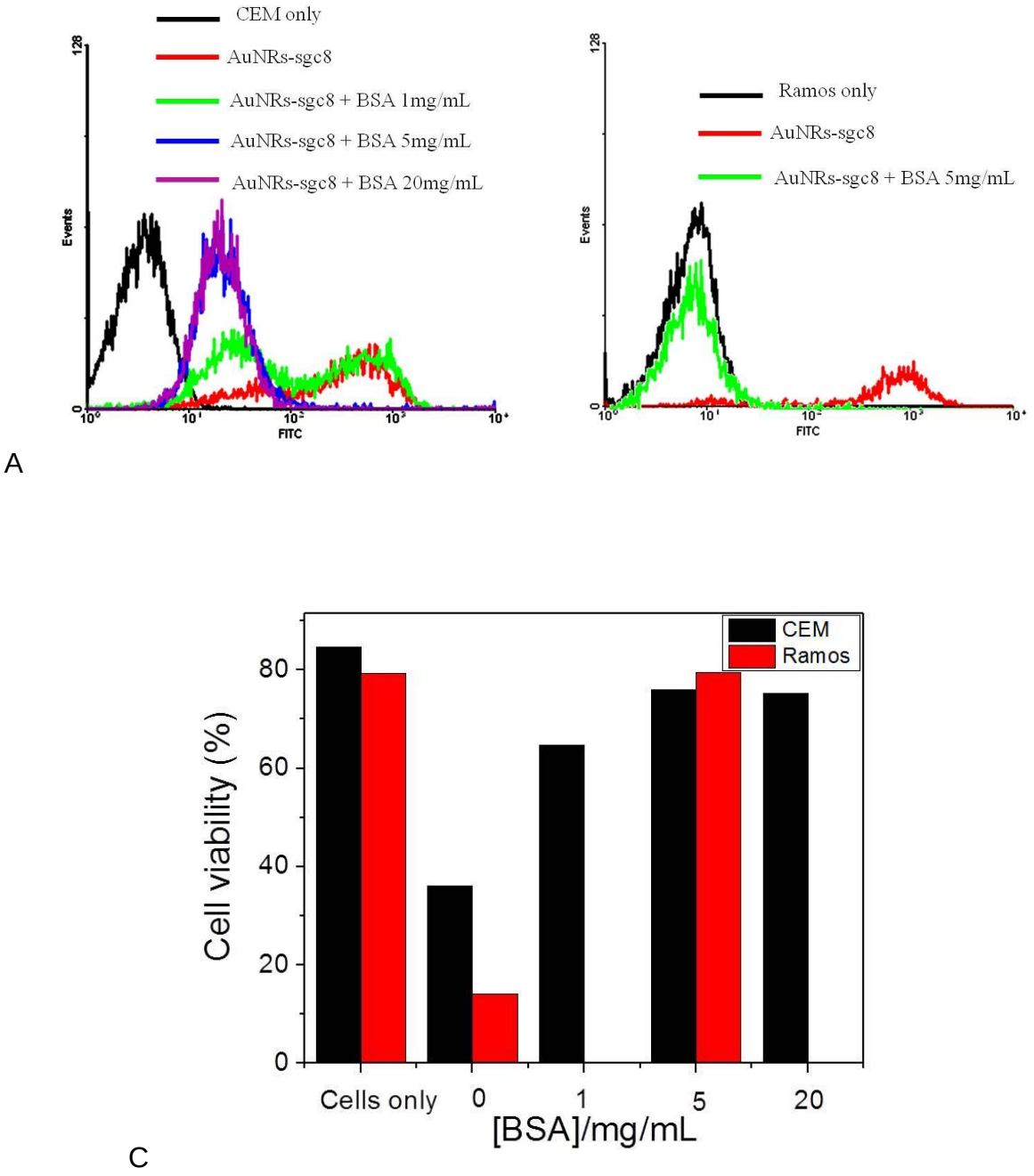

Figure 2-8. Specificity and cytotoxicity test of AuNR-sgc8c (0.47 nM) to CEM and Ramos cells. Flow cytometric assay to monitor the binding of AuNR-sgc8c with A) CEM under different BSA concentrations, B) Ramos under 5mg/mL BSA after the incubation at 37°C for 2 h. C) Cell viability of CEM and Ramos cells was analyzed with PI staining.

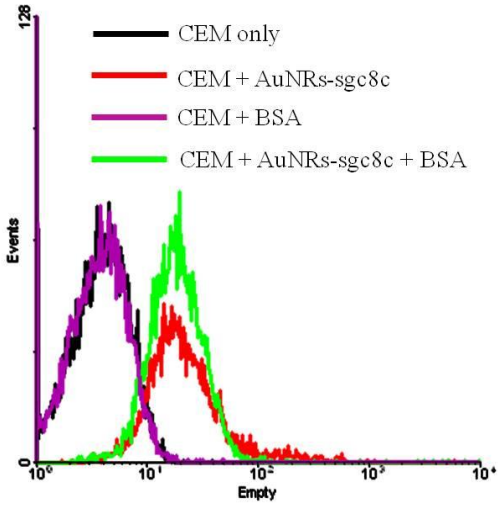

A

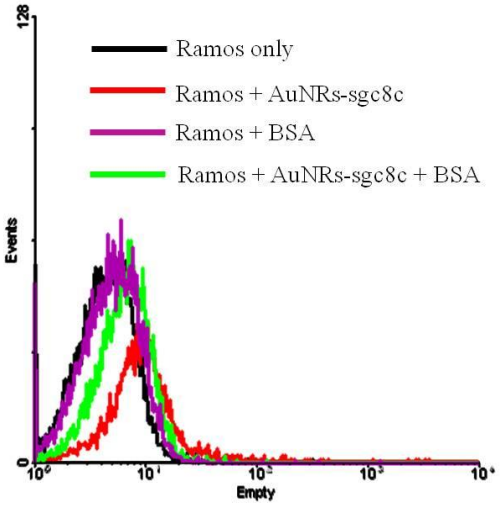

B

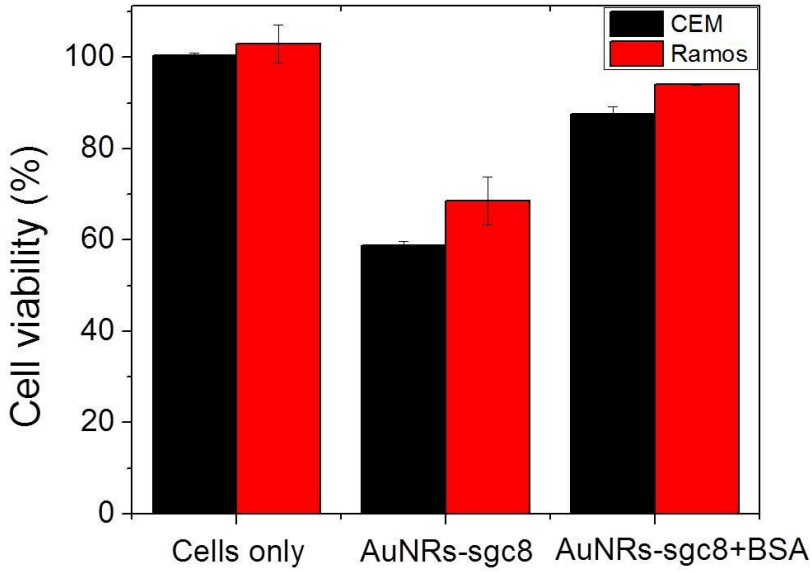

C

Figure 2-9. Specificity and cytotoxicity test of AuNR-sgc8c (0.3 nM) to CEM and Ramos cells. Flow cytometric assay to monitor the binding of AuNR-sgc8c with A) CEM, B) Ramos under 5mg/mL BSA after the incubation at 37°C for 2 h. C) Cell viability of CEM and Ramos cells was analyzed with PI staining.

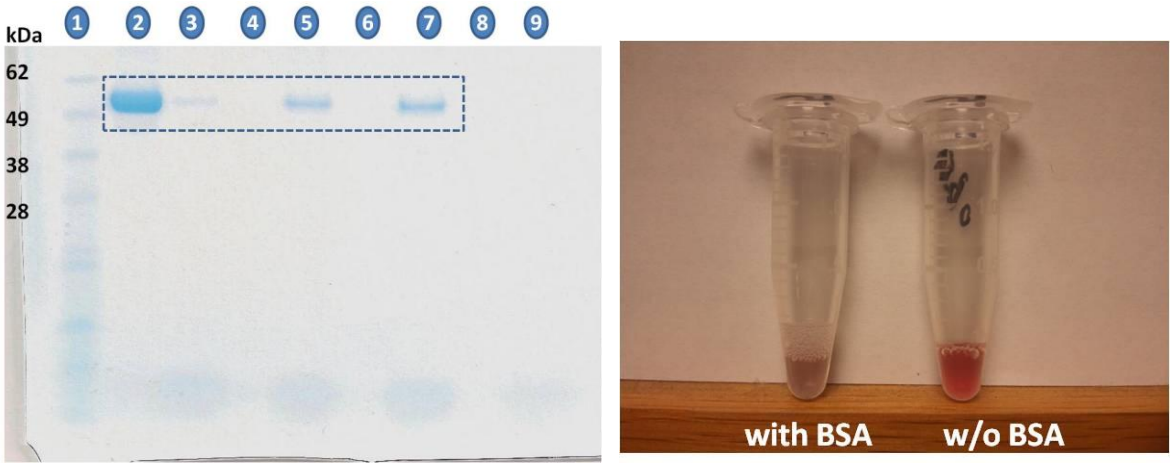

A B

Figure 2-10. Monitoring the BSA modification on AuNRs. A) Gel electrophoresis of captured BSA: lane 1, protein marker; lane 2, BSA protein standard (10 µg); lanes 3, 5, 7, BSA captured, respectively via 0.1, 0.3 and 0.5 nM of AuNRs that were incubated with 100 µg of BSA; lane 9, 0.5 nM of AuNR only. B) The picture of 0.5 nM of AuNR solutions before and after BSA modification.

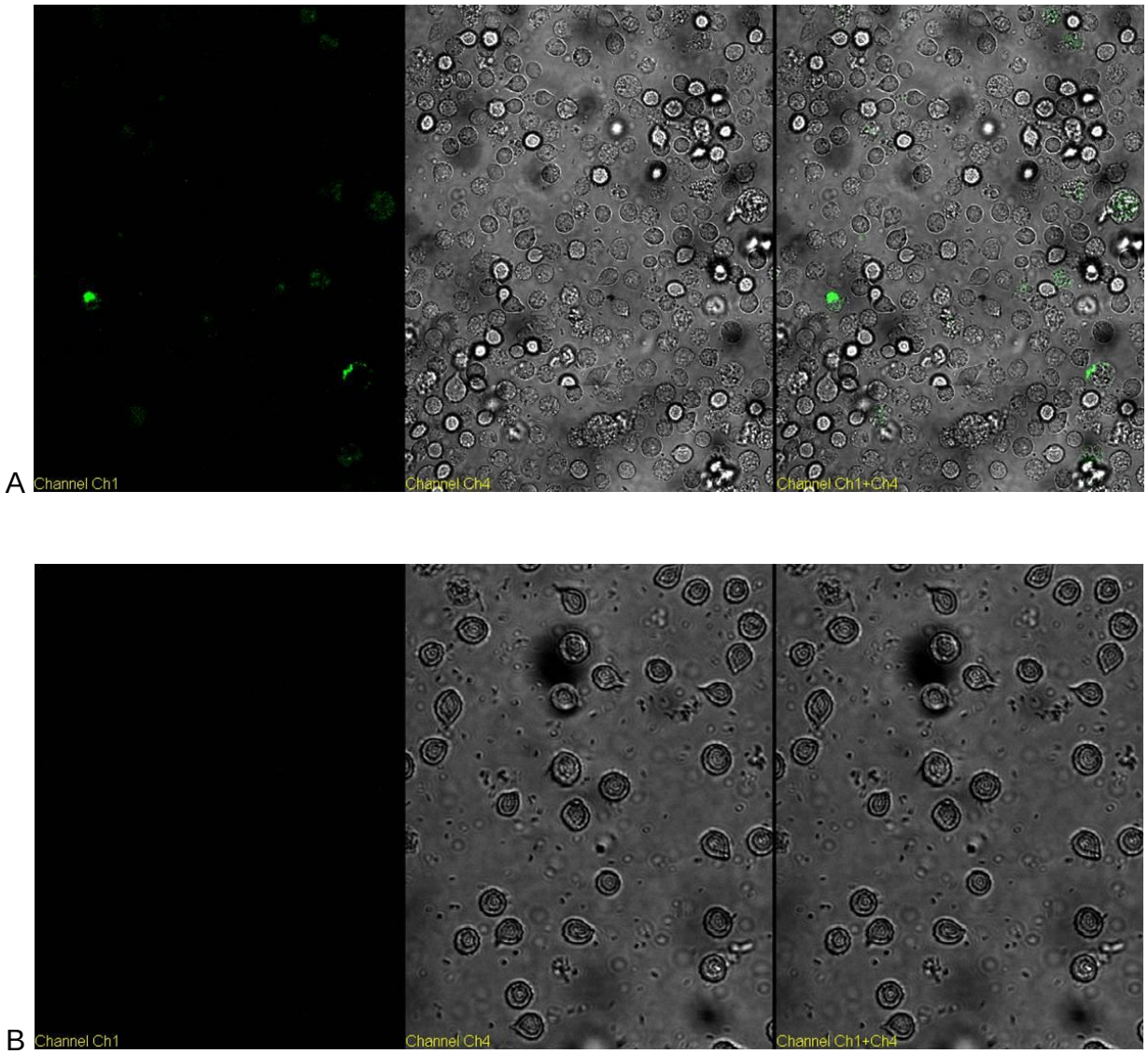

Figure 2-11. Confocal images of Ramos cells incubated with AuNR-sgc8c (0.5 nM) that were A) not treated with BSA and B) treated with 5mg/mL BSA. The cells were incubated with AuNR-sgc8c at 37°C for 2 h.

CHAPTER 3
ENRICHMENT AND DETECTION OF RARE PROTEINS WITH APTAMER-CONJUGATED GOLD NANORODS

Introduction

Rare protein enrichment has great significance in clinical applications, biomedical studies, proteomic studies and signal transduction. Because changes in rare protein abundances or structures are often associated with disease pathogenesis, recognition of these indications may lead to early diagnosis.[1-5] Previous attempts to capture and detect low-abundance proteins from biological media have met with limited success, generally from the lack of robust, sensitive and specific capturing probes.[2] In order to achieve these designer features, surface modification of nanoparticles, as capture scaffolds, plays an essential role.

Specific capturing can be accomplished with affinity tags like proteins[94], antibodies[95] and aptamers[5] that can be conjugated to nanomaterials. Affinity tag proteins can be used as bait for direct detection of their target proteins. However, this type of protein-protein interaction is limited by weak binding, which is further decreased when the bait protein is used outside of the context of the native protein. This weak binding affinity can also lead to nonspecific binding with more abundant proteins in the medium.[94] Antibodies are used as affinity tags in immunoprecipitation (IP) experiments, which are usually performed with gel-conjugated antibodies that can specifically bind to their target proteins.[95] However, because these agarose or sepharose beads have highly porous structures, large target protein molecules may not be able to diffuse adequately into the pores. In addition, the porous structure can also increase the nonspecific binding of smaller molecules that can easily diffuse into the pores. Another drawback of gel beads is rapid precipitation caused by their large sizes (>1μm), which

can cause incomplete interactions with the proteins of interest.[96] As an alternative to gel beads, monodispersed, superparamagnetic beads with diameters varying from nm to μm are used to minimize sample loss and facilitate the isolation process via magnetic separation.[18,19,21] However, in order to fabricate magnetic nanoparticles (MNPs) with good size control and narrow size distribution, they are generally synthesized in the presence of hydrophobic surfactants in organic solvents by thermal decomposition of the precursors. For further biological applications in aqueous solutions, hydrophilic polymers should be tethered to the surface of hydrophobic MNPs, which is fairly challenging due to the inert MNP surface.[97] Gold nanoparticles (AuNPs) have become attractive choices for biomedical applications because of their unique physical and chemical properties. Gold nanoparticles have been used for the detection of specific DNAs[40-42] and proteins[3-5,98] because they can be easily functionalized via simple thiolate chemistry, and they show significant size-dependent color differences. In these "self-assembled monolayer" modifications, the dispersibility of AuNPs in solutions can be increased. For example, after PEG (polyethylene glycol) modification, AuNPs can remain suspended for months.[5] Despite the facile isolation of MNPs, AuNPs are preferred over MNPs due to their easy surface functionalization. Moreover, surface-only binding can avoid limitations in the sizes of the target proteins and eliminate the necessity of pore penetration, thereby decreasing nonspecific binding. Aptamers represent another type of affinity protein tag, consisting of single-stranded oligonucleotides that bind to target molecules, such as small biomolecules and proteins, with affinities equal to those of antibodies. In contrast to other affinity tags, aptamers have many advantages, including small size, nontoxicity, relatively easy preparation and

functionalization with no batch-to-batch variations and easy surface immobilization via their functional groups.[15,18-21]

Proteins captured via affinity tag-conjugated nanoparticles can generally be analyzed using 2-D gels, SDS-PAGE or mass spectrometry (MS) techniques.[4] Besides the challenges described above for protein capturing probes, even detection of captured proteins is limited, to some extent, by the sensitivity of these analytical tools. In SDS-PAGE, the proteins can be stained with Coomassie Brilliant Blue or silver staining methods, with detection limits of 50 ng and 1 ng, respectively.[99,100] On the other hand, MS can achieve detection limits in the femtomole range.[101,102] Regardless of the analytical method, existing affinity enrichment techniques for capture of low-abundance proteins from complex biological fluids still need improvement.

Therefore, in this chapter, we demonstrate the use of surface-modified, aptamer-conjugated gold nanorods (AuNRs) for efficient capture and isolation of target proteins. As a model capturing platform, 15-mer thrombin aptamers are immobilized on the surface of gold nanorods. To increase the binding efficiency, thrombin aptamers are modified with different lengths of hexaethyloxy-glycol (EG_6) linker prior to immobilization on the gold nanorod surface.

Materials and Methods

Materials

Cetyltrimetylammonium bromide (CTAB) ≥ 96.0% was obtained from Fluka (52370), and sodium tetrachloroaurate (III) dihydrate (99%), sodium borohydride (98%), and tris(2-carboxyethyl)phosphine (TCEP) were obtained from Sigma-Aldrich. Ascorbic acid, glycine, Tris, and silver nitrate (99%) were obtained from Fisher Scientific. Thiol-terminated methoxypoly (ethylene glycol) (mPEG-SH, MW 5000) was purchased from

Nanocs. Deoxyribonucleotides, spacer phosphoramidite 18, and 5'-thiol modifiers were purchased from Glen Research. The pH value of the solution containing glycine (0.5 M) was adjusted with 2.0 M NaOH to 8.0. 20X of NuPAGE MOPS SDS running buffer, 4X of NuPAGE LDS sample buffer, and 4-12% Bis-Tris SDS-polyacrylamide gel with 10 wells were purchased from Invitrogen. Deionized water (18.2 MΩ·cm) was used to prepare all of the aqueous solutions.

Preparation of AuNR Seed Solution

Five mL 0.2 M CTAB solution and 5 mL 0.5 mM $NaAuCl_4$ solution were mixed in a 50 mL plastic tube, and then 0.6 mL 0.01 M freshly prepared $NaBH_4$ was added. Following sonication for 3 min, the mixture turned brownish-yellow. This reaction mixture was protected from the light with aluminum foil and placed in a water bath at 25˚C for 1 h.

Preparation of AuNR Growth Solution

Fifty mL 0.2 M CTAB solution and 50 mL 1 mM $NaAuCl_4$ solution were mixed in a 100 mL glass bottle. Then 3.25 mL 0.004 M $AgNO_3$ was added to this mixture, followed by 0.7 mL 0.0788 M ascorbic acid. After addition of ascorbic acid, the color of the solution changed from dark yellow to colorless. Then 0.12 mL of the seed solution was added, and the overall mixture was protected from the light with aluminum foil. Finally, the reaction mixture was placed in a water bath at 25˚C for 1 h. The solution changed to dark pink within 30 min.

Synthesis of AuNRs

Forty mL 0.5 M Glycine (adjusted pH 8.0) was prepared in a 200 mL glass bottle, and 60 mL DI water was added, followed by 100 mL of the growth solution. The reaction

mixture was protected from light with aluminum foil and was placed in a water bath at 25˚C for 12 h.

Removing Excess CTAB from AuNRs

Aliquots (25 mL) of nanorod solution were added to centrifuge tubes and were centrifuged at 14000 rpm for 8 min. For each fraction, 22.5 mL of the supernatant was removed and replaced with 22.5 mL DI water. The solutions were again centrifuged at 14000 rpm at 25°C for 5 min. Then 22.5 mL of the supernatant was removed from each fraction and replaced with 22.5 mL 0.5 mM CTAB solution. The centrifugation step was repeated with the CTAB solution twice at the same speed and temperature for each fraction, and, finally, 2.5 mL of the solution was collected from each fraction.

Characterization of AuNRs

After removing excess CTAB, all fractions were combined to have approximately 10 times concentrated gold nanorod solution. Then this nanorod solution was diluted 1:20, and the UV/Vis spectrum was taken using a Cary Bio-300 (Varian, Walnut Creek, CA) to find its concentration. Two absorbance peaks were obtained at ca. 530 nm (transverse band) and ca. 860 nm (longitudinal band). TEM images of gold nanorods were obtained with a JEOL TEM 2010F transmission electron microscope on a copper grid. The sizes of gold nanorods were calculated with FemtoScan software as 77 ± 6 nm and 17 ± 1 nm in length and width, respectively.

Synthesis of Thrombin Aptamer

The 15-mer thrombin aptamer was selected as a model capture agent: (SH-2EG_6-Apt-FAM): 5` HS-$C_6$-2$(EG)_6$-GGT TGG TGT GGT TGG-FAM 3`; (SH-3EG_6-Apt-FAM): 5` HS-$C_6$-3$(EG)_6$-GGT TGG TGT GGT TGG-FAM 3`. All aptamers were coupled with 5′-thiol modifier for conjugation to the gold nanorod surface and were labeled with

fluorescein at the 3′-end using 3′-(6-fluorescein) CPG to detect and quantify the aptamer modification on the gold nanorod surface. Also, either two or three hexaethyloxy-glycol units (EG_6) were added between the thiol and thrombin aptamer sequence as spacers to observe the length effect on thrombin capture. All oligonucleotides were synthesized by solid-state phosphoramidite chemistry at a 1-µmol scale using an ABI3400 DNA/RNA synthesizer (Applied Biosystems, Foster City, CA). The completed sequences were then deprotected in AMA (ammonium hydroxide/40% aqueous methylamine 1:1) at 65 °C for 20 min and further purified using a ProStar HPLC (Varian, Walnut Creek, CA) with a C18 column (Econosil, 5 µm, 250×4.6 mm) from Alltech (Deerfield, IL). A Cary Bio-300 UV spectrometer (Varian, Walnut Creek, CA) was used to measure absorbance to quantify the concentrations of the product sequences.

Aptamer Immobilization to the Surface of AuNRs

Before aptamer immobilization, 0.1 mM 5` S-S tagged thrombin aptamers were incubated with 5 mM TCEP in 50 mM Tris/HCl (pH=7.5) buffer for 1 hour at room temperature to reduce S-S to SH groups. 5` SH-thrombin aptamers were then collected in small portions by eluting the TCEP mixture through a NAP-5 column. Concentrations of these portions were calculated by measuring their absorbance using a Cary Bio-300 UV spectrometer (Varian, Walnut Creek, CA). Then a 100 µL sample of 0.96 nM gold nanorod solution was centrifuged at 14000 rpm at 25°C for 3 min. The supernatant was removed, and the precipitate was resuspended in 100 µL 2 mM CTAB. Then 850 µL of DNA grade water, 50 µL 2mM thiol-PEG (MW 5000) and 0.25 µL 100 µM (25 nM as final concentration) thrombin aptamer were added to the gold nanorod solution. The solution was incubated for 12 hours at room temperature. Then the reaction solution was centrifuged at 14000 rpm at 25°C for 5 minutes to remove the unbound aptamers

and SH-PEG as a supernatant. The precipitate was resuspended in 100 µL of DI or DNA grade water. Gold nanorods conjugated with thiol-PEG-only (MW 5000) were prepared in the same manner.

Thrombin Capture with Aptamer-Conjugated AuNRs

Three samples, including 20, 50 and 100 µL of 0.96 nM gold nanorod-thrombin aptamer ($2EG_6$-or $3EG_6$-modified), and 50 µL 0.96 nM of only SH-PEG-modified gold nanorod were centrifuged at 14000 rpm for 5 minutes, and the supernatants were removed. Then 100 µL of thrombin activation buffer and human plasma samples containing 338 ng, 100 ng or 1ng human α-thrombin were prepared separately for each precipitated gold nanorod solution. The activation buffer solutions also contained 10mg/mL BSA (3000 times more concentrated than α-thrombin in the 338 ng α-thrombin-spiked buffer solutions) to mimic multiplex biological fluids. Thrombin-spiked activation buffer (20 mM Tris-HCl pH=7.4, 140 mM NaCl, 5mM KCl, 1mM $CaCl_2$, 1mM $MgCl_2$) and plasma samples were added to the precipitates of gold nanorod solutions separately, and the mixtures were vortexed, or briefly sonicated, to mix the contents. The mixtures were incubated for 20 minutes at room temperature and were then centrifuged at 14000 rpm for 3 min. The precipitates were washed three times with 200 µL of washing buffer and centrifuged at 14000 rpm for 3 min after each buffer addition; the precipitates were then dispersed in 10 µL of DI water.

One-Dimensional Gel Electrophoresis and Gel Staining

A volume of 10 µL of the prepared α-thrombin protein standards and the gold nanorod solutions with α-thrombin captured from human plasma or buffer were mixed with 10 µL gel loading buffer (NuPAGE LDS sample buffer; Invitrogen). The mixtures and 2 µL of the prestained protein marker solution were heated at 95°C for 5 minutes

and loaded into the gel (4-12% Bis-Tris SDS-polyacrylamide (Invitrogen)) with a thickness of 1.0 mm. Gel separation in running buffer proceeded at a constant voltage of 200V for 1 hour. After separation, the gels that were loaded with 338 ng or 100 ng thrombin samples were washed with DI water three times at 10 minute increments, and the gels were stained with Coomassie Blue dye (GelCode Blue Stain Reagent, Thermo Scientific) for 1 hour. The gels that were loaded with 1 ng thrombin samples were stained by the silver staining method using a SilverQuest Staining Kit (Invitrogen). Then the stained gels were scanned with a scanner, and the bands in the gels were analyzed by ImageJ software. To determine the thrombin capture efficiency, the peak areas of the protein standard bands were considered to represent 100% yield.

Results and Discussion

Characterization of AuNRs

In order to synthesize gold nanorods, a seed-mediated method was used.[33,89-91] The synthesized gold nanorods were characterized by their UV-Vis absorption and by their TEM images, as shown in Figure 3-1. The prepared gold nanorods showed good uniformity, as indicated by their TEM image. The characteristic transverse and longitudinal bands[33] were observed at 530 nm and 860 nm, respectively, in the UV-Vis absorption spectrum (Figure 3-1).

Optimization of the Surface Modification of AuNRs

Surface modification of gold nanorods utilizing thiolate reaction consisted of PEGylation of the surface using SH-PEG (MW 5000) and immobilization of thiol-labeled 15-mer thrombin aptamers that were previously modified with different hexaethyloxy-glycol (EG_6) lengths (Figure 3-2). Gold nanorods were functionalized with thiol-PEG (MW 5000) to avoid agglomeration and decrease nonspecific binding.[5,103-107]

The immobilization of thiol-PEG was optimized by monitoring the fluorescence intensities of the FAM-labeled aptamer-conjugated gold nanorods and the unbound aptamers for different concentrations of SH-PEG. As shown in Figure 3-3, the highest fluorescence intensity of aptamer-conjugated gold nanorods and the least fluorescence intensity of the unbound aptamers were obtained when 100 µM SH-PEG was used, and that concentration was subsequently used for AuNRs with either 2 or 3 EG_6 units. This amount of SH-PEG also led to well-dispersed AuNR solutions (Figure 3-4). The average number of aptamers bound on the surface per nanorod was found by dividing the concentration of aptamers bound on the surface by the concentration of the gold nanorods used in conjugation. In order to find the concentration of the bound aptamers, the concentration of the unbound aptamers was subtracted from the overall aptamer concentration that was used in the modification. The concentrations of the aptamers were evaluated using a fluorescence standard calibration curve for standard solutions of the thrombin aptamer.[47,70] According to these calculations, approximately 162 and 157 of $2EG_6$- and $3EG_6$- modified 15-mer thrombin aptamers were immobilized on each gold nanorod surface, respectively, while using 100 µM SH-PEG (MW 5000) (Figures 3-5 and Figure 3-6). Since the aptamer immobilization did not differ significantly for either of these modifications, the thrombin capture efficiency can be compared with the change in the linker length.

The aptamer accessibility towards its target can be increased by using linkers, such as Thymidine[108] and PEG[109]. In previous reports, arbitrarily chosen lengths of these linkers were used.[107,108] Balamurugan *et al.* showed that there are two factors affecting the target capture efficiency, surface density and the distance from the

immobilization surface of the aptamers. In their study, thymidine linkers in 4 different increments (T_0, T_5, T_{10}, T_{20}) decreased the surface density of thrombin aptamers immobilized on gold slides, resulting in decreased target capturing efficiency in $T_5 \rightarrow T_{10}$ and $T_{10} \rightarrow T_{20}$ increment change, however in T_0 to T_5 modification the distance effect suppressed the surface density decrease, which increased the accessibility of aptamers towards its target.[107] In this study, 15-mer thrombin binding aptamers were modified with either 2 or 3 units of hexaethyloxy-glycol to determine which length resulted in more efficient thrombin capture. Instead of thymidine, hexaethyloxy-glycol was chosen as a linker because it does not affect the surface density of the aptamers.[107] On the other hand, one unit of hexaethyloxy-glycol is approximately as long as a T_5 linker.

Gold surfaces have a high tendency to quench fluorescence of nearby fluorophores.[110,111] Consequently, before starting the thrombin capturing efficiency comparison experiments, it was necessary to estimate the distance between aptamer and AuNR surface. Therefore, the fluorescence quenching percentages of $3EG_6$- and $2EG_6$- modified thrombin aptamers having FAM dye on their 3' ends were compared. The fluorescence quenching percentage of $3EG_6$-modified aptamers was found to be 10% less than that for aptamers with $2EG_6$ units, indicating that the $3EG_6$- modified aptamers were farther away from the AuNR surface (Figure 3-7).

Thrombin Capturing Efficiency Comparison

Thrombin capturing efficiency comparison experiments were then conducted by an SDS-PAGE technique. Different concentrations (0.19, 0.48 and 0.96 nM) of gold nanorods conjugated with $3EG_6$- or $2EG_6$- modified thrombin aptamers were incubated with 338 ng, 100 ng or 1ng human α-thrombin-spiked buffer or human plasma samples. The enriched α-thrombin on these gold nanorods and a standard human α-thrombin

sample were loaded in a 4-12% Bis-Tris SDS-polyacrylamide gel for electrophoresis. Also, gold nanorods that were conjugated only to thiol-PEG (MW 5000) were incubated with the samples containing human α-thrombin protein to determine any contribution from nonspecific enrichment.

As shown in Figure 3-8, an increase in concentration of the AuNRs conjugated with $2EG_6$-modified thrombin aptamers from 0.19 nM to 0.96 nM resulted in an increase in thrombin capturing efficiency from 48% to 84% for the buffer sample containing 338 ng (~84 nM, 3.38 ppm) of human α-thrombin (Figure 3-8 A, lanes 2-4). However, when the concentration of the AuNRs conjugated with $3EG_6$-modified thrombin aptamers increased from 0.19 nM to 0.96 nM, the thrombin capturing efficiency decreased from 90% to 28% for the same thrombin standard (Figure 3-8 A, lane 5-7). Therefore, the most efficient capturing occurred with the 0.19 nM $3EG_6$-modified aptamer-conjugated AuNRs. A similar thrombin capturing trend occurred for the buffer sample containing 100 ng (~25nM, 1.00 ppm) of α-thrombin. In Figure 3-8 B, the thrombin capture efficiency difference between the 0.19 nM $3EG_6$- and $2EG_6$-modified thrombin aptamer-conjugated AuNRs is even more evident (lane 5 and lane 4, respectively). Thus, even a one unit change of hexaethyloxy-glycol increased the thrombin capturing efficiency by 47%.

As it was reported by Balamurugan *et al*.[107], the thrombin binding capacity was controlled by two different factors, surface density and the distance from the immobilization surface of the aptamers. In this study, since the numbers of $2EG_6$- and $3EG_6$-modified thrombin aptamers immobilized on each gold nanorod surface were close to each other, the distance of aptamers from gold surface became the major effect

on thrombin capture efficiency. For AuNRs conjugated with $2EG_6$- modified thrombin aptamers, which had shorter linkers, the thrombin capture efficiency was greatly affected by the steric effect. Thus larger concentrations of AuNRs were needed to increase the chance of α-thrombin to come close to the aptamers immobilized on gold surface. That is the reason of the increase in the thrombin capture efficiency with the increase of the concentration of AuNRs conjugated with $2EG_6$-modified thrombin aptamers. However, AuNRs conjugated with $3EG_6$-modified thrombin aptamers, which had longer linkers showed slight steric effects on thrombin binding to aptamer, so even low concentrations of AuNRs (0.19 nM) conjugated with $3EG_6$-modified thrombin aptamers could reach up to 90% of thrombin capture efficiency. On the other hand, with the increase of the concentration of AuNRs, the $3EG_6$-modified thrombin aptamers on the adjacent AuNRs may have twisted around each other due to their longer distance from the gold surface and flexibility. Therefore the effective number of aptamers that can bind to thrombin was reduced. That's maybe the reason of the decrease in thrombin capture efficiency with the concentration increase of AuNRs conjugated with $3EG_6$-modified thrombin aptamers.

In both Figures 3-8 A and B, lane 8 shows the nonspecifically captured α-thrombin from buffer solutions via gold nanorods conjugated only with thiol-PEG (MW 5000).[5] Since the band intensities for this nonspecifically captured α-thrombin were so low, it can be concluded that the nonspecific capture of α-thrombin in the absence of the affinity tag conjugation was negligible.

These buffer solutions contained α-thrombin, as well as high concentrations of BSA (10mg/mL), to mimic complex biological fluids. As shown in Figure 3-9, thrombin

aptamer-conjugated gold nanorods showed some nonspecific binding to BSA (66 kDa), but the band intensities were very low compared to the bands for captured α-thrombin (37kDa), indicating that the nonspecific binding was negligible. The gel in Figure 3-9 also shows that the thrombin capture efficiency increased with an increase in the concentration of $2EG_6$-modified aptamer-conjugated AuNRs, but it decreased with an increase in the concentration of $3EG_6$-modified aptamer-conjugated AuNRs. Moreover, 0.96 nM aptamer-$2EG_6$-AuNRs and 0.19 nM aptamer-$3EG_6$-AuNRs again showed similar band intensities for captured α-thrombin, which is an indication of the efficacy of aptamer-$3EG_6$-AuNRs, despite their low concentration.

Thrombin capturing efficiency comparison experiments were also conducted with 1 ng (~250 pM, 10 ppb) human α-thrombin-spiked buffer and human plasma samples. This concentration was chosen since 1ng is close to the detection limit of the silver staining method for proteins after gel electrophoresis.[99,100] Significant differences in thrombin capture efficiency for different probes from 1 ng α-thrombin-spiked buffer solutions were not observed, as shown in Figure 3-10.

Similarly, the α-thrombin capture efficiency trend observed with thrombin aptamer activation buffer solutions was not observed with the 1ng α-thrombin-spiked human plasma sample (Figure 3-11). The band intensities of the captured α-thrombin (red dashed lines, Figure 3-11) via different concentrations of $2EG_6$- or $3EG_6$-modified thrombin aptamer-conjugated AuNRs did not differ significantly from each other (except in lane 7, which could have resulted from a staining error), and they even showed slightly higher intensities than thrombin standard (lane 1) by the presence of some α-thrombin in the original plasma sample. Even though one hexaethyloxy-glycol unit

change of the spacer in the surface modification of gold nanorods did not affect the thrombin capturing efficiency significantly in plasma samples, 1 ng (10 ppb) of α-thrombin was successfully enriched from human plasma with the aptamer-conjugated gold nanorods. An unexpected band could also be seen in the gel electrophoresis of the α-thrombin standard (blue dashed lines, lane 1, Figure 3-11). In order to identify this band, MALDI-MS spectrum of the α-thrombin standard was taken. Besides the expected mass-to-charge ratio peak at around 36000 m/z, another peak was obtained at around 72000 m/z (Figure 3-12). This was most likely caused by the prothrombin content of the α-thrombin standard solution, since α-thrombin (~37kDa) is generated by proteolysis of two peptide bonds in prothrombin (~72kDa) via prothrombinase enzyme.[112,113] The same band (~72 kDa) occurred for the lanes of the captured α-thrombin in Figure 3-11. This result indicates that 15-mer thrombin aptamer can also bind to prothrombin. This correlates with some previous studies, which found that a 15-mer thrombin aptamer can block the clotting activity of thrombin either by binding to exosite I or prothrombin to inhibit its activation by prothrombinase enzyme, which also leads to the inhibition of thrombin generation.[114] The band intensity for prothrombin in the standard (lane 1, Figure 3-11) did not substantially differ from band intensities recorded for captured prothrombin via aptamer-conjugated gold nanorods modified with different linker lengths (lanes 2-6). Thus, it may be concluded that effective capturing was achieved at ppb levels for prothrombin using 15-mer thrombin aptamer-conjugated gold nanorods as well.

Conclusions

The overall results in this study demonstrate the applicability of the surface-modified, aptamer-conjugated gold nanorods for the enrichment of low-abundance

proteins (in ppb range) from plasma samples and the vital role of surface modification to generate robust, sensitive, specific and efficient protein capturing platforms. This new method can enrich proteins at ppb levels using very low amounts of the capturing platform (0.19 nM gold nanorods) and with negligible nonspecificity. The dramatic increase in thrombin capturing efficiency with only one unit change of hexaethyloxy-glycol linker proves the significance of surface modification in protein enrichment techniques. This study also outscores similar, but more complex, methods only capable of enriching down to 6 ng of captured thrombin.[115] In addition to the detection of proteins using gel electrophoresis, this work can also open new avenues for aptamer-conjugated gold nanorods to be used as an LDI – MS matrix[116] where NIR lasers are used. In this way, aptamer-conjugated gold nanorods can be used as a dual platform for enrichment and detection of rare proteins utilizing MS, as shown in our previous work with aptamer-conjugated graphene oxide.[117] It may be concluded that aptamer-conjugated gold nanorods are promising protein capturing platform candidates for biomarker discovery studies involving capture and detection of low-abundance proteins from biological fluids.

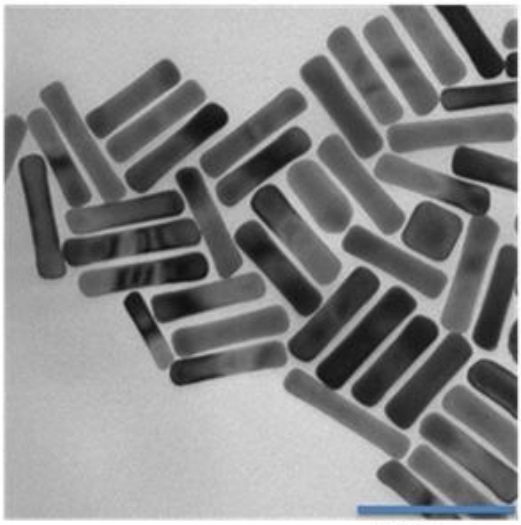

A

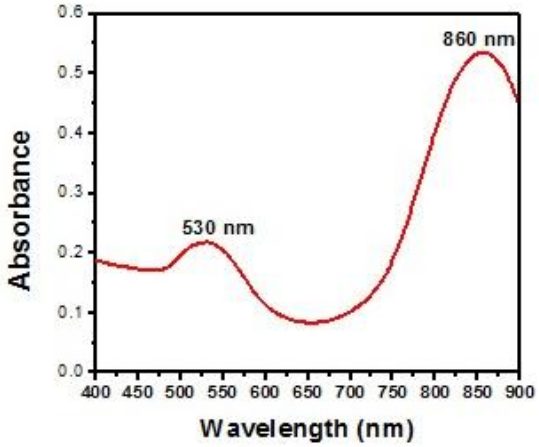

B

Figure 3-1. Characterization of AuNRs. A) TEM image of the gold nanorods with the dimensions 77 ± 6 nm and 17 ± 1 nm. B) Absorption spectrum of gold nanorods with two absorption maxima at 530 and 860 nm.

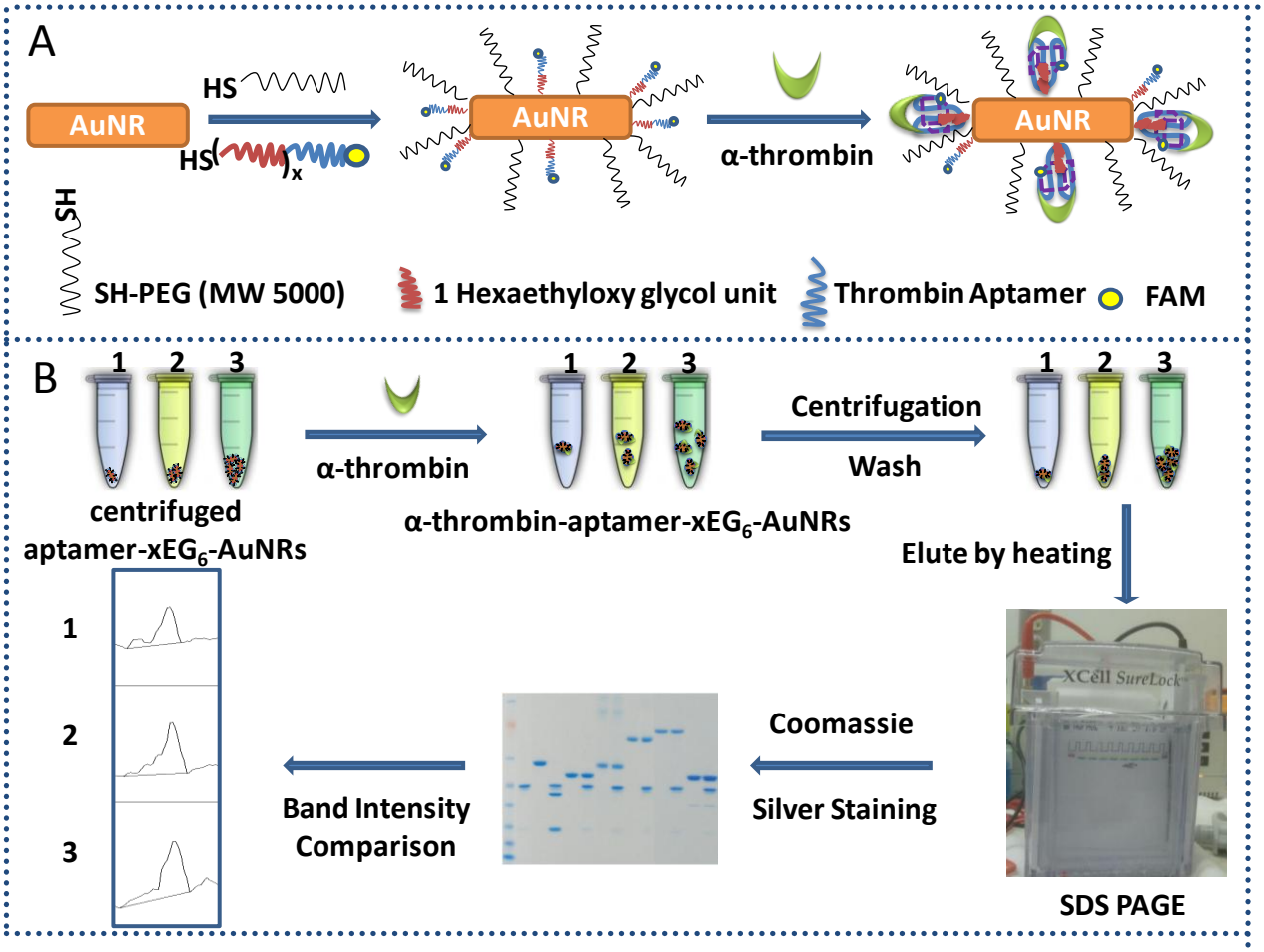

Figure 3-2. General scheme for the α-thrombin capturing process. A) Surface modification design of gold nanorods. B) Scheme of the α-thrombin capturing protocol: 1, 2, 3 represent 0.19, 0.48 and 0.96 nM gold nanorods conjugated with 3EG6- or 2EG6-modified thrombin aptamers, respectively.

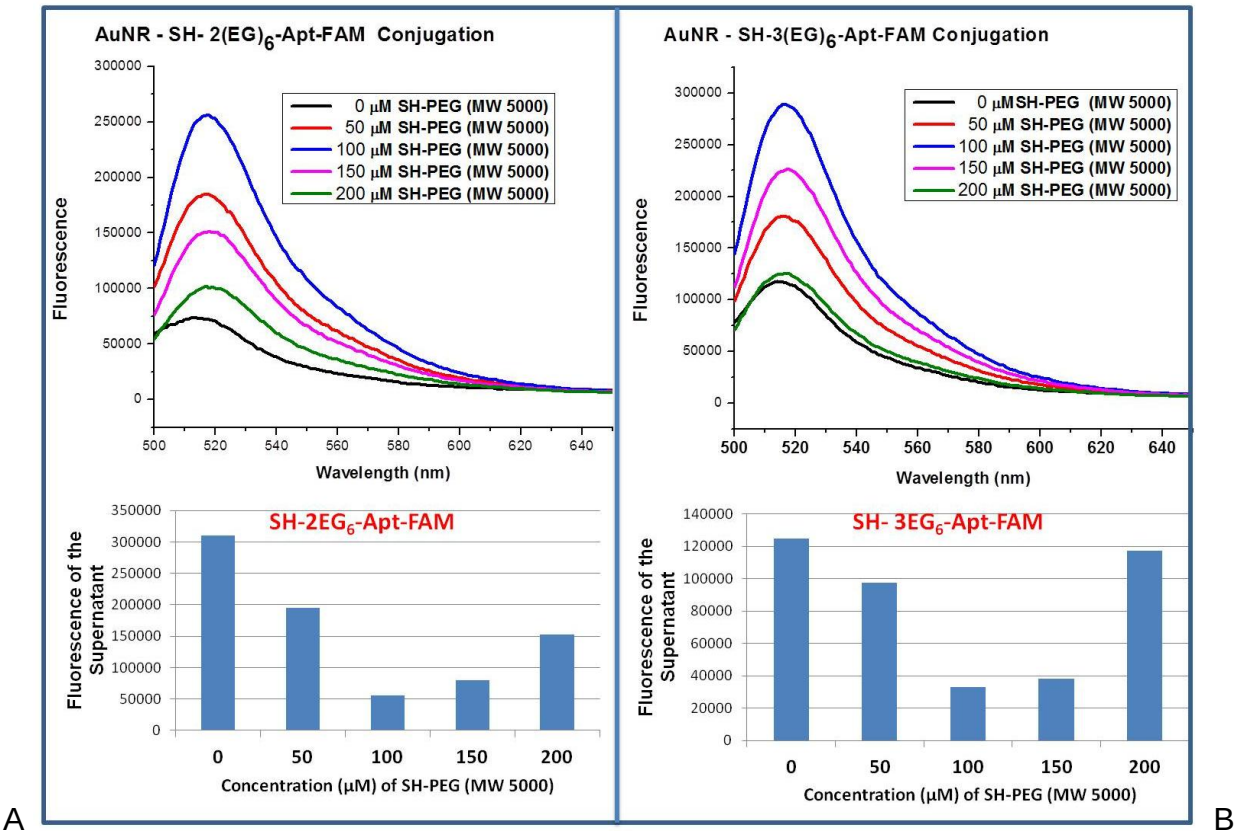

A B

Figure 3-3. Optimization of aptamer immobilization on AuNR surface. The fluorescence intensities of A) $2EG_6$-modified aptamers, B) $3EG_6$-modified aptamers, (upper figures) aptamer-conjugated AuNRs, (lower figures) unbound aptamers, while varying the concentrations of SH-PEG (MW 5000) in the surface modification of AuNRs.

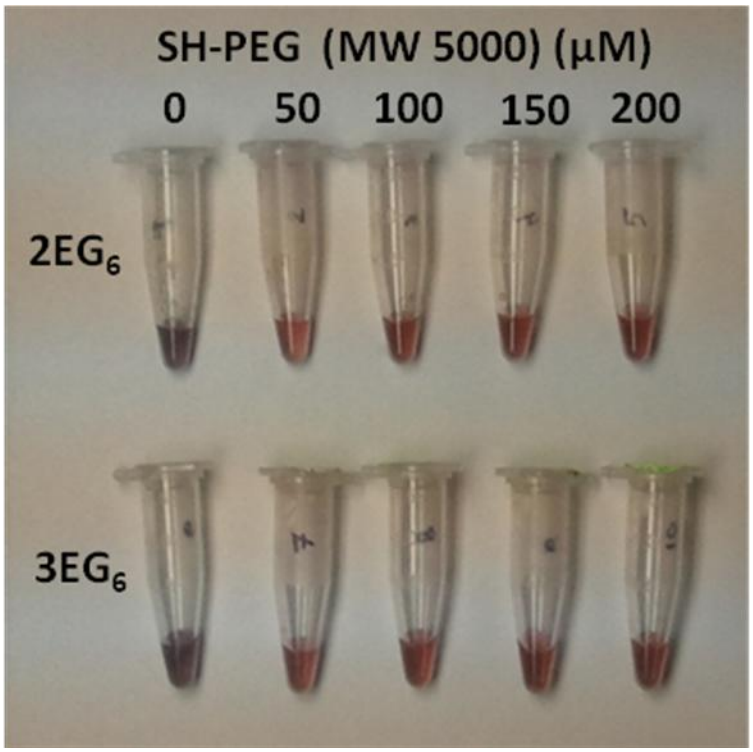

Figure 3-4. The effect of SH-PEG (MW 5000) concentration on the agglomeration of gold nanorods conjugated with either $2EG_6$- or $3EG_6$- modified 15-mer thrombin aptamers.

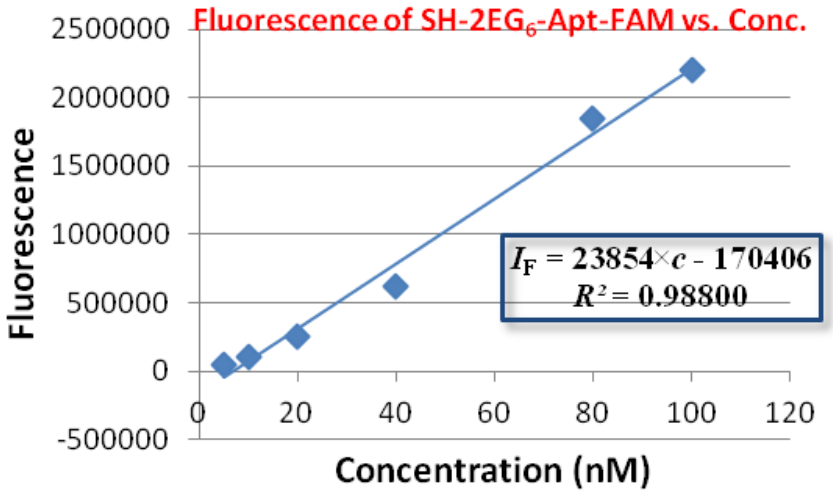

A

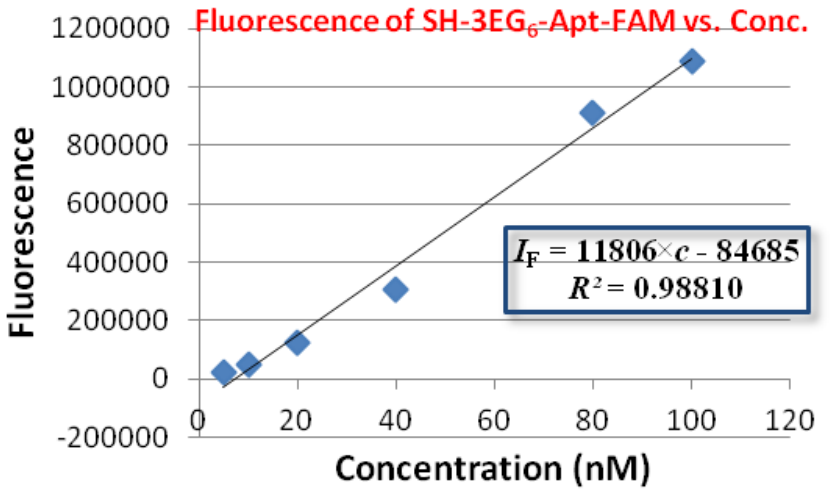

B

Figure 3-5. The fluorescence standard calibration curves for A)2EG_6- and B) 3EG_6-modified 15-mer thrombin aptamers labeled with FAM dyes.

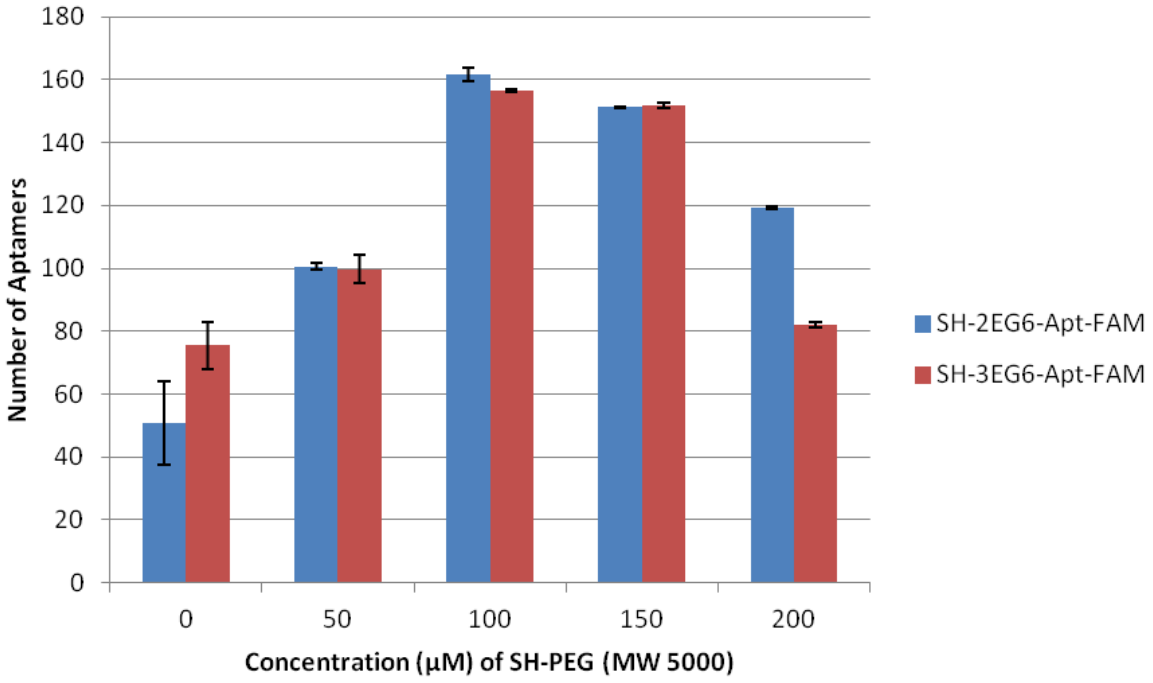

Figure 3-6. The effect of SH-PEG (MW 5000) concentration on $2EG_6$- or $3EG_6$-modified 15-mer thrombin aptamer immobilization.

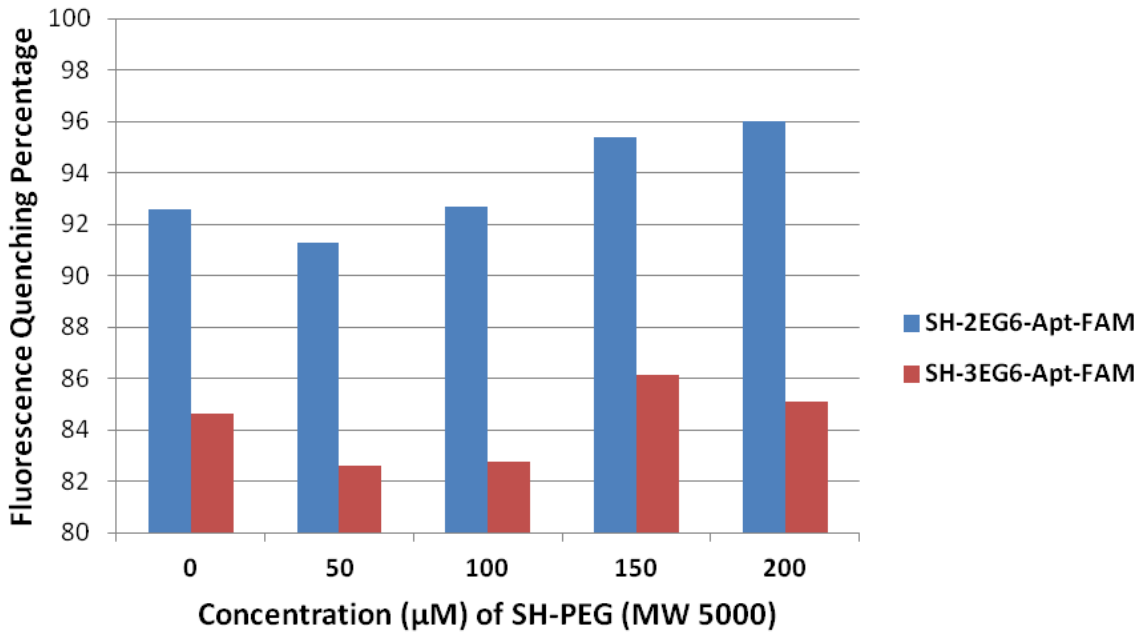

Figure 3-7. The fluorescence quenching percentages for the $2EG_6$- or $3EG_6$-modified 15-mer thrombin aptamer immobilized on the gold nanorod surface.

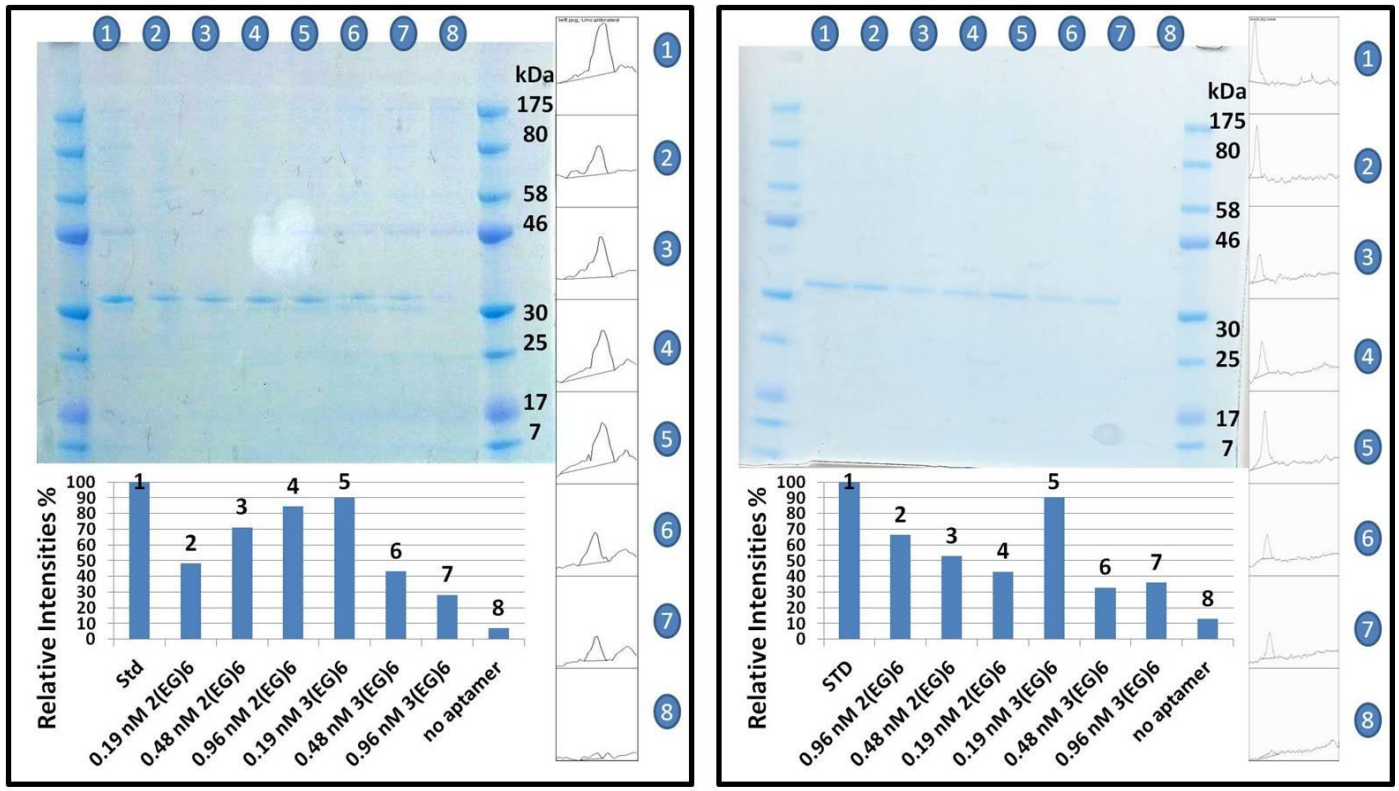

Figure 3-8. Upper panels: Gel electrophoresis of enriched α-thrombin A) from 338 ng of α-thrombin-spiked activation buffer: lane 1, α-thrombin standard; lanes 2, 3, 4, α-thrombin captured, respectively, via 0.19, 0.48 and 0.96 nM aptamer-2EG_6-AuNRs; lanes 5, 6, 7, α-thrombin captured, respectively, via 0.19, 0.48 and 0.96 nM aptamer-3EG_6-AuNRs; lane 8, α-thrombin captured via 0.48 nM of PEGylated-only gold nanorods and B) from 100 ng of α-thrombin-spiked activation buffer: lane 1, α-thrombin standard; lanes 2, 3, 4, α-thrombin captured, respectively, via 0.96, 0.48 and 0.19 nM aptamer-2EG_6-AuNRs; lanes 5, 6, 7, α-thrombin captured, respectively, via 0.19, 0.48 and 0.96 nM aptamer-3EG_6-AuNRs; lane 8, α-thrombin captured via 0.48 nM of PEGylated-only gold nanorods. Figures on the right: Pixel intensity peaks of each band drawn by ImageJ software. Lower Panels: Relative band intensities calculated by ImageJ software for the captured α-thrombin compared to α-thrombin standards to demonstrate the thrombin capture percentage.

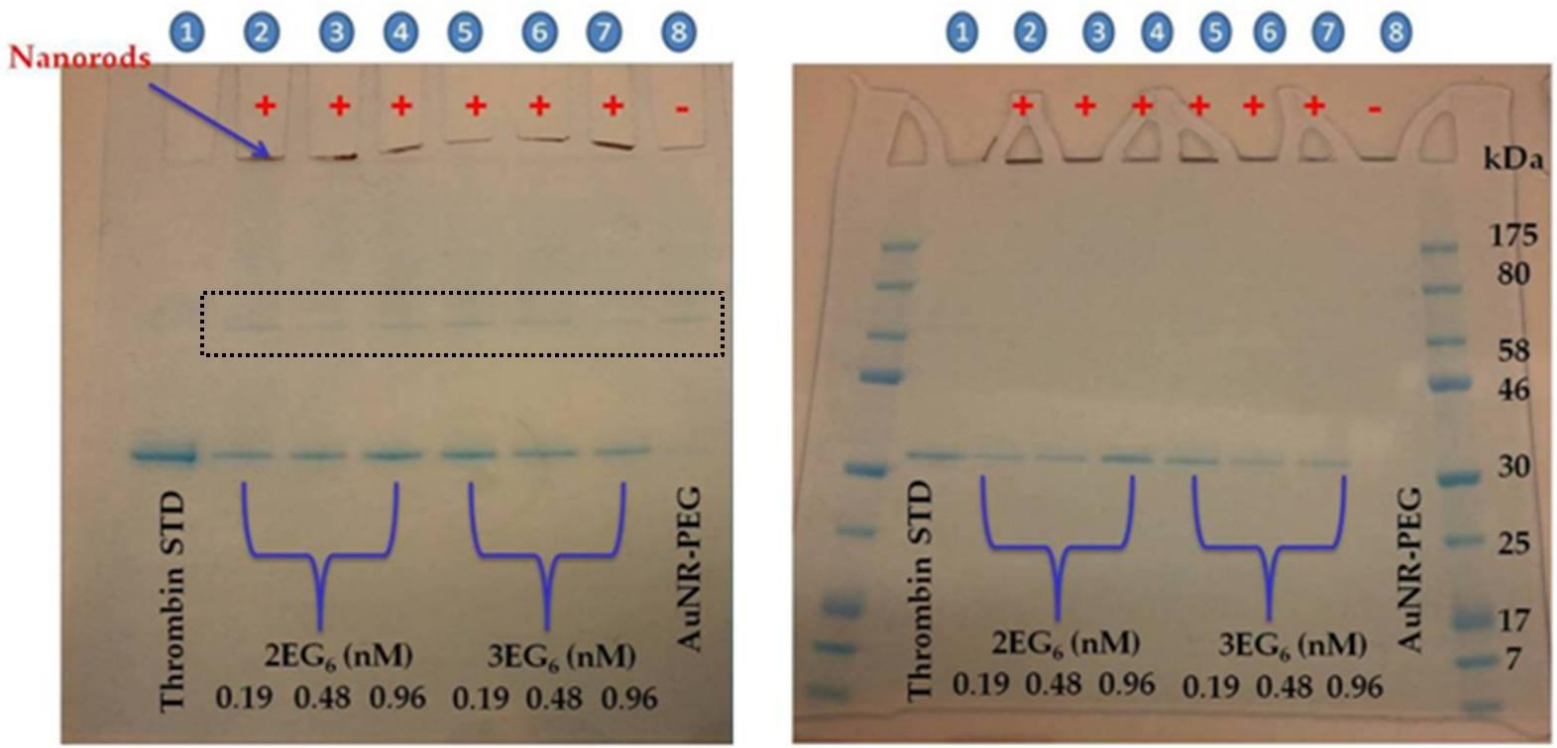

A. B

Figure 3-9. Gel electrophoresis of enriched α-thrombin from A) 338 ng and B) 100 ng of α-thrombin-spiked activation buffer: lane 1, α-thrombin standard; lanes 2, 3, 4, α-thrombin captured, respectively via 0.19, 0.48 and 0.96 nM aptamer-2EG_6-AuNRs; lanes 5, 6, 7, α-thrombin captured, respectively via 0.19, 0.48 and 0.96 nM aptamer-3EG_6-AuNRs; lane 8, α-thrombin captured via 0.48 nM of PEGylated-only gold nanorods. Dashed lines show the nonspecific BSA (66 kDa) capture via aptamer- and thiol-PEG-only-conjugated gold nanorods. "**+**" indicates the positive control, and "**-**" indicates the negative control for the thrombin band.

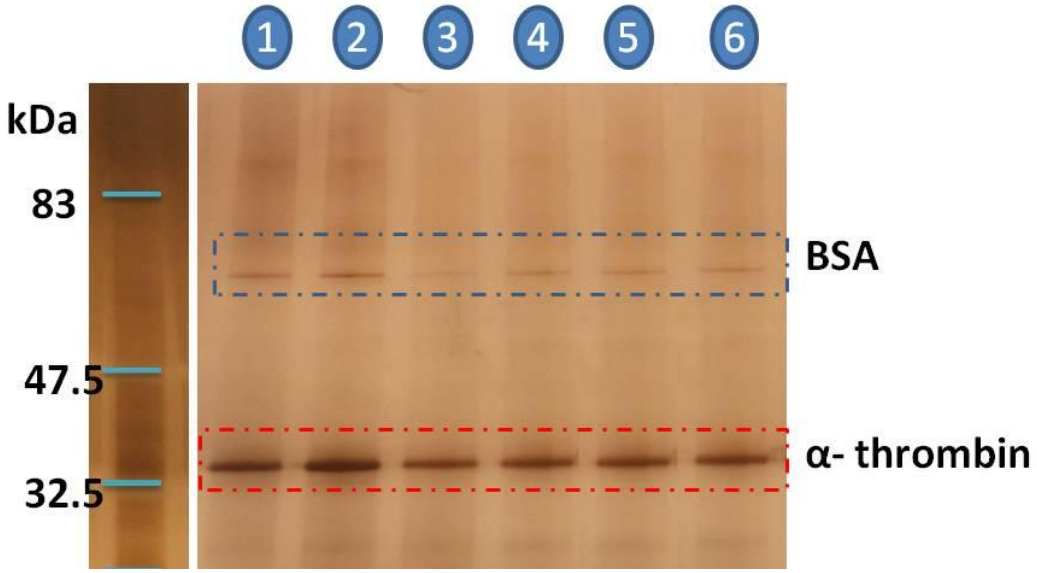

Figure 3-10. Gel electrophoresis of enriched α-thrombin from activation buffer containing 1 ng of α-thrombin: lanes 1, 2, 3, α-thrombin captured, respectively via 0.19, 0.48 and 0.96 nM aptamer-2EG_6-AuNRs; lanes 4, 5, 6, α-thrombin captured, respectively via 0.19, 0.48 and 0.96 nM aptamer-3EG_6-AuNRs.

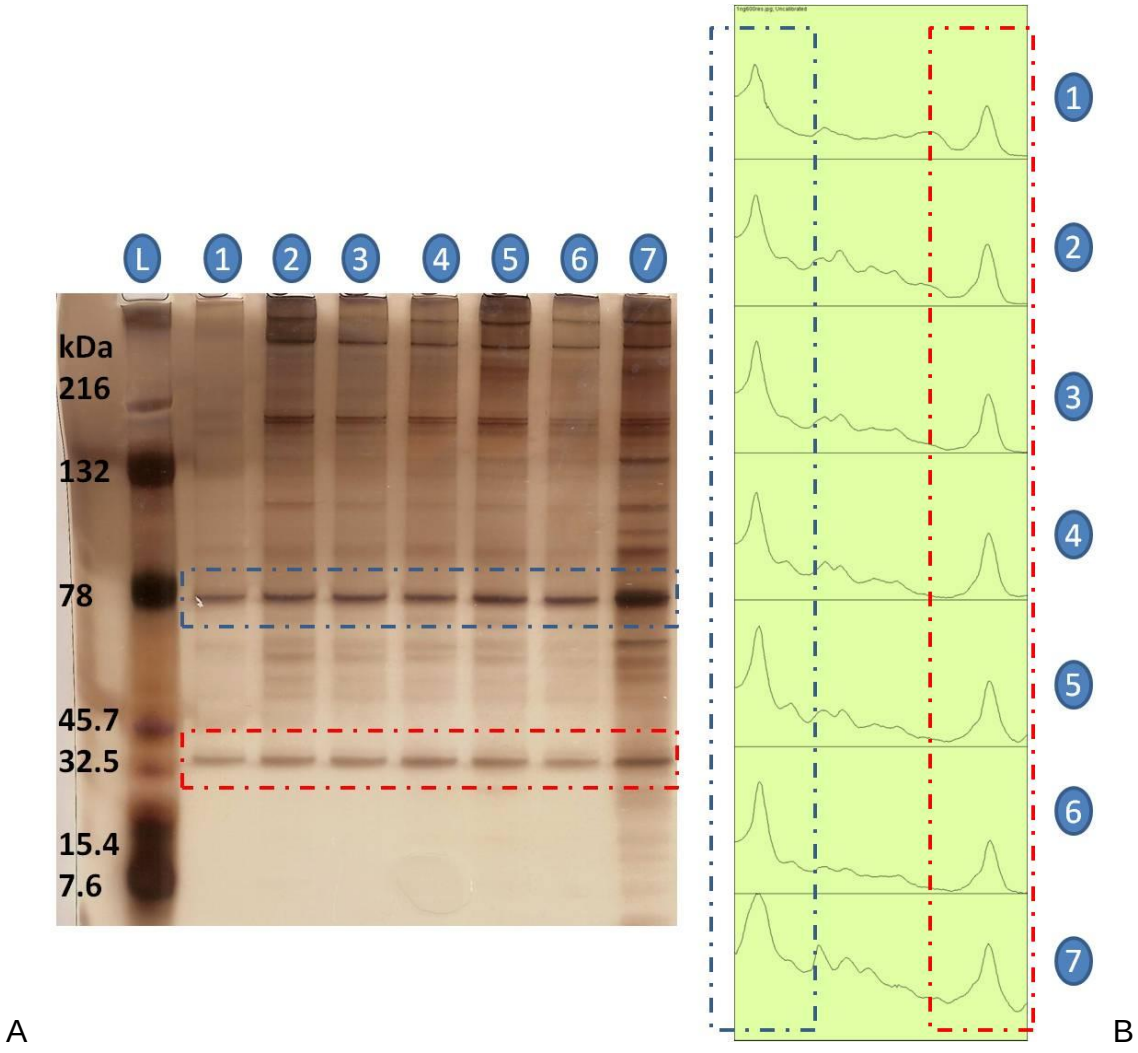

Figure 3-11. A) Gel electrophoresis of enriched α-thrombin from 1 ng α-thrombin-spiked human plasma: lane 1, α-thrombin standard; lanes 2, 3, 4, α-thrombin captured, respectively, via 0.19, 0.48 and 0.96 nM aptamer-2EG$_6$-AuNRs; lanes 5, 6, 7, α-thrombin captured, respectively, via 0.19, 0.48 and 0.96 nM aptamer-3EG$_6$-AuNRs. B) Pixel intensity peaks of each lane drawn by ImageJ software; blue dashed lines show the upper bands (72 kDa), and red dashed lines show the lower bands (37kDa).

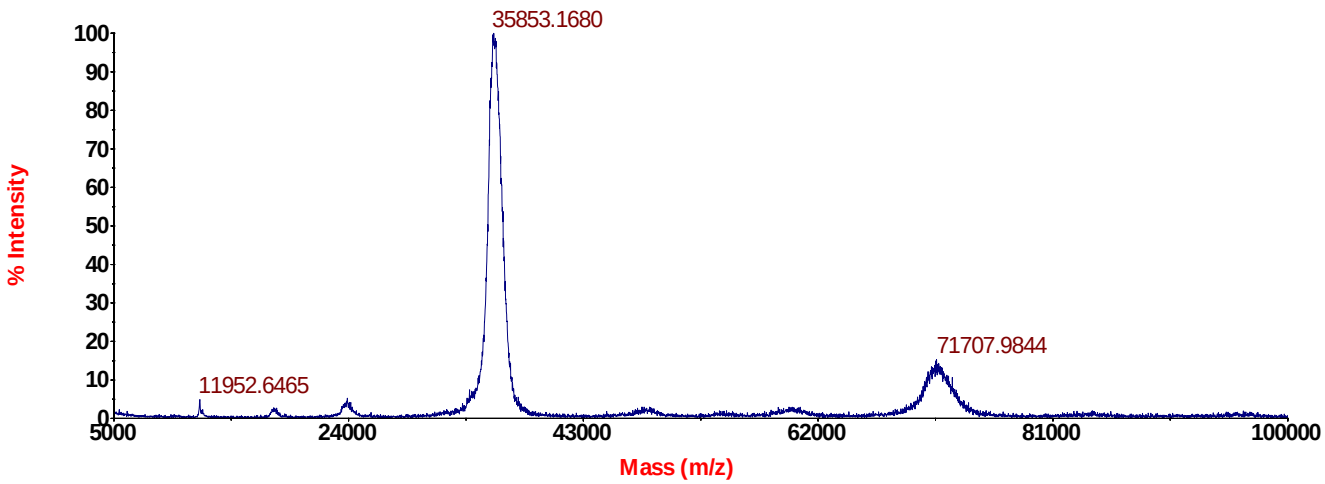

Figure 3-12. The MALDI-MS spectrum of α-thrombin (6.4µg/µL).

CHAPTER 4
IDENTIFYING RARE CANCER PROTEINS WITH APTAMER-CONJUGATED GOLD NANORODS

Introduction

In Dr. Tan's lab, Dr. Shangguan followed a two step strategy to find a protein ligand to which the corresponding aptamer binds.[15] First step is the aptamer selection through the cell-SELEX method for the related cancer cell line, and the second step is the biomarker discovery to identify the protein ligand of the selected aptamer. Firstly, a group of aptamers were generated for the CCRF-CEM cell line or also called as T-cell acute lymphoblastic leukemia (T-ALL). The aptamer, sgc8c showed high specificity and binding affinity to the T-ALL cells, but it didn't show binding to the normal human bone marrow cells or lymphoma cells. This can be an indication that the target protein of sgc8c can be a biomarker for leukemia. So the biotin modified sgc8c aptamers were incubated with the cell lysate of CCRF-CEM cell line, and then the protein-sgc8c complex was captured by incubating them with streptavidin modified magnetic beads (Figure 4-1). After capturing the protein-sgc8c complex, magnetic beads were collected by applying a magnetic field. The captured proteins were isolated by heating the beads and analyzed by SDS-PAGE technique. They were loaded into a SDS-polyacrylamide gel (12%) and after the gel electrophoresis; the gel was stained with Colloidal Blue. In order to realize, if the protein was specifically captured, a nonbinding sequence was also incubated with the cell lysate and the captured proteins from this sequence were also loaded into the same gel. After comparing with the ones captured with nonbinding sequence, the differential protein bands in the gel captured with the sgc8c aptamer were excised and digested in situ to be analyzed by QSTAR LC-MS/MS and a MASCOT database search at the Protein Chemistry Core Facility, University of Florida.

After MS analysis and database matching, protein tyrosine kinase-7 (PTK7) was identified as the biomarker.

After the model work done in Chapter 3, in this study, aptamer conjugated AuNRs were used to capture the biomarkers of DLD-1 (colorectal adenocarcinoma), a colon cancer cell line. This cell line was chosen since two aptamers were selected from our lab that can bind to it in high affinities. And gold nanorods were chosen for the reasons listed in Chapter 3.

Colon cancer cells highly express PTK7, actually PTK7 was discovered from colon cancer cell lines. This gene was thought to be expressed in colon carcinomas, but not in normal colon. Thus it can be a biomarker and may be involved in tumor progression. Therefore, sgc8c aptamer can bind to DLD-1 cell line very well. Also Dr. Sefah from Dr. Tan's lab had selected an aptamer that binds to DLD 1, KCHA10a[118], but the biomarker protein for this aptamer is still unknown. The goal of this study is to capture and detect both biomarkers simultaneously with sgc8c and KCHA10a modified gold nanorods, utilizing SDS-PAGE technique (Figure 4-3). In order to achieve this, nonbinding aptamer modified gold nanorods can be used as a negative control. For this study, TDO5 aptamer was chosen as the nonbinding aptamer. TDO5 is the aptamer for Ramos cells[20], but it doesn't show any affinity against DLD-1 cell line (Figure 4-4).

Materials and Methods

Cell Culturing

DLD-1 (CCL-221, epithelial cell, human colorectal adenocarcinoma) as target cells were cultured at 37 °C under a 5% CO_2 atmosphere. The cell culture medium consists of RPMI 1640 medium (American Type Culture Collection), 10% heat inactivated fetal bovine serum (FBS, Invitrogen, Carlsbad, USA) and penicillin-streptomycin (100 IU/mL,

GIBCO). After splitting the cells, when the dishes of DLD-1 reached a certain number (20 dishes), the cells were scrapped. The scrapped cells were collected and removed from their cell medium by low speed centrifugation at 1500 rpm for 5 min. The pellet of the cells was then washed twice with cold PBS buffer (10 mL) by centrifuging at 1500 rpm for 5 min. The final pellet of the cells was then resuspended in 3 mL PBS buffer and stored at -80°C.

Synthesis of Aptamers

The aptamers that were selected to target the DLD-1 cell line: sgc8c, 5`-ATC TAA CTG CTG CGC CGC CGG GAA AAT ACT GTA CGG TTA GA-3`. KCHA10a, 5`-ACG CAG CAG GGG AGG CGA GAG CGC ACA ATA ACG ATG GTT GGG ACC CAA CTG TTT GGA CA-3`. The nonbinding aptamer that was selected: TDO5, 5`-AAC ACC GGG AGG ATA GTT CGG TGG CTG TTC AGG GTC TCC TCC CGG TG-3`.

The selected aptamers were coupled with 5′-thiol modifier for conjugation to the gold nanorod surface and were labeled with fluorescein (FITC, FAM) at the 3′-end using 3′-(6-fluorescein) CPG to detect and quantify the aptamer modification on the gold nanorod surface. Also, two hexaethyloxy-glycol units (EG_6) were added between the thiol and aptamer sequences as a spacer. The aptamers were synthesized by solid-state phosphoramidite chemistry at a 1-µmol scale using an ABI3400 DNA/RNA synthesizer (Applied Biosystems, Foster City, CA). The completed sequences were then deprotected in AMA (ammonium hydroxide/40% aqueous methylamine 1:1) at 65 °C for 20 min and further purified using a ProStar HPLC (Varian, Walnut Creek, CA) with a C18 column (Econosil, 5 µm, 250×4.6 mm) from Alltech (Deerfield, IL). A Cary

Bio-300 UV spectrometer (Varian, Walnut Creek, CA) was used to measure the absorbance to quantify the concentrations of the product sequences.

Membrane Protein Extraction Process

The scrapped cells were collected and removed from their cell medium by low speed centrifugation (1500 rpm for 5 min). The pellet of the cells was then washed twice with cold PBS buffer (10 mL) by centrifuging at 1500 rpm for 5 min. The final pellet was then resuspended in 2 mL of buffer A (Invent Biotechnologies, Inc.). Followed by the protein inhibitor addition (10X, 200 µL), the mixture was incubated on ice for 5-10 min. Then the mixture was vortexed vigorously for a minute. After that, the mixture was sonicated to fasten the cell breaking and it was incubated in cold room (at 4°C) for 30 min. After the incubation, the cell suspension was transferred to centrifuge tube filters and centrifuged at 14 000 rpm for 30 seconds. Then the filters were discarded and the pellets were resuspended by vortexing them vigorously for 10 seconds. The collected suspensions were centrifuged at 3000 rpm for 1 min. Then the precipitates were discarded and the supernatants were transferred to fresh 1.5 mL microcentrifuge tubes and centrifuged at 4°C for 10 min at 14 000 rpm. Followed by removing the supernatants (cytosol protein fraction) the pellets were resuspended (the total membrane protein fraction) in 600 µL buffer B (Invent Biotechnologies, Inc.) by repeatedly pipetting up and down or vortexing to dissolve membrane proteins. The suspension was then centrifuged at 10 000 rpm for 5 min at 4°C (the pellet contains organelle membrane proteins). The supernatant was transferred to a fresh 2.0 mL microcentrifuge tube and 1.4 mL cold PBS was added. The suspension was mixed by inverting the tube a few times. Followed by centrifuging the suspension at 16 000 rpm for 15 min, the supernatant was discarded and the pellet (isolated plasma membrane

proteins) was dissolved in 500 µL Pierce IP Lysis Buffer (Thermo Scientific, effectively solubilizes cellular proteins, 25 mM Tris-HCl pH 7.4, 150 mM NaCl, 1 mM EDTA, 1% NP-40 and 5% glycerol). To dilute the whole mixture and reduce the detergent concentration (for aptamer to bind to its target well) 500 µL of Tris-HCl buffer (25 mM Tris-HCl pH 7.4, 150 mM NaCl, 1 mM EDTA) was added. Then 200 µL of activated Deoxyribonucleic acid, single stranded from salmon testes (Sigma Aldrich, blocking agent to reduce nonspecific bindings) was added to the suspension. The whole mixture was then incubated at 4°C overnight. Finally, the suspension was divided into three groups, each consist of 400 µL fraction of the membrane proteins, before the capturing probe addition.

Also as an alternative step, since the membrane proteins were not solubilized efficiently, after the salmon DNA incubation, the suspension was centrifuged at 12 000 rpm for 4 minutes to remove the unsolubilized portion of the proteins as a pellet. Then the supernatant was used as the solubilized portion of the membrane proteins.

Incubation of Membrane Proteins with Aptamer Conjugated AuNRs

A volume of 100 µL of 1 nM AuNR-Aptamer (Sgc8c, KCHA10a and TDO5) were centrifuged at 14 000 rpm for 4 min. The supernatant was removed and the pellets were resuspended in 100 µL of Tris-HCl buffer (25 mM Tris-HCl pH 7.4, 150 mM NaCl, 1 mM EDTA). Then each 100 µL of AuNR-Aptamer (Sgc8c, KCHA10a, and TDO5) were incubated with 400 µL fraction of the isolated membrane proteins at 4°C for 2 h. After the incubation, the mixtures were washed three times with 500 µL of washing buffer (20 mM Tris-HCl, 0.5% NP-40) by centrifuging at 12 500 rpm for 4 minutes at 4°C. Finally, the pellets were resuspended in 10 µL of Tris-HCl buffer (25 mM Tris-HCl pH 7.4, 150 mM NaCl, 1 mM EDTA).

One-Dimensional Gel Electrophoresis and Gel Staining

A volume of 10 µL of the AuNR-Aptamer (Sgc8c, KCHA10a and TDO5) with the proteins captured from membrane extracts were mixed with 10 µL of gel loading buffer (NuPAGE LDS sample buffer; Invitrogen). The AuNR-Aptamer-protein mixtures were then heated at 95°C for 5 minutes to elute the captured proteins and they were loaded into the gel (4-12% Bis-Tris SDS-polyacrylamide (Invitrogen)) with a thickness of 1.0 mm. Gel separation in running buffer proceeded at a constant voltage of 200 V for 35 min. After separation, the gel was washed with DI water three times at 10 minute increments, and the gel was stained with Coomassie Blue dye (GelCode Blue Stain Reagent, Thermo Scientific) for 1 hour. If necessary, the gel was also stained by the silver staining method using a SilverQuest Staining Kit (Invitrogen). Then the stained gel was scanned with a scanner, and the bands in the gel were analyzed to see any differential bands for the positive controls (AuNR-sgc8c and AuNR-KCHA10a) compared to the negative control (AuNR-TDO5).

Results and Discussion

Aptamer Binding Tests

In Figure 4-4, it can be seen that, both sgc8c and KCHA10a aptamer showed a good binding against DLD-1 cell line. Also TDO5 aptamer didn’t show any affinity against the DLD-1 cell line, so it can easily be used as a nonbinding sequence (negative control) for the protein capturing experiments. Moreover, despite the high affinity of sgc8c against the DLD-1 cell line, KCHA10a didn’t show any affinity against CEM cell line, which can indicate that there is no competition between the sgc8c and KCHA10a aptamers (They don’t both bind to PTK7 protein).

Verification and Quantification of Aptamer Immobilization on AuNRs

As it was mentioned earlier, the average number of aptamers immobilized on the surface per gold nanorod was found by dividing the concentration of aptamers immobilized on the surface by the concentration of the gold nanorods used in conjugation.[47,70] After the necessary calculations, the average numbers of aptamers immobilized on the surface per gold nanorod were found to be 95, 137 and 147 for KCHA10a, sgc8c and TDO5 aptamers, respectively (Figure 4-5). Even though, the same procedure was followed for the aptamer conjugation, the quantity of the aptamers per gold nanorod surface differs for each aptamer. This is probably due to the differences in the length and tertiary structures of the aptamers. The number of bases of each aptamer is 59, 41 and 48 for KCHA10a, sgc8c and TDO5 aptamers, respectively (Figure 4-5)

Capturing of Cancer Proteins with Aptamer Conjugated AuNRs

Firstly, the membrane proteins were isolated from the cell lysate of 100 million DLD-1 cells (Figure 4-2). After the incubation of AuNR-Aptamer (sgc8c, TDO5 and KCHA10a) with the isolated membrane proteins, the AuNR-Aptamer-Protein complex was heated at 65°C for 5 minutes to elute the captured proteins. However, as it can be seen in the gel image (Figure 4-6), this temperature was not enough to isolate the captured proteins from the AuNR surface. The captured proteins couldn't run into the gel and they accumulated at the top of the wells because AuNRs can't run into the gel and the captured proteins were still on the AuNRs. Also after the incubation, AuNR-Aptamer-Protein complex couldn't be collected fully, since the centrifuging speed was arranged to be 3 000 rpm because at higher centrifuging speeds, membrane proteins

could also precipitate with AuNRs nonspecifically. These are the main reasons to observe very weak and smear bands in the gel in Figure 4-6.

So in the second trial (Figure 4-7), the isolated membrane proteins were first centrifuged at 12 000 rpm for 4 minutes to remove the unsolubilized portion of the proteins as a pellet. Then the supernatant, as the solubilized portion of the membrane proteins were incubated with the aptamer conjugated AuNRs. Also after the incubation, AuNR-Aptamer-Protein complex was heated at 95°C for 5 minutes to elute the captured proteins, instead of heating at 65°C. However, no strong differential bands could be observed for the positive controls (AuNR-sgc8c and AuNR-KCHA10a). Then the number of cells was increased to prepare the cell lysate of DLD-1. Even though the number of cells were doubled (from 100 million to 200 million cells) to prepare the cell lysate, again no strong differential bands could be obtained for the positive controls (Figure 4-8 and Figure 4-9).

In order to test, if the isolated membrane protein suspension indeed contained the biomarker proteins, an ELISA-like assay was applied to the membrane protein solution that was washed off after the incubation with aptamer conjugated AuNRs (Figure 4-10). In this assay, the protein solutions were incubated with the sgc8c-FITC aptamer and then the unbound aptamers were washed away. Then the HRP (horseradish peroxidase) modified antibody that can bind to FITC was introduced and then unbound antibodies were washed away. Thus, if there is PTK7 in the protein solution, then with the addition of the substrate, the enzyme will cleave the substrate, which causes a color change in the substrate solution as a signal. The signal for the washed off membrane protein solution was considerably high compared to the controls, which indicates the

high content of PTK7 that couldn't be captured by the AuNR-sgc8c. Finally, the number of cells were increased up to 380 million to prepare the cell lysate of DLD-1 cells,but again no strong differential bands could be obtained for the positive controls (Figure 4-11).

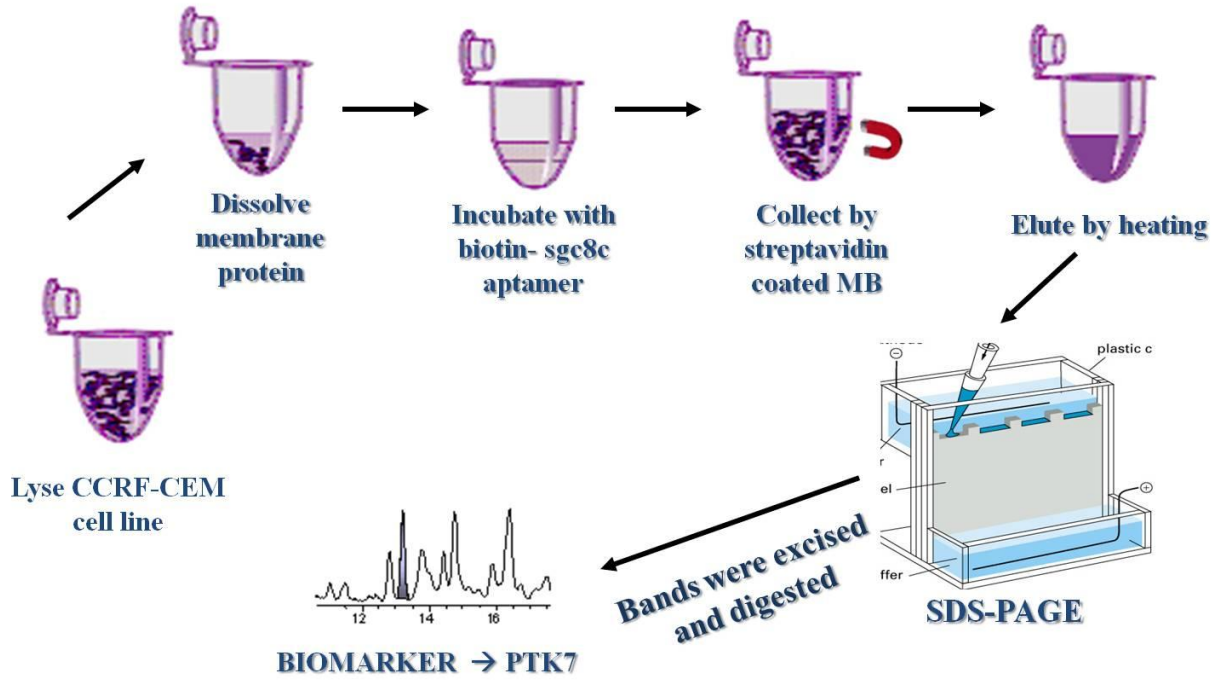

Figure 4-1. The biomarker discovery route of CCRF-CEM cell line.

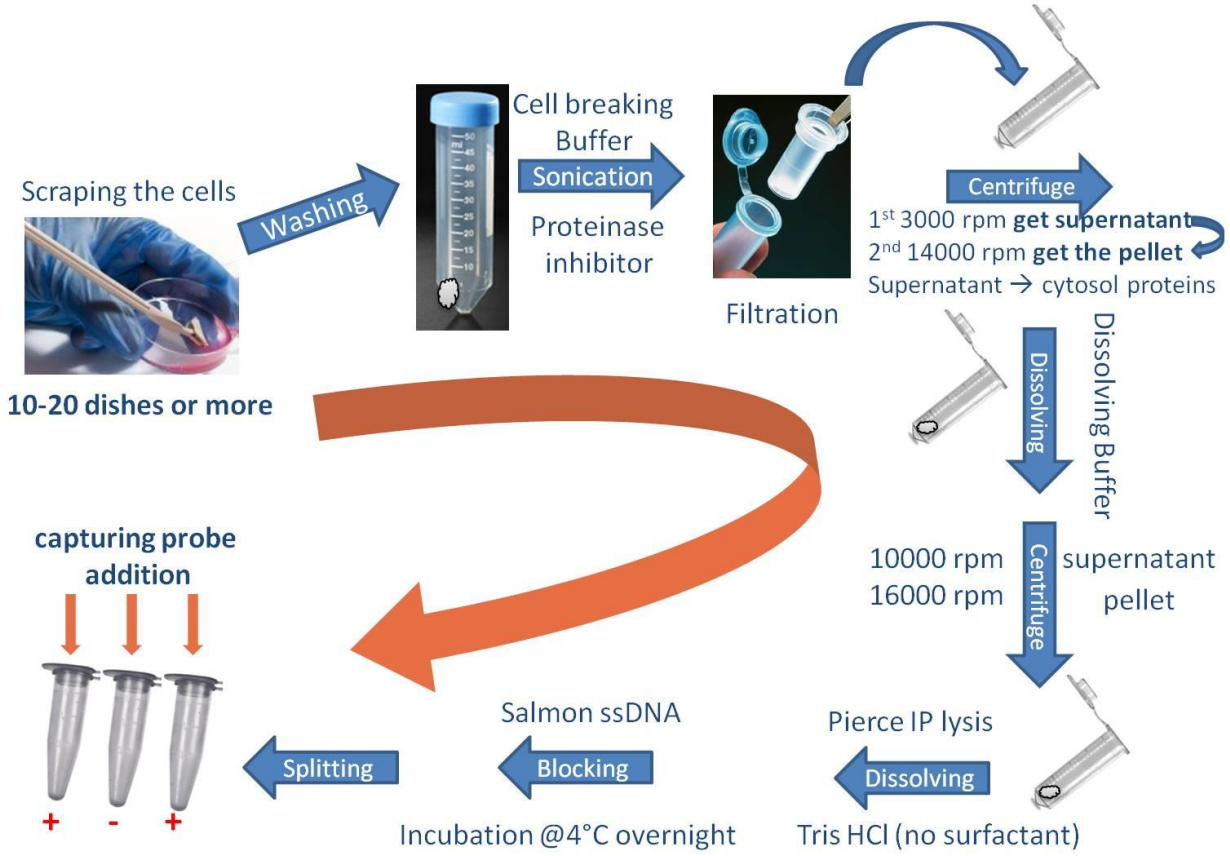

Figure 4-2. The steps for the membrane protein extraction. ("+" refers to the binding probes "-" refers to the nonbinding probes)

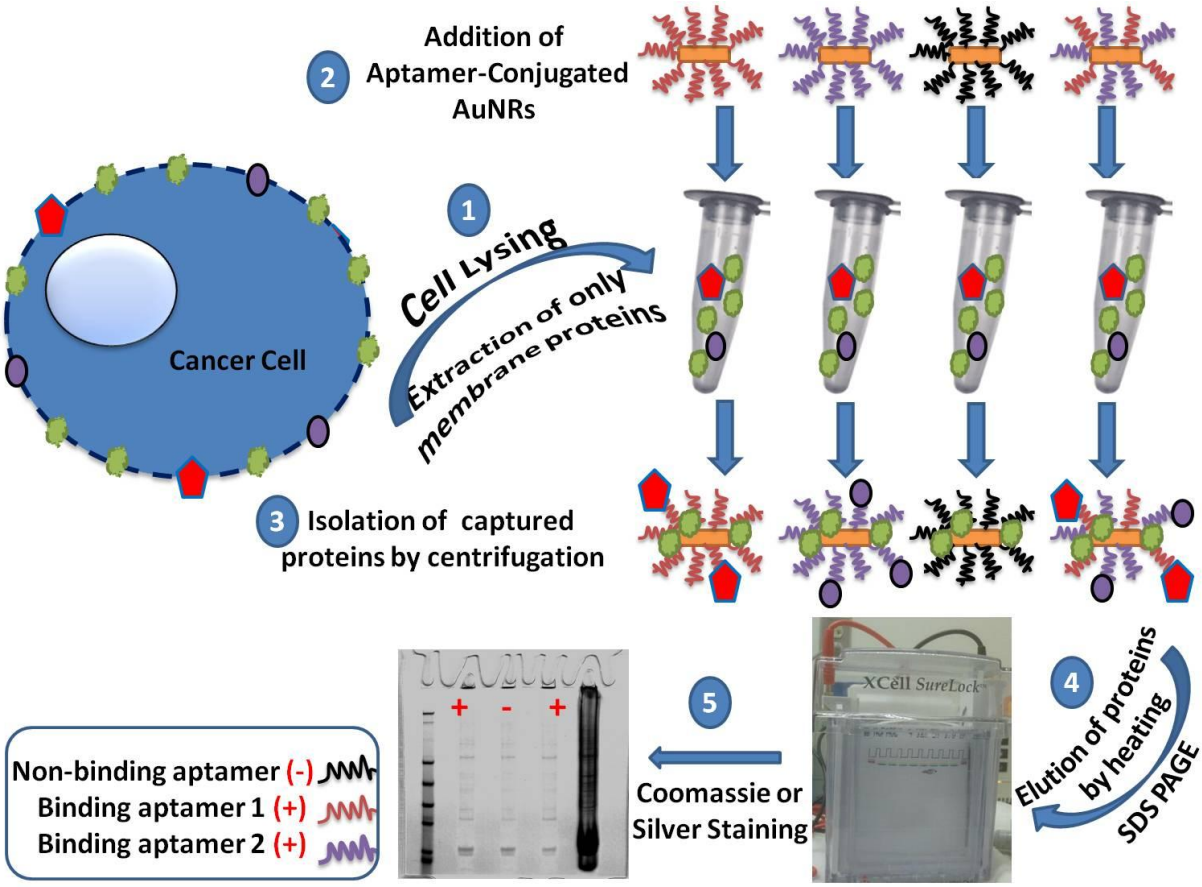

Figure 4-3. The general scheme for the rare cancer protein capturing and detection via aptamer conjugated gold nanorods.

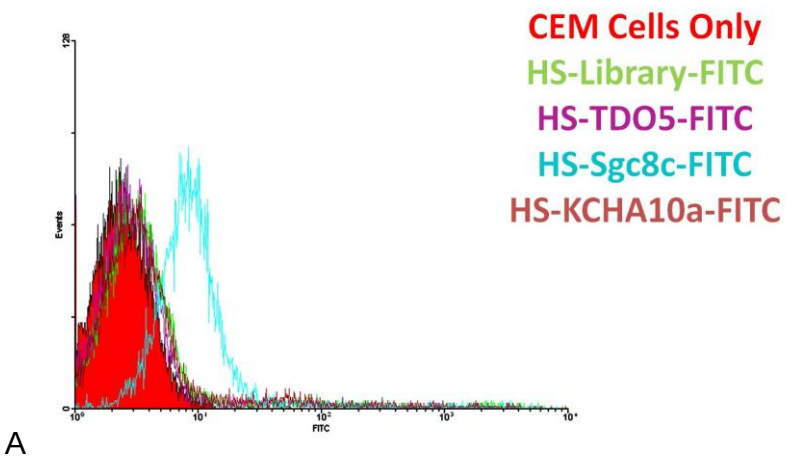

A

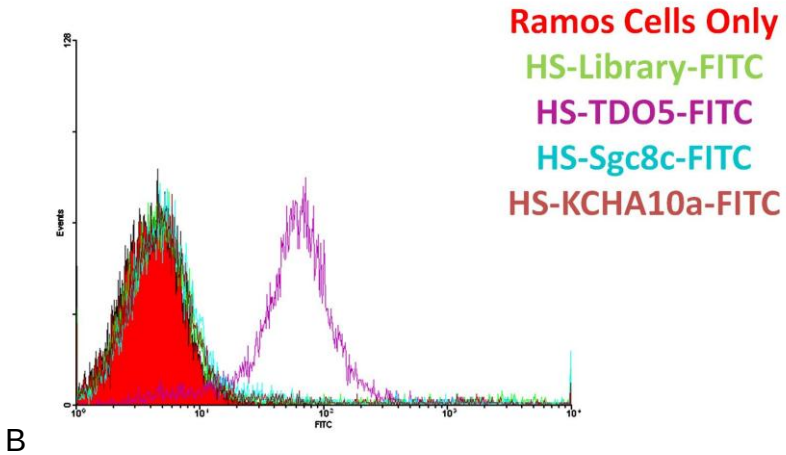

B

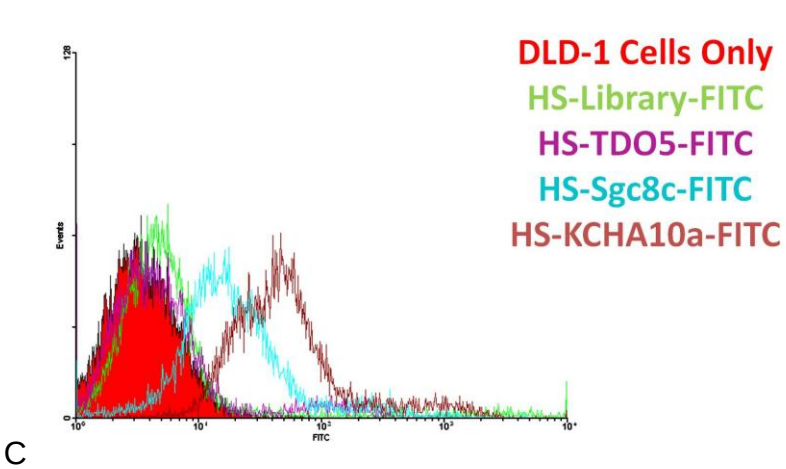

C

Figure 4-4. Flow cytometric assay to monitor the binding of aptamers (200 nM): sgc8c, TDO5, KCHA10a with A) CEM cells, B) Ramos Cells, C) DLD-1 Cells (1 million cells for each).

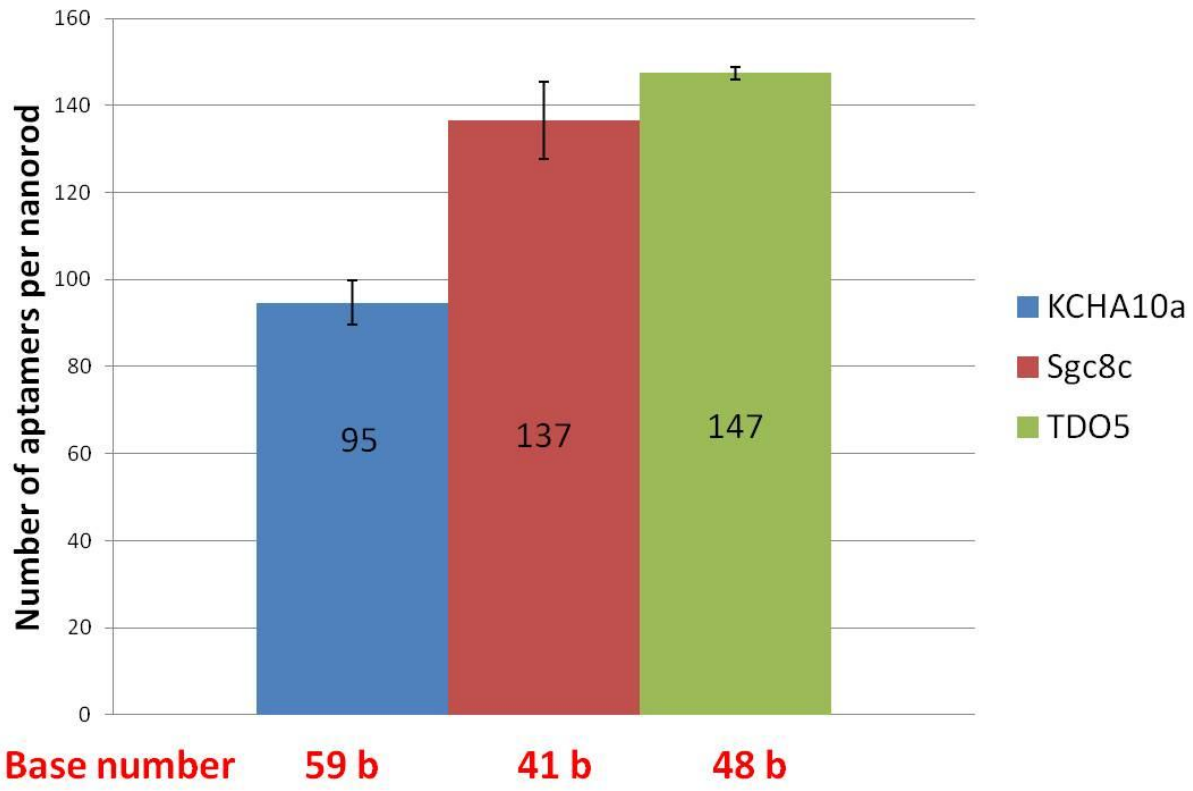

Figure 4-5. The average number of aptamers immobilized on a gold nanorod surface. ("b" refers to the bases)

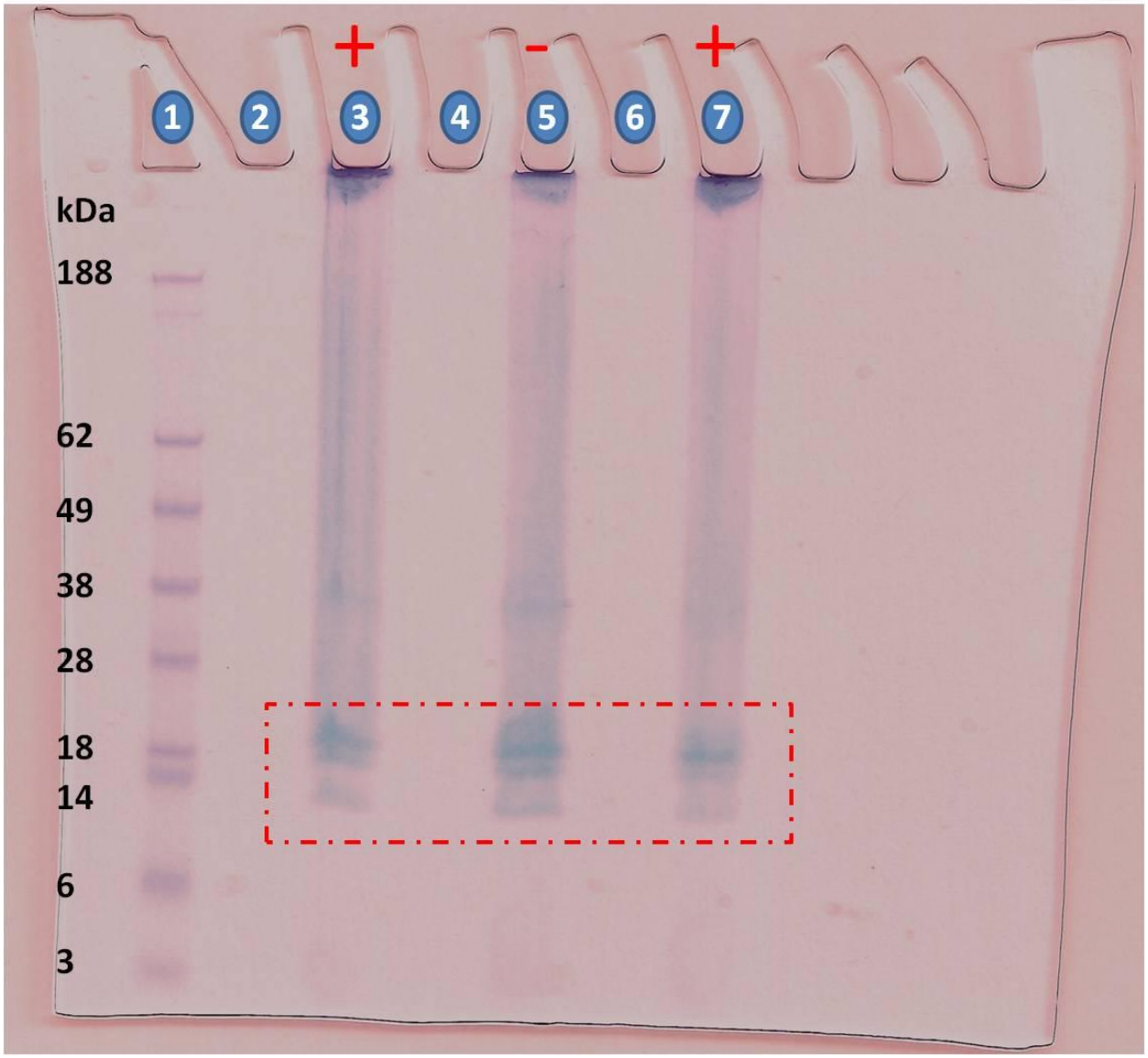

Figure 4-6. Gel electrophoresis of captured proteins from the membrane proteins isolated from the cell lysate of 100 million DLD-1 cells: lane 1, protein marker; lane 3, proteins captured with AuNR-sgc8c (positive control); lane 5, proteins captured with AuNR-TDO5 (negative control); lane 7, proteins captured with AuNR-KCHA10a (positive control). AuNR-Aptamer-Protein complex was heated at 65°C for 5 minutes to elute the captured protein before loading into the gel.

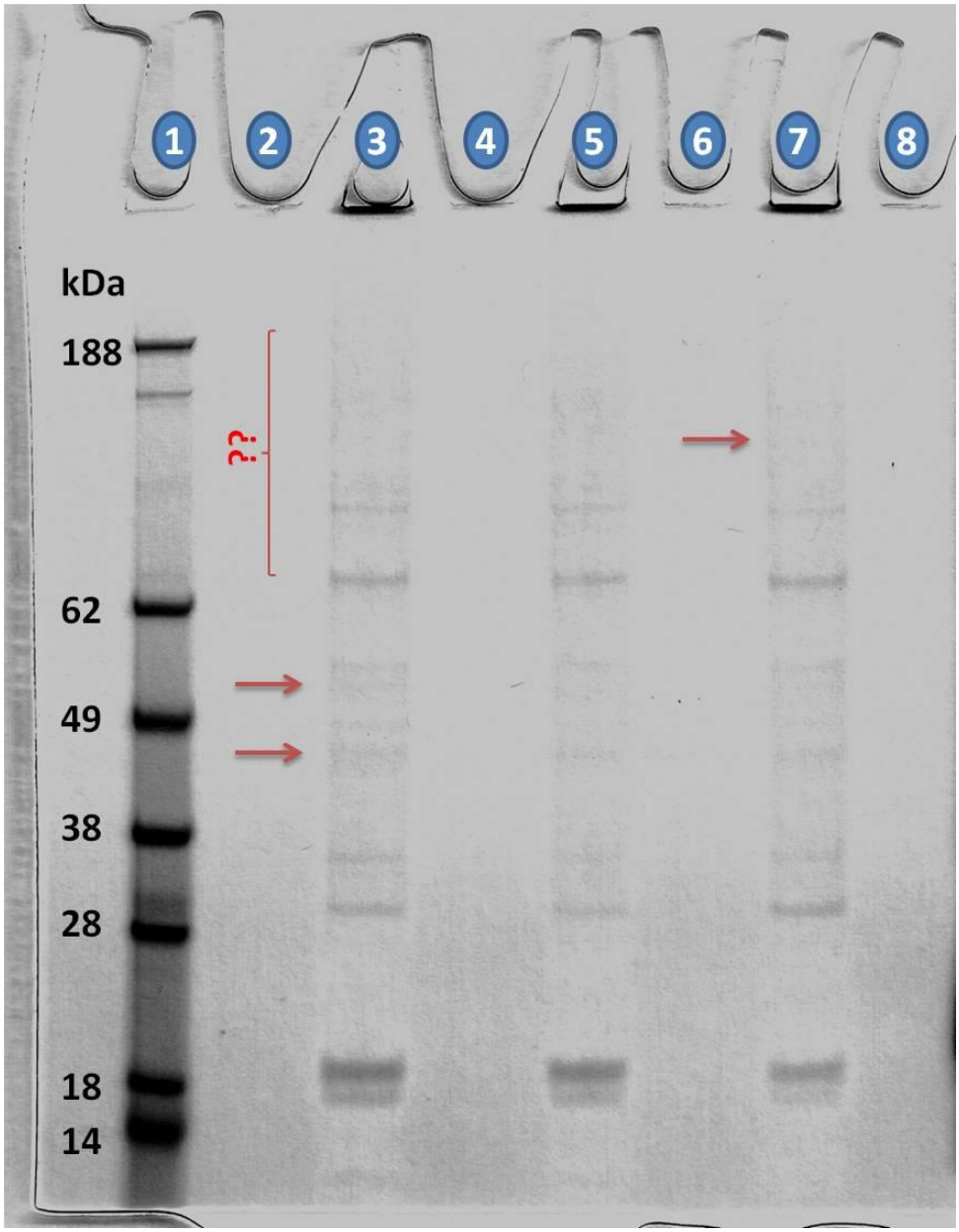

Figure 4-7. Gel electrophoresis of captured proteins from the membrane proteins isolated from the cell lysate of 100 million DLD-1 cells: lane 1, protein marker; lane 3, proteins captured with AuNR-sgc8c (positive control); lane 5, proteins captured with AuNR-TDO5 (negative control); lane 7, proteins captured with AuNR-KCHA10a (positive control). AuNR-Aptamer-Protein complex was heated at 95°C for 5 minutes to elute the captured protein before loading into the gel. ("→" refers to possible different bands)

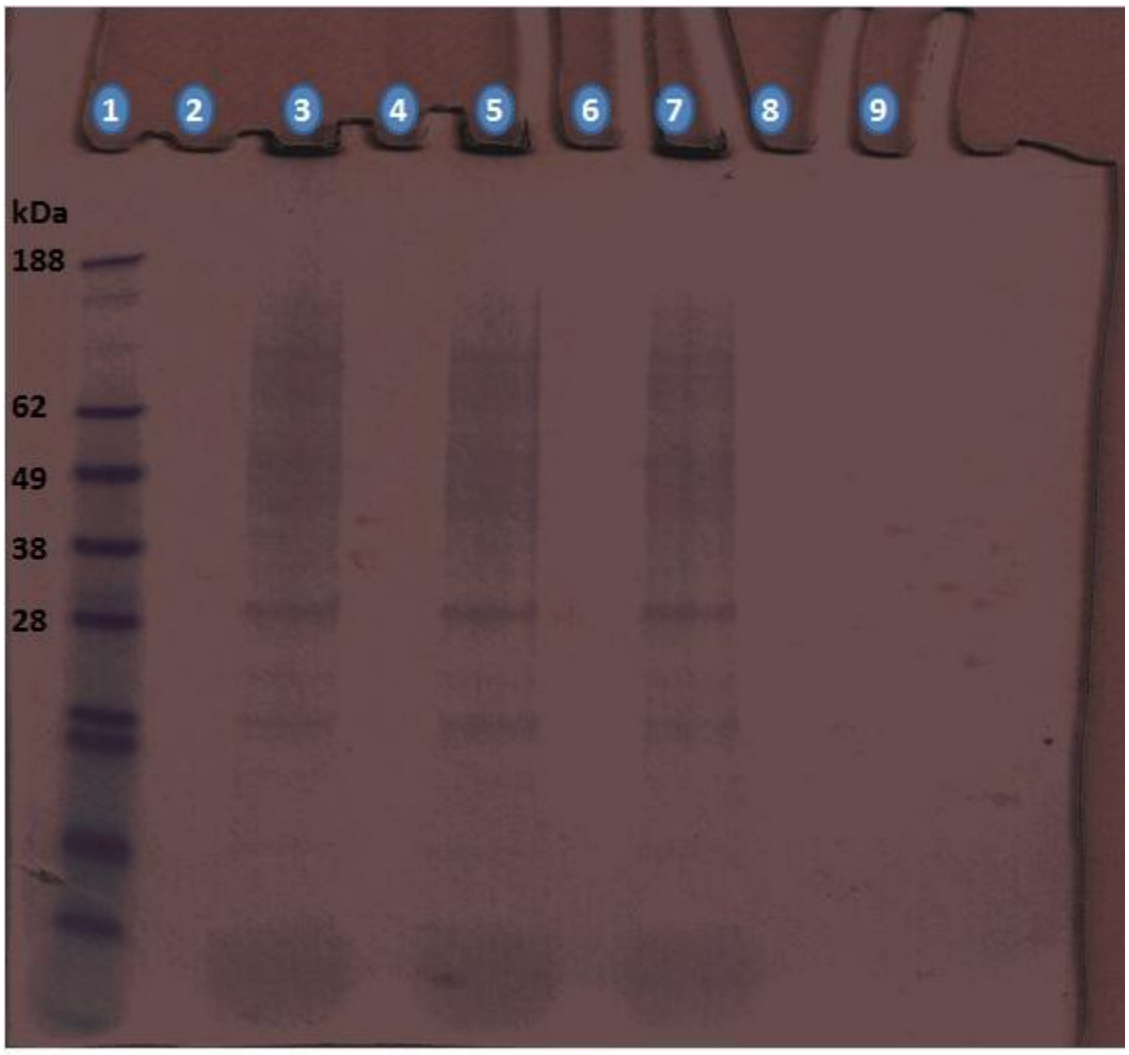

Figure 4-8. Gel electrophoresis of captured proteins from the membrane proteins isolated from the cell lysate of 200 million DLD-1 cells: lane 1, protein marker; lane 3, proteins captured with AuNR-sgc8c (positive control); lane 5, proteins captured with AuNR-TDO5 (negative control); lane 7, proteins captured with AuNR-KCHA10a (positive control). AuNR-Aptamer-Protein complex was heated at 95°C for 5 minutes to elute the captured protein before loading into the gel.

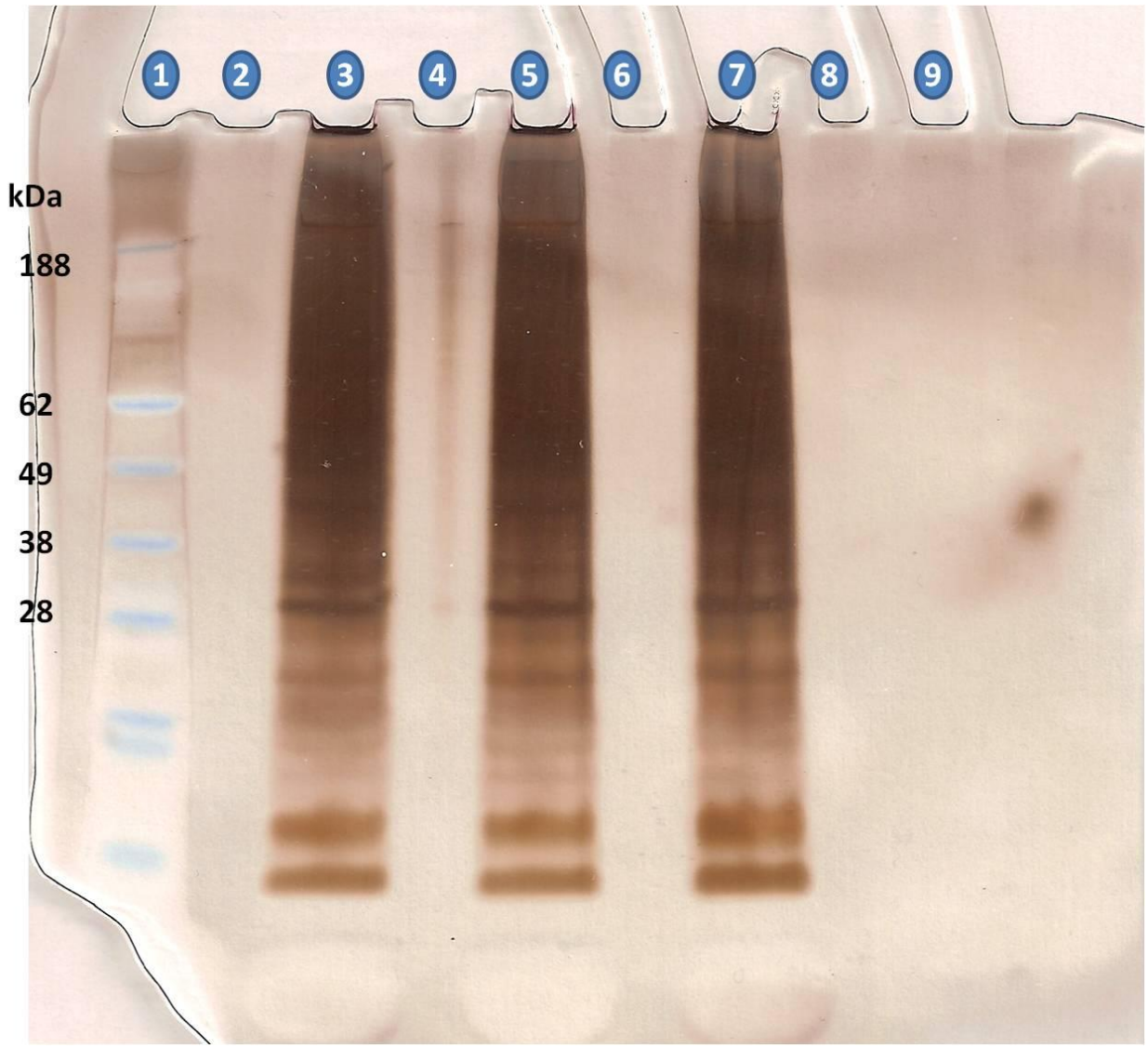

Figure 4-9. The previous gel (Figure 4-8) was stained with silver staining.

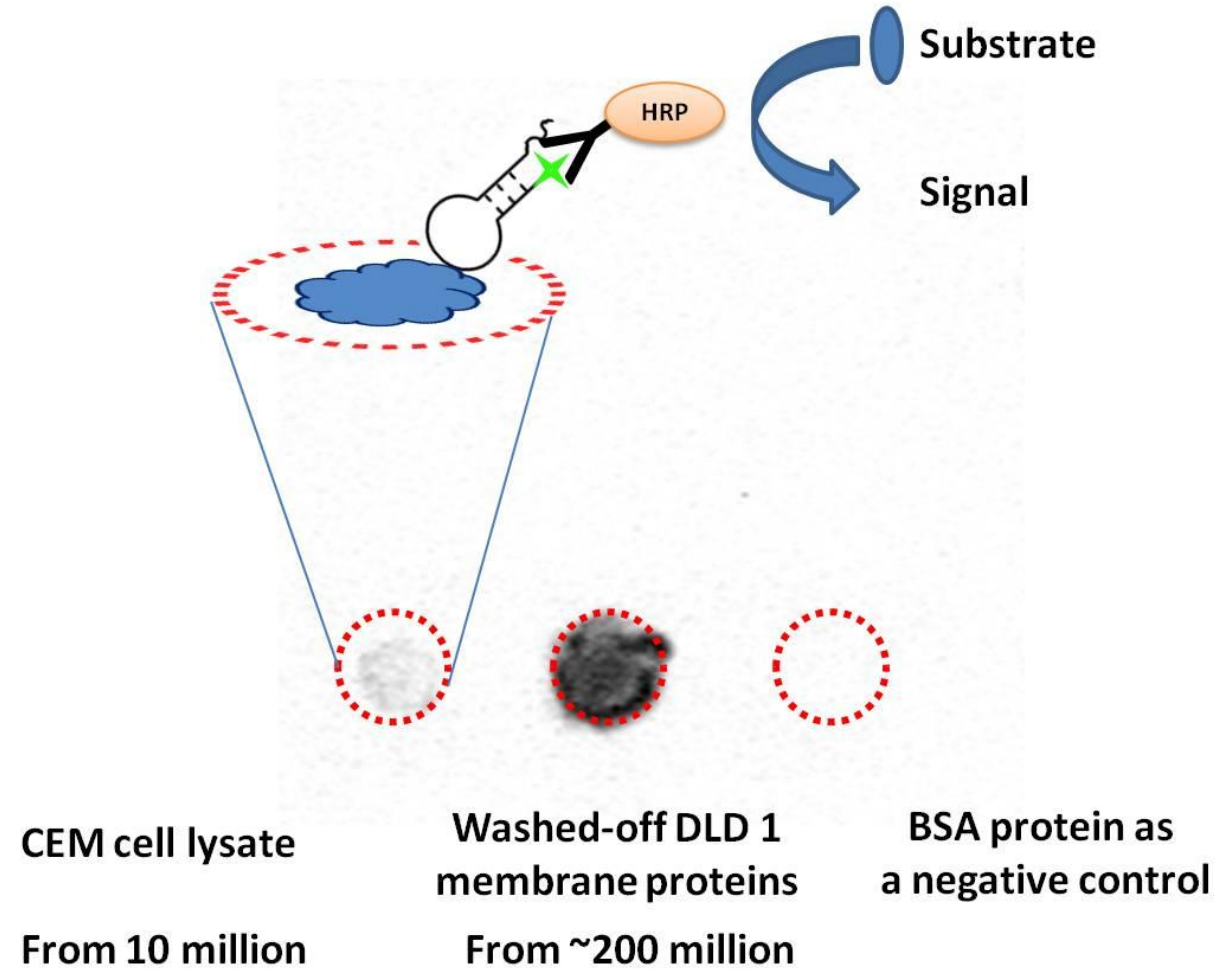

Figure 4-10. Testing for the PTK7 existence in the membrane protein solution that was washed off after the incubation with the AuNR-sgc8c.

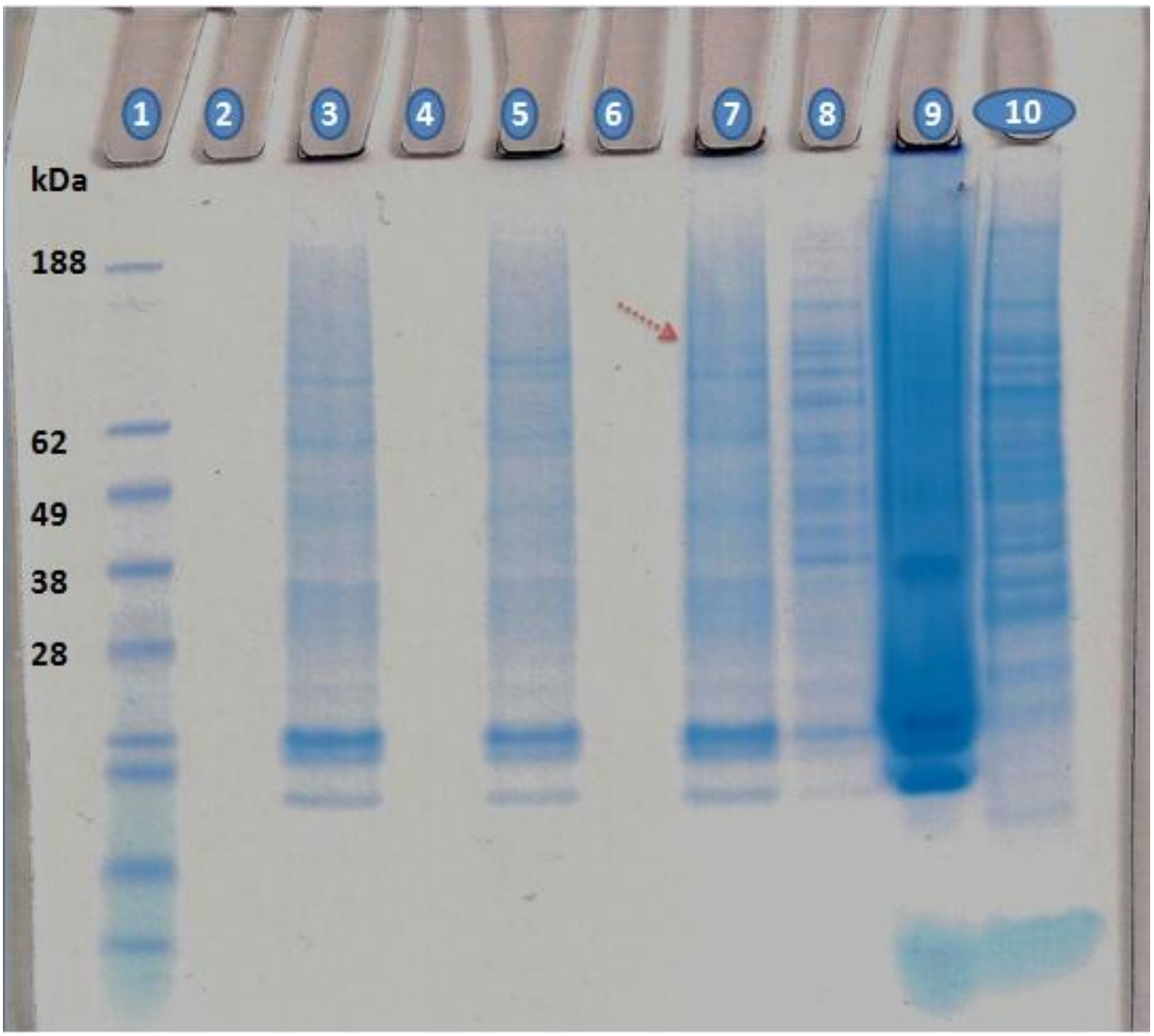

Figure 4-11. Gel electrophoresis of captured proteins from the membrane proteins isolated from the cell lysate of 380 million DLD-1 cells: lane 1, protein marker; lane 3, proteins captured with AuNR-sgc8c (positive control); lane 5, proteins captured with AuNR-TDO5 (negative control); lane 7, proteins captured with AuNR-KCHA10a (positive control); lane 8, cytosol proteins isolated from the cell lysate; lane 9, proteins captured with AuNR-KCHA10a from cytosol proteins; lane 10, membrane proteins isolated from the cell lysate. AuNR-Aptamer-Protein complex was heated at 95°C for 5 minutes to elute the captured protein before loading into the gel.

CHAPTER 5
FACILE ISOLATION AND DETECTION OF RARE CANCER PROTEINS WITH APTAMER-CONJUGATED SILVER MICROSPHERES

Introduction

Until now, various types of aptamer conjugated nano/micro particles have been used to isolate the biomarker proteins from the corresponding cancer cell lines. The most commonly used isolation techniques depending on the intrinsic properties of those particles are centrifugation[5] and magnetic separation[15,20] upon the capture of target protein. However, in this very recent work, silver microspheres (SMSs) offer a novel separation method, gravitational separation[76-78] owing to their heavy nature. They can be suspended in their solutions while shaking and when they are set aside, they can come down easily with the things bound on their surface (Figure 5-1). In this way, there is no need for external stimuli to separate the captured proteins and protein isolation can take only seconds. On the other hand, silver microspheres can be relatively easily synthesized compared to other nanoparticles without using any surfactants as templates. The lack of surfactants will avoid them to suspend in the solutions. So the combination of specificity provided by the aptamers towards the target cancer proteins and the easy separation provided by the silver microspheres might ease the separation and detection of the biomarker proteins.

Materials and Methods

Synthesis of Silver Microspheres

A volume of 1108 µL of 0.675 M $AgNO_3$ was added to 1240 µL of 2.45 M NH_2OH aqueous solution. This leads to a large amount of precipitate (SMSs) formation in seconds. Then this mixture was washed with DI water for three times and resuspended in 2.35 mL of DI water.[77]

Aptamer Immobilization to the surface of Silver Microspheres

A volume of 35 µL of 25 µM TCEPylated aptamers were incubated with 20 µL of SMSs while oscillating at room temperature for 2 h. Then the mixture was washed three times with DNA grade water. Finally, the aptamer conjugated SMSs were dispersed in 20 µL of DNA grade water.

Results and Discussion

According to the TEM images, SMSs likes to form clusters (Figure 5-2 A). They don't have uniform shape due to the lack of surfactants as templates in the synthesis route. They have this spiky spherical-like shape. The average size of those SMSs is 993 ± 269 nm in diameter (Figure 5-2 A).

In order to see, if the aptamer conjugated SMSs can bind to the target cells, SMS-sgc8c was incubated with DLD-1 cells. From the confocal images (Figure 5-3), it can be seen that the aptamer immobilization on the surface of the SMSs was efficient and also SMS-sgc8c could bind to DLD-1 cells. The SMSs clusters wrapped around the DLD-1 cells with high fluorescence signals coming from the FITC dye on the sgc8c aptamers.

Figure 5-4 shows the first trial of the protein capturing with SMS-Aptamer from the membrane proteins isolated from the cell lysate of 100 million DLD-1 cells. Even though, no differential bands were observed for the positive controls, the background of the gel was clearer (except the scattered SMSs that were accumulated at the top of the wells) and the band of the proteins were stronger compared to the gel in Figure 4-7.

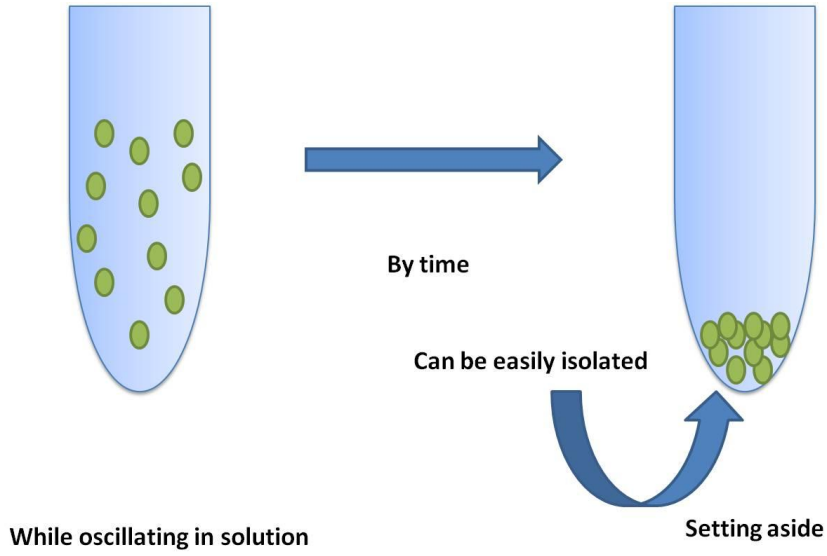

Figure 5-1. The easy isolation of the silver microspheres via gravitational separation.

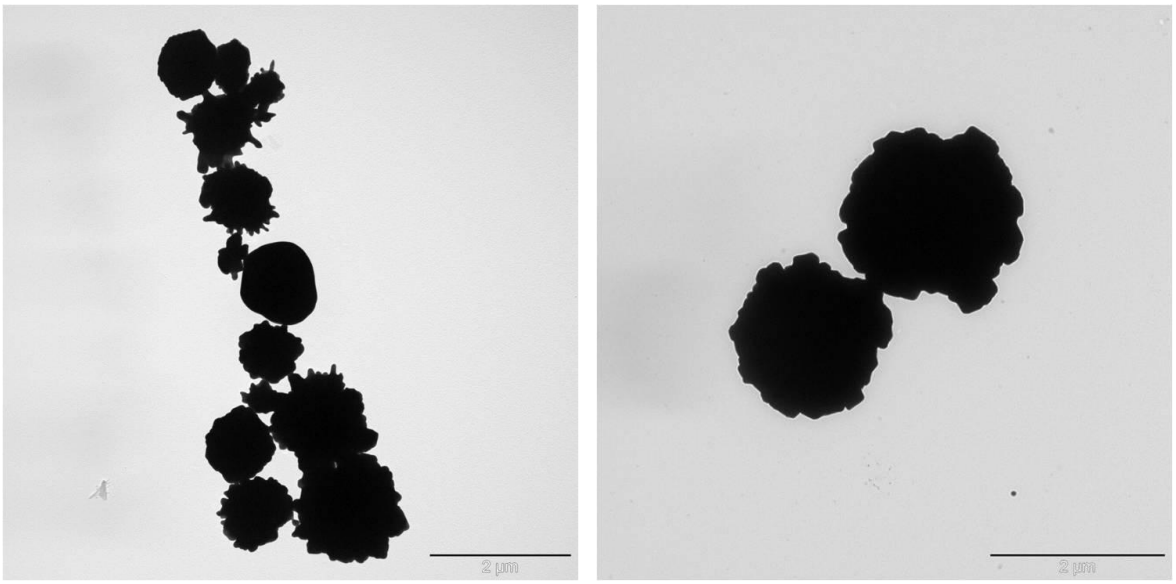

A B

Figure 5-2. The TEM images of the synthesized Silver Microspheres. A) Clustering of Silver Microspheres, B) Individual Silver Microspheres.

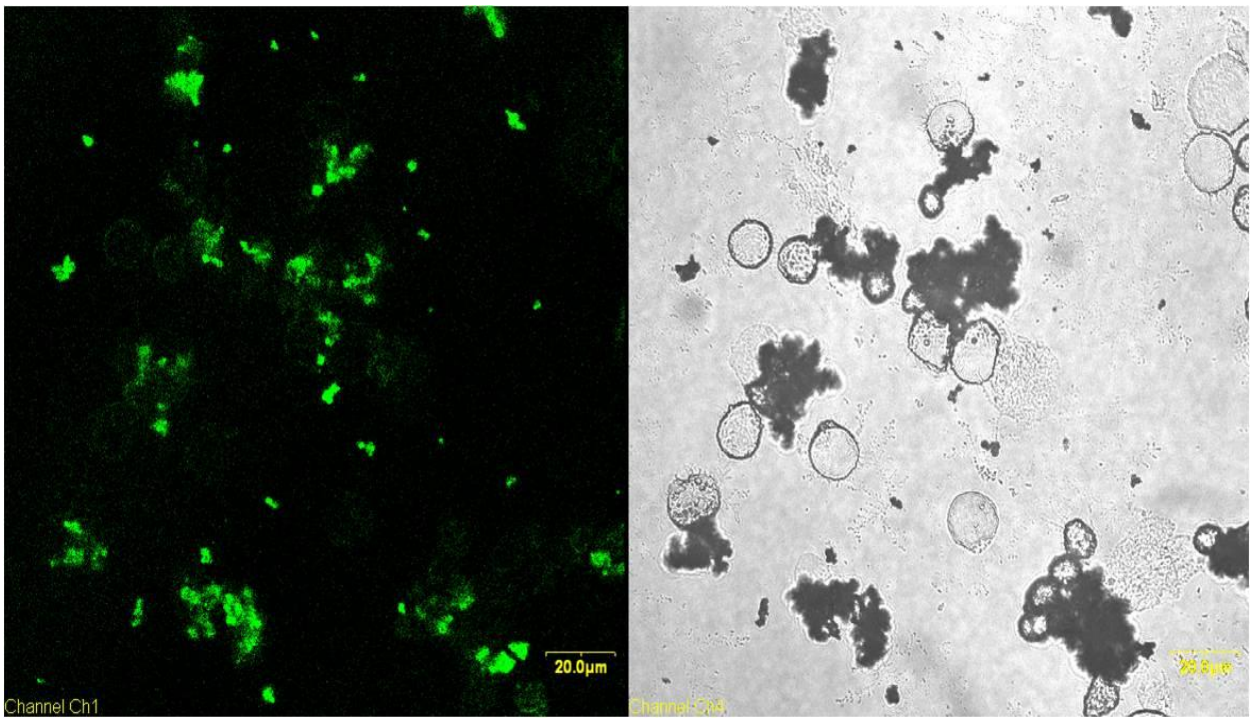

Figure 5-3. Confocal images of DLD-1 cells (1 million) incubated with SMS-sgc8c (10 µL) at 4°C for 30 min.

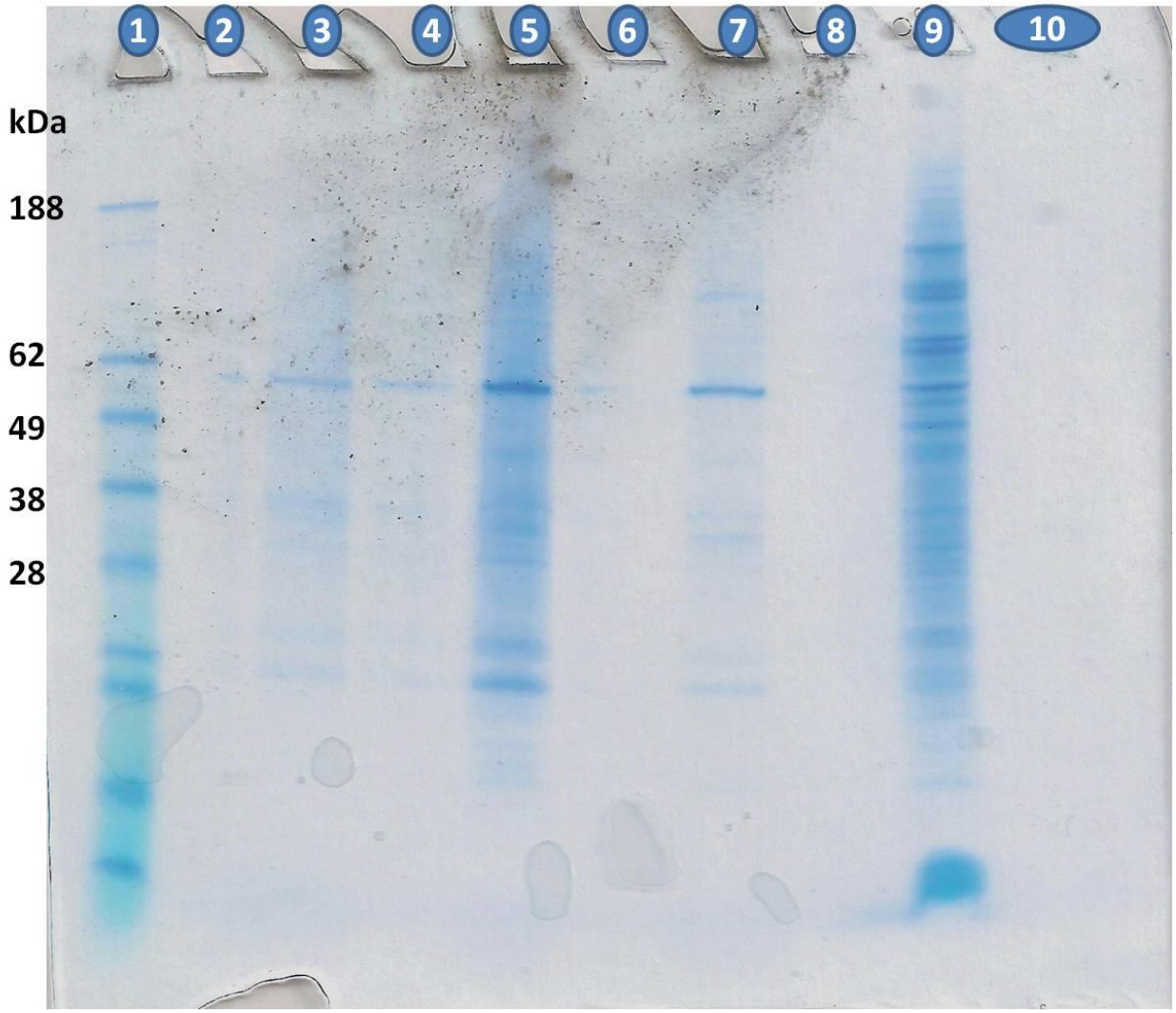

Figure 5-4. Gel electrophoresis of captured proteins from the membrane proteins isolated from the cell lysate of 100 million DLD-1 cells: lane 1, protein marker; lane 3, proteins captured with SMS-sgc8c (positive control); lane 5, proteins captured with SMS-TDO5 (negative control); lane 7, proteins captured with SMS-KCHA10a (positive control); lane 9, membrane proteins isolated from the cell lysate. 20 µL of SMS-Aptamer was used in the incubations. SMS-Aptamer-Protein complex was heated at 95°C for 5 minutes to elute the captured protein before loading into the gel.

CHAPTER 6
SUMMARY AND FUTURE DIRECTIONS

In the first project, CTAB induced nonspecificity and toxicity, the major challenges encountered in photothermal therapy applications of gold nanorods were dramatically decreased prior to the NIR treatment with BSA modification of the aptamer conjugated gold nanorods. This is an indication of the vital role of the surface modification where gold nanorods and aptamers couldn't show their superior properties.

After capturing the model protein, α-thrombin in ppb levels from plasma samples with aptamer conjugated gold nanorods, the same system was used to capture biomarkers of DLD-1 (a colon cancer cell line). Unfortunately, the biomarker proteins couldn't be captured to be identified. The reason could be the sizes of AuNRs. The sizes of AuNRs are not big enough to capture these big membrane proteins. For example, in the α-thrombin capturing project, almost all of the α-thrombin that was spiked in plasma samples could be captured, since the size of thrombin protein was only 4 nm, whereas the size of AuNR was about 70 nm. However, membrane proteins could be much bigger than thrombin protein. For example, BSA protein (66 kDa) has an ellipsoid shape and one of its dimensions is 14 nm. So PTK7 should be much bigger than that with the MW of 120 kDa (maybe 30 nm or even bigger). These sizes of the proteins can cause some steric hindrance while binding to the surface of AuNRs that have a limited space, even though there are lots of aptamers (hundreds) ready to bind to its target protein on the surface. In the light of these, silver microspheres can be a remedy. They have a huge surface area (in micron size like magnetic beads) and facilitate the isolation by gravitational separation owing to their heavy nature.[76-78] This can also avoid the problem of losing the membrane proteins that are not fully

solubilized, since before incubation with the AuNR-Aptamer, the membrane protein solution was centrifuged at 12 000 rpm to get rid of the unsolubilized portion of the membrane proteins as a precipitate and the supernatant, which consists of the solubilized portion was incubated with the AuNR-Aptamer. Then the mixture was centrifuged at 12 500 rpm to pull down the complex of protein-Aptamer-AuNRs. In this process, obviously some of the membrane proteins were lost, but gravitational isolation is a promising separation technique, which will eliminate these centrifuging steps. So the number of the cells will be increased up to 400 million to prepare the cell lysate of DLD-1 cells to increase the overall protein content. Then the same protein capturing procedure will be repeated with the aptamer conjugated SMSs.

LIST OF REFERENCES

(1) Anderson, N. L.; Anderson, N. G. *Mol. Cell. Proteomics* **2002**, *1*, 845-867.

(2) Darmanis, S.; Nong, R. Y.; Hammond, M.; Gu, J.; Alderborn, A.; Vanelid, J.; Siegbahn, A.; Gustafsdottir, S.; Ericsson, O.; Landegren, U.; Kamali-Moghaddam, M. *Mol. Cell. Proteomics* **2010**, *9*, 327-335.

(3) Kirk, J. S.; Bohn, P. W. *J. Am. Chem. Soc.* **2004**, *126*, 5920-5926.

(4) Wang, A.; Wu, C. J.; Chen, S. H. *J. Proteome. Res.* **2006**, *5*, 1488-1492.

(5) Cheng, P. C.; Chang, H. K.; Chen, S. H. *Mol. Cell. Proteomics* **2010**, *9*, 209-224.

(6) Olsson, A. K.; Dimberg, A.; Kreuger, J.; Claesson-Welsh, L. *Nat. Rev. Mol. Cell. Biol.* **2006**, *7*, 359-371.

(7) Osborne, C. K.; Hamilton, B.; Titus, G.; Livingston, R. B. *Cancer Res* **1980**, *40*, 2361-2366.

(8) Ariad, S.; Seymour, L.; Bezwoda, W. R. *Breast Cancer Res. Treat.* **1991**, *20*, 11-17.

(9) Wu, C. C.; Yates, J. R. *Nat. Biotechnol.* **2003**, *21*, 262-267.

(10) Schiess, R.; Wollscheid, B.; Aebersold, R. *Mol Oncol* **2009**, *3*, 33-44.

(11) Longo, C.; Patanarut, A.; George, T.; Bishop, B.; Zhou, W.; Fredolini, C.; Ross, M. M.; Espina, V.; Pellacani, G.; Petricoin, E. F., 3rd; Liotta, L. A.; Luchini, A. *PLoS ONE* **2009**, *4*, e4763.

(12) Lawson, E. L.; Clifton, J. G.; Huang, F.; Li, X.; Hixson, D. C.; Josic, D. *Electrophoresis* **2006**, *27*, 2747-2758.

(13) Chang, P. S.; Absood, A.; Linderman, J. J.; Omann, G. M. *Anal. Biochem.* **2004**, *325*, 175-184.

(14) Shangguan, D.; Li, Y.; Tang, Z.; Cao, Z. C.; Chen, H. W.; Mallikaratchy, P.; Sefah, K.; Yang, C. J.; Tan, W. *Proc. Natl. Acad. Sci. U.S.A.* **2006**, *103*, 11838-11843.

(15) Shangguan, D.; Cao, Z.; Meng, L.; Mallikaratchy, P.; Sefah, K.; Wang, H.; Li, Y.; Tan, W. *J. Proteome. Res.* **2008**, *7*, 2133-2139.

(16) Wang, K. Y.; Krawczyk, S. H.; Bischofberger, N.; Swaminathan, S.; Bolton, P. H. *Biochemistry* **1993**, *32*, 11285-11292.

(17) Neves, M. A.; Reinstein, O.; Saad, M.; Johnson, P. E. *Biophys Chem* **2010**, *153*, 9-16.

(18) Sefah, K.; Phillips, J. A.; Xiong, X.; Meng, L.; Van Simaeys, D.; Chen, H.; Martin, J.; Tan, W. *Analyst* **2009**, *134*, 1765-1775.

(19) Meir, A.; Marks, R. S.; Stojanovic, M. N. In *Handbook of Biosensors and Biochips*; John Wiley & Sons, Ltd: 2008.

(20) Mallikaratchy, P.; Tang, Z.; Kwame, S.; Meng, L.; Shangguan, D.; Tan, W. *Mol. Cell. Proteomics* **2007**, *6*, 2230-2238.

(21) Shangguan, D.; Tang, Z.; Mallikaratchy, P.; Xiao, Z.; Tan, W. *ChemBioChem* **2007**, *8*, 603-606.

(22) Connor, E. E.; Mwamuka, J.; Gole, A.; Murphy, C. J.; Wyatt, M. D. *Small* **2005**, *1*, 325-327.

(23) Jain, P. K.; Lee, K. S.; El-Sayed, I. H.; El-Sayed, M. A. *J. Phys. Chem. B* **2006**, *110*, 7238-7248.

(24) Lee, K. S.; El-Sayed, M. A. *J. Phys. Chem. B* **2006**, *110*, 19220-19225.

(25) Sperling, R. A.; Rivera Gil, P.; Zhang, F.; Zanella, M.; Parak, W. J. In *Chem Soc Rev*; 2008/09/03 ed.; The Royal Society of Chemistry: 2008; Vol. 37, p 1896-1908.

(26) Frens, G. *Nature* **1973**, *241*, 20-22.

(27) Jana, N. R.; Gearheart, L.; Murphy, C. J. *Adv. Mater.* **2001**, *13*, 1389-1393.

(28) Martin, B. R.; Dermody, D. J.; Reiss, B. D.; Fang, M. M.; Lyon, L. A.; Natan, M. J.; Mallouk, T. E. *Adv. Mater.* **1999**, *11*, 1021-1025.

(29) van der Zande, B. M. I.; Böhmer, M. R.; Fokkink, L. G. J.; Schönenberger, C. *Langmuir* **2000**, *16*, 451-458.

(30) Cepak, V. M.; Martin, C. R. *J. Phys. Chem. B* **1998**, *102*, 9985-9990.

(31) Govindaraj, A.; Satishkumar, B. C.; Nath, M.; Rao, C. N. R. *Chem. Mater.* **2000**, *12*, 202-205.

(32) Jana, N. R.; Gearheart, L.; Murphy, C. J. *J. Phys. Chem. B* **2001**, *105*, 4065-4067.

(33) Nikoobakht, B.; El-Sayed, M. A. *Chem. Mater.* **2003**, *15*, 1957-1962.

(34) Grzelczak, M.; Perez-Juste, J.; Mulvaney, P.; Liz-Marzan, L. M. *Chem Soc Rev* **2008**, *37*, 1783-1791.

(35) Ahmadi, T. S.; Wang, Z. L.; Green, T. C.; Henglein, A.; El-Sayed, M. A. *Science* **1996**, *272*, 1924-1926.

(36) Huang, C. C.; Huang, Y. F.; Cao, Z.; Tan, W.; Chang, H. T. *Anal. Chem.* **2005**, *77*, 5735-5741.

(37) Lin, T. E.; Chen, W. H.; Shiang, Y. C.; Huang, C. C.; Chang, H. T. *Biosens. Bioelectron.* **2011**, *29*, 204-209.

(38) Chen, C. K.; Huang, C. C.; Chang, H. T. *Biosens. Bioelectron.* **2010**, *25*, 1922-1927.

(39) Xia, F.; Zuo, X.; Yang, R.; Xiao, Y.; Kang, D.; Vallee-Belisle, A.; Gong, X.; Yuen, J. D.; Hsu, B. B.; Heeger, A. J.; Plaxco, K. W. *Proc. Natl. Acad. Sci. U.S.A.* **2010**, *107*, 10837-10841.

(40) Elghanian, R.; Storhoff, J. J.; Mucic, R. C.; Letsinger, R. L.; Mirkin, C. A. *Science* **1997**, *277*, 1078-1081.

(41) Storhoff, J. J.; Elghanian, R.; Mucic, R. C.; Mirkin, C. A.; Letsinger, R. L. *J. Am. Chem. Soc.* **1998**, *120*, 1959-1964.

(42) Storhoff, J. J.; Lazarides, A. A.; Mucic, R. C.; Mirkin, C. A.; Letsinger, R. L.; Schatz, G. C. *J. Am. Chem. Soc.* **2000**, *122*, 4640-4650.

(43) Medley, C. D.; Smith, J. E.; Tang, Z.; Wu, Y.; Bamrungsap, S.; Tan, W. *Anal. Chem.* **2008**, *80*, 1067-1072.

(44) Hirsch, L. R.; Stafford, R. J.; Bankson, J. A.; Sershen, S. R.; Rivera, B.; Price, R. E.; Hazle, J. D.; Halas, N. J.; West, J. L. *Proc. Natl. Acad. Sci. U.S.A.* **2003**, *100*, 13549-13554.

(45) Huang, X.; El-Sayed, I. H.; Qian, W.; El-Sayed, M. A. *J. Am. Chem. Soc.* **2006**, *128*, 2115-2120.

(46) Dickerson, E. B.; Dreaden, E. C.; Huang, X.; El-Sayed, I. H.; Chu, H.; Pushpanketh, S.; McDonald, J. F.; El-Sayed, M. A. *Cancer Lett* **2008**, *269*, 57-66.

(47) Huang, Y. F.; Sefah, K.; Bamrungsap, S.; Chang, H. T.; Tan, W. *Langmuir* **2008**, *24*, 11860-11865.

(48) Goodrich, G. P.; Bao, L.; Gill-Sharp, K.; Sang, K. L.; Wang, J.; Payne, J. D. *J Biomed Opt* **2010**, *15*, 018001.

(49) Chen, J.; Wang, D.; Xi, J.; Au, L.; Siekkinen, A.; Warsen, A.; Li, Z. Y.; Zhang, H.; Xia, Y.; Li, X. *Nano Lett.* **2007**, *7*, 1318-1322.

(50) Wang, Y. W.; Xie, X. Y.; Wang, X. D.; Ku, G.; Gill, K. L.; O'Neal, D. P.; Stoica, G.; Wang, L. V. *Nano Lett.* **2004**, *4*, 1689-1692.

(51) Eghtedari, M.; Oraevsky, A.; Copland, J. A.; Kotov, N. A.; Conjusteau, A.; Motamedi, M. *Nano Lett.* **2007**, *7*, 1914-1918.

(52) Oraevsky, A. A.; Li, P.-C.; Wei, C.-W.; Liao, C.-K.; Chen, C.-D.; Pao, K.-C.; Wang, C.-R. C.; Wu, Y.-N.; Shieh, D.-B.; Wang, L. V. *Proc SPIE* **2006**, *6086*, 60860M.

(53) Agarwal, A.; Huang, S. W.; O'Donnell, M.; Day, K. C.; Day, M.; Kotov, N.; Ashkenazi, S. *J. Appl. Phys.* **2007**, *102*, 064701.

(54) Song, K. H.; Kim, C.; Maslov, K.; Wang, L. V. *Eur J Radiol* **2009**, *70*, 227-231.

(55) Yang, X.; Skrabalak, S. E.; Li, Z. Y.; Xia, Y.; Wang, L. V. *Nano Lett.* **2007**, *7*, 3798-3802.

(56) Kang, H.; Trondoli, A. C.; Zhu, G.; Chen, Y.; Chang, Y. J.; Liu, H.; Huang, Y. F.; Zhang, X.; Tan, W. *ACS Nano* **2011**, *5*, 5094-5099.

(57) Anderson, R. R.; Parrish, J. A. *Journal of Investigative Dermatology* **1981**, *77*, 13-19.

(58) Yang, X.; Stein, E. W.; Ashkenazi, S.; Wang, L. V. *Wiley Interdiscip. Rev. Nanomed. Nanobiotechnol.* **2009**, *1*, 360-368.

(59) Huang, X.; El-Sayed, I.; El-Sayed, M. In *Cancer Nanotechnology*; Grobmyer, S. R., Moudgil, B. M., Eds.; Humana Press: 2010; Vol. 624, p 343-357.

(60) Didychuk, C. L.; Ephrat, P.; Chamson-Reig, A.; Jacques, S. L.; Carson, J. J. L. *Nanotechnology* **2009**, *20*, 195102.

(61) Kennedy, L. C.; Bickford, L. R.; Lewinski, N. A.; Coughlin, A. J.; Hu, Y.; Day, E. S.; West, J. L.; Drezek, R. A. *Small* **2011**, *7*, 169-183.

(62) Hu, M.; Chen, J. Y.; Li, Z. Y.; Au, L.; Hartland, G. V.; Li, X. D.; Marquez, M.; Xia, Y. N. *Chem. Soc. Rev.* **2006**, *35*, 1084-1094.

(63) Lee, K. S.; El-Sayed, M. A. *J. Phys. Chem. B* **2005**, *109*, 20331-20338.

(64) von Maltzahn, G.; Park, J. H.; Agrawal, A.; Bandaru, N. K.; Das, S. K.; Sailor, M. J.; Bhatia, S. N. *Cancer Res* **2009**, *69*, 3892-3900.

(65) Esumi, K.; Matsuhisa, K.; Torigoe, K. *Langmuir* **1995**, *11*, 3285-3287.

(66) Yu; Chang, S.-S.; Lee, C.-L.; Wang, C. R. C. *J. Phys. Chem. B* **1997**, *101*, 6661-6664.

(67) Murphy, C. J.; Sau, T. K.; Gole, A. M.; Orendorff, C. J.; Gao, J.; Gou, L.; Hunyadi, S. E.; Li, T. *J. Phys. Chem. B* **2005**, *109*, 13857-13870.

(68) Perezjuste, J.; Pastorizasantos, I.; Lizmarzan, L.; Mulvaney, P. *Coord. Chem. Rev* **2005**, *249*, 1870-1901.

(69) Yasun, E.; Gulbakan, B.; Ocsoy, I.; Yuan, Q.; Shukoor, M. I.; Li, C.; Tan, W. *Anal. Chem.* **2012**, *84*, 6008-6015.

(70) Huang, Y. F.; Chang, H. T.; Tan, W. *Anal. Chem.* **2008**, *80*, 567-572.

(71) Yuan, Z.; Jiang, H. In *Cancer Nanotechnology*; Grobmyer, S. R., Moudgil, B. M., Eds.; Humana Press: 2010; Vol. 624, p 309-324.

(72) Jiang, H.; Iftimia, N. V.; Xu, Y.; Eggert, J. A.; Fajardo, L. L.; Klove, K. L. *Acad Radiol* **2002**, *9*, 186-194.

(73) Ntziachristos, V.; Yodh, A. G.; Schnall, M.; Chance, B. *Proc. Natl. Acad. Sci. U.S.A.* **2000**, *97*, 2767-2772.

(74) Cerussi, A. E.; Berger, A. J.; Bevilacqua, F.; Shah, N.; Jakubowski, D.; Butler, J.; Holcombe, R. F.; Tromberg, B. J. *Acad Radiol* **2001**, *8*, 211-218.

(75) Li, P. C.; Wang, C. R. C.; Shieh, D. B.; Wei, C. W.; Liao, C. K.; Poe, C.; Jhan, S.; Ding, A. A.; Wu, Y. N. *Opt. Express* **2008**, *16*, 18605-18615.

(76) Zhu, J.; Yang, X.; Zhang, L.; Zhang, L.; Lou, B.; Dong, S.; Wang, E. *Chem Commun (Camb)* **2013**, *49*, 5459-5461.

(77) Guo, S.; Du, Y.; Yang, X.; Dong, S.; Wang, E. *Anal. Chem.* **2011**, *83*, 8035-8040.

(78) Yang, X.; Sun, X.; Lv, Z.; Guo, W.; Du, Y.; Wang, E. *Chem Commun (Camb)* **2010**, *46*, 8818-8820.

(79) Yasun, E.; Kang, H.; Erdal, H.; Cansiz, S.; Ocsoy, I.; Huang, Y. F.; Tan, W. *Interface Focus* **2013**, *3*, 20130006.

(80) Nikoobakht, B.; El-Sayed, M. A. *Langmuir* **2001**, *17*, 6368-6374.

(81) Wang, L.; Jiang, X.; Ji, Y.; Bai, R.; Zhao, Y.; Wu, X.; Chen, C. *Nanoscale* **2013**, *5*, 8384-8391.

(82) Hauck, T. S.; Ghazani, A. A.; Chan, W. C. *Small* **2008**, *4*, 153-159.

(83) Alkilany, A. M.; Nagaria, P. K.; Hexel, C. R.; Shaw, T. J.; Murphy, C. J.; Wyatt, M. D. *Small* **2009**, *5*, 701-708.

(84) Niidome, T.; Yamagata, M.; Okamoto, Y.; Akiyama, Y.; Takahashi, H.; Kawano, T.; Katayama, Y.; Niidome, Y. *Journal of controlled release : official journal of the Controlled Release Society* **2006**, *114*, 343-347.

(85) Qiu, Y.; Liu, Y.; Wang, L.; Xu, L.; Bai, R.; Ji, Y.; Wu, X.; Zhao, Y.; Li, Y.; Chen, C. *Biomaterials* **2010**, *31*, 7606-7619.

(86) Vigderman, L.; Manna, P.; Zubarev, E. R. *Angew Chem Int Edit* **2012**, *51*, 636-641.

(87) Wang, L.; Liu, Y.; Li, W.; Jiang, X.; Ji, Y.; Wu, X.; Xu, L.; Qiu, Y.; Zhao, K.; Wei, T.; Li, Y.; Zhao, Y.; Chen, C. *Nano Lett.* **2011**, *11*, 772-780.

(88) Alkilany, A. M.; Nagaria, P. K.; Wyatt, M. D.; Murphy, C. J. *Langmuir* **2010**, *26*, 9328-9333.

(89) Johnson, C. J.; Dujardin, E.; Davis, S. A.; Murphy, C. J.; Mann, S. *J. Mater. Chem.* **2002**, *12*, 1765-1770.

(90) Gole, A.; Murphy, C. J. *Chem. Mater.* **2004**, *16*, 3633-3640.

(91) Gao, J.; Bender, C. M.; Murphy, C. J. *Langmuir* **2003**, *19*, 9065-9070.

(92) Chithrani, B. D.; Ghazani, A. A.; Chan, W. C. *Nano Lett.* **2006**, *6*, 662-668.

(93) Peng, Z. G.; Hidajat, K.; Uddin, M. S. *J Colloid Interface Sci* **2005**, *281*, 11-17.

(94) Schulze, W. X.; Mann, M. *J. Biol. Chem.* **2004**, *279*, 10756-10764.

(95) Phizicky, E. M.; Fields, S. *Microbiol. Rev.* **1995**, *59*, 94-123.

(96) Alber, F.; Dokudovskaya, S.; Veenhoff, L. M.; Zhang, W.; Kipper, J.; Devos, D.; Suprapto, A.; Karni-Schmidt, O.; Williams, R.; Chait, B. T.; Sali, A.; Rout, M. P. *Nature* **2007**, *450*, 695-701.

(97) Tong, S.; Hou, S.; Ren, B.; Zheng, Z.; Bao, G. *Nano Lett.* **2011**, *11*, 3720-3726.

(98) Teng, C. H.; Ho, K. C.; Lin, Y. S.; Chen, Y. C. *Anal. Chem.* **2004**, *76*, 4337-4342.

(99) Williams, L. *Biotech. Histochem.* **2001**, *76*, 127-132.

(100) Roegener, J.; Lutter, P.; Reinhardt, R.; Blüggel, M.; Meyer, H. E.; Anselmetti, D. *Anal. Chem.* **2003**, *75*, 157-159.

(101) Aebersold, R.; Goodlett, D. R. *Chem. Rev.* **2001**, *101*, 269-295.

(102) Aebersold, R.; Mann, M. *Nature* **2003**, *422*, 198-207.

(103) Karakoti, A. S.; Das, S.; Thevuthasan, S.; Seal, S. *Angew. Chem., Int. Ed. Engl.* **2011**, *50*, 1980-1994.

(104) Liu, Z.; Robinson, J. T.; Sun, X.; Dai, H. *J. Am. Chem. Soc.* **2008**, *130*, 10876-10877.

(105) Jokerst, J. V.; Lobovkina, T.; Zare, R. N.; Gambhir, S. S. *Nanomedicine (Lond)* **2011**, *6*, 715-728.

(106) Suh, J.; Choy, K. L.; Lai, S. K.; Suk, J. S.; Tang, B. C.; Prabhu, S.; Hanes, J. *Int. J. Nanomed.* **2007**, *2*, 735-741.

(107) Balamurugan, S.; Obubuafo, A.; McCarley, R. L.; Soper, S. A.; Spivak, D. A. *Anal. Chem.* **2008**, *80*, 9630-9634.

(108) Balamurugan, S.; Obubuafo, A.; Soper, S. A.; Spivak, D. A. *Anal. Bioanal. Chem.* **2008**, *390*, 1009-1021.

(109) Balamurugan, S.; Obubuafo, A.; Soper, S. A.; McCarley, R. L.; Spivak, D. A. *Langmuir* **2006**, *22*, 6446-6453.

(110) Lakowicz, J. R. *Anal. Biochem.* **2004**, *324*, 153-169.

(111) Swierczewska, M.; Lee, S.; Chen, X. *Phys. Chem. Chem. Phys.* **2011**, *13*, 9929-9941.

(112) Lundblad, R. L.; Kingdon, H. S.; Mann, K. G. In *Methods in Enzymology*; Laszlo, L., Ed.; Academic Press: 1976; Vol. Volume 45, p 156-176.

(113) Michael E. Nesheim, K. G. M. *J. Biol. Chem.* **1983**, *258*, 5386-5391.

(114) Kretz, C. A.; Cuddy, K. K.; Stafford, A. R.; Fredenburgh, J. C.; Roberts, R.; Weitz, J. I. *Thromb. Haemostasis* **2010**, *103*, 83-93.

(115) Li, F.; Li, J.; Wang, C.; Zhang, J.; Li, X. F.; Le, X. C. *Anal. Chem.* **2011**, *83*, 6464-6467.

(116) Castellana, E. T.; Gamez, R. C.; Gomez, M. E.; Russell, D. H. *Langmuir* **2010**, *26*, 6066-6070.

(117) Gulbakan, B.; Yasun, E.; Shukoor, M. I.; Zhu, Z.; You, M.; Tan, X.; Sanchez, H.; Powell, D. H.; Dai, H.; Tan, W. *J. Am. Chem. Soc.* **2010**, *132*, 17408-17410.

(118) Sefah, K.; Meng, L.; Lopez-Colon, D.; Jimenez, E.; Liu, C.; Tan, W. *PLoS ONE* **2010**, *5*, e14269.

BIOGRAPHICAL SKETCH

Emir Yasun was born in Bursa, Turkey. He obtained his BS degree in Chemistry from Bilkent University, in 2008, in Turkey with Honors. In 2008, he joined the chemistry graduate program at the University of Florida, where he obtained his PhD in Chemistry in 2013, under the supervision of Dr. Weihong Tan.